Research on the potential of electrolysis and gasification of solid fuels for the production of synthetic natural gas in a polygeneration system

DARIA KATLA

Supervisors:

Anna Skorek-Osikowska

Michał Jurczyk

Doctoral Thesis in Environmental Engineering, Mining and Energy

Silesian University of Technology

Gliwice, Poland, 2023

Author:

Daria Katla, MEng.

Silesian University of Technology

Joint Doctoral School

daria.katla@polsl.pl

Supervisor:

Anna Skorek-Osikowska, Prof.

Silesian University of Technology

Faculty of Energy and Environmental Engineering

Department of Power Engineering and Turbomachinery

anna.skorek-osikowska@polsl.pl

Co-Supervisor:

Michał Jurczyk, PhD

Silesian University of Technology

Faculty of Energy and Environmental Engineering

Department of Power Engineering and Turbomachinery

michal.jurczyk@polsl.pl

Polish title:

Badanie potencjału procesów elektrolizy i zgazowania paliw stałych do produkcji syntetycznego gazu ziemnego w układzie poligeneracyjnym

Acknowledgements

I would like to express my sincere gratitude to my supervisor Prof. Anna Skorek-Osikowska for her invaluable support, guidance, and fruitful discussions. It would be my pleasure to continue this relationship on academic and personal ground.

I gratefully acknowledge the contribution of Dr Michał Jurczyk, my co- supervisor. I am thankful for all the support, suggestions, countless hours spent in the lab and cooperation during the realisation of this research project.

My sincere thanks also go to Dr Daniel Węcel. I appreciate all the shared knowledge and experience, which was invaluable for the preparation of the experimental part of this thesis.

In addition, I would like to acknowledge all the people that I had a chance to collaborate with during last years. Sincere thanks go to Łukasz Bartela, Wojciech Uchman, Bartosz Stanek, Jakub Ochmann, Iwona Adamczewska and Katarzyna Janusz-Szymańska.

I would like to acknowledge the contribution of Dr Shareq Mohd Nazir (KTH Royal Institute of Technology, Stockholm, Sweden). I am glad for the support and all the advice I have received from him during and after my internship at KTH.

I gratefully acknowledge the support of the National Science Centre, Poland. Financial assistance was provided by grant no. 2017/27/B/ST8/02270 within the framework of the research project entitled *Utilization of electrolysis and oxygen gasification processes for the production of synthetic natural gas in a polygeneration system*.

This doctoral thesis was carried within the framework of the European Social Fund programme Power for Student, Stuff, Science, no. POWR.03.05.00-00-Z305, which I would like to gratefully acknowledge.

Finally, my deep and sincere gratitude goes to my loved family and dearest friends. I am thankful for all the care, opportunities and support I was given by my mom and my grandmothers during all my youth. Finally, thank you Mati for being my safe place at all times.

Table of Contents

List of Figures

List of Tables

List of important denotations

A - depreciation, €

CF - cash flows, €

c_i - unit investment cost, e.g. €/MW

C_{op} - operating costs, €

CR - carbon recovery

C_{SNG} - SNG selling price, €

E_{ch} - chemical energy, MWh

E_{el} - electricity consumption, MWh

FOM - fixed operation and maintenance costs, €

GHSV - Gas Hourly Space Velocity, h^{-1}

HHV - Higher Heating Value, MJ/kg

J - investment costs, €

L - salvage value, €

LHV - Lower Heating Value, MJ/kg

$\dot{m}$ - mass flow, kg/s

$\dot{n}$ - mole flow, kmol/s

N_{el} - electric power, W

p - pressure, bar

Q - heat stream, W

r - discount rate, %

S - revenue from sales, €

T - temperature, °C

T_{in} - income tax, €

V - volume, dm^3

$\dot{v}$ - volumetric flow, dm^3/h

VOM - variable operation and maintenance costs, €

WHSV - Weighted Hourly Space Velocity, h^{-1}

x_{CO_2} - carbon dioxide conversion coefficient

η - efficiency, %

List of important acronyms

AEL - alkaline electrolyzers

AEM - anion exchange membrane electrolyzers

AFBR - adiabatic fixed bed reactor

a-MDEA - activated methyldiethanolamine

BFB - bubbling fluidized-bed gasifier

C - compressor

CAES - Compressed Air Energy Storage

CAPEX - capital expenditures

CCS - Carbon Capture and Storage

CFB - circulating fluidized-bed gasifier

CFBR - cooled fixed bed reactor

CHP - Combined Heat and Power

DFB - dual fluidized-bed gasifier

EU - European Union

FBR - fluidised bed reactor

FICFB - fast internally circulating fluidised bed

HX - heat exchanger

M - motor

MR - methanation reactor

NG - natural gas

NPV - Net Present Value

OPEX - operational expenditures

PEM - polymer electrolyte membrane

PG - process gas

PHES - Pumped Hydroelectric Energy Storage

PtG - Power to Gas

PtH_2 - Power to H_2

PtSNG - Power to SNG

RES - Renewable Energy Sources

SEP - separator

SNG - Synthetic Natural Gas

SOE - solid oxide electrolyzers

SR - structured reactor

3PR - three-phase reactor

1. General introduction

1.1. Background

The European Union (EU) has established a growing number of new energy policy objectives in recent years. EU energy policy focuses on improving energy efficiency, increasing energy security, diversifying power generation structure, developing renewable energy sources (RES), developing competitive fuel and energy markets, and reducing environmental impact.

In 2020, the share of RES in the European energy mix was 22% [1]. Figure 1.1 illustrates the most important renewable energy share 2030 targets with later modifications. In October 2014 the EU leaders agreed on setting a target of at least 27% share of energy consumption produced from renewable resources, 27% improvement in the EU's energy efficiency, 40% reduction of greenhouse gas emissions from 1990 level [2].

The recasted Renewable Energy Directive 2018/2001/EU [3] established a new legally binding objective of at least 32% of renewable energy share for 2030. However, additional implementations are required in order to achieve the objectives outlined in the European Green Deal [4] in 2019. Its aim is to make the EU's economy more sustainable and reduce the EU's greenhouse gas emissions to net-zero by 2050. The Green Deal includes a broad range of policy measures and initiatives covering areas such as climate neutrality, energy transition, sustainable transport, agriculture, biodiversity, circular economy, and sustainable finance. The proposal to amend the Renewable Energy Directive was presented in 2021, with the objective of raising the target of 40% renewable energy share in the EU's energy mix by 2030 [5]. In light of Russia's aggression against Ukraine in 2022, the European Commission proposed a new plan to reduce reliance on Russian fossil fuels. According to the REPowerEU plan, the renewable energy target should be increased by up to 45% by 2030 [6]. To achieve this goal significant investments in the renewable energy sector will be needed. Also, diversification of the gas supplied is highly important and the main emphasis is on increasing the levels of bio-methane and hydrogen produced [6].

A massive acceleration and scaling-up of RES in power generation, transportation, industry and buildings will speed up the transition away from Russian

fossil fuels. It will also reduce electricity prices and lower the amount of imported fossil fuels over time.

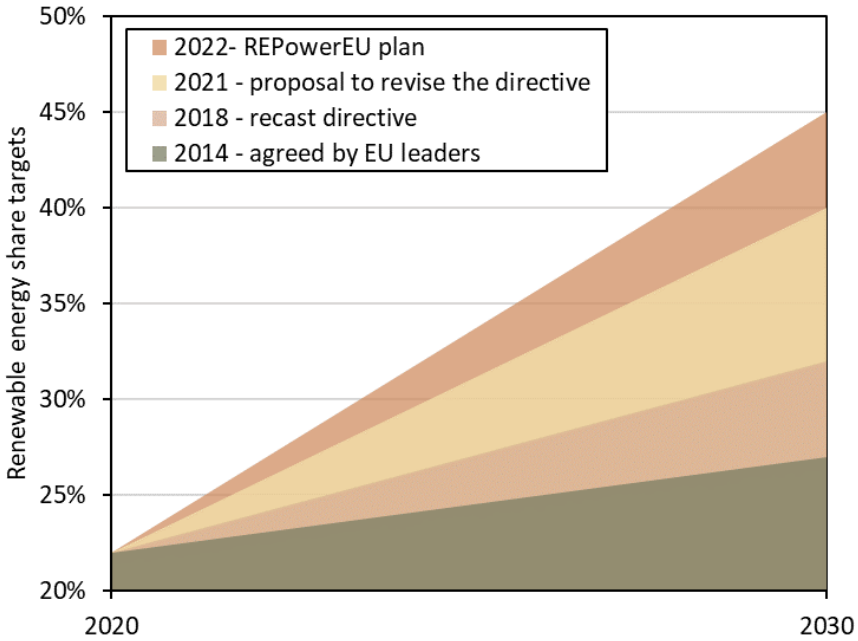

Figure 1.1 Evolution of EU renewable energy targets [1]

To achieve climate-neutrality by 2050, antropogenic emissions of CO_2 must approach net zero. The primary goal of the Paris Agreement is to keep global temperature rise well below 2 °C above pre-industrial levels. The carbon budget described in the Agreement refers to the maximum amount of greenhouse gas emissions that can be released into the atmosphere while still limiting global warming to a specific temperature target. All parties pledged in the Paris Agreement to preserve global warming below 2 °C (with the remaining carbon budget of 1170-1500 Gt_{CO_2}), while enduring efforts to keep it below 1.5 °C (with the remaining carbon budget of 420-580 Gt_{CO_2}) [7]. The shift to a carbon-neutral economy will be difficult for the global energy system. However, if existing power infrastructure (based mainly on fossil fuels) is used as it has been so far, by 2050 it will emit approximately 658 Gt_{CO_2}, which already surpasses the 1.5 °C carbon budget [8]. The power sector contributes to over half of all those emissions (358 Gt_{CO_2}), which highlights the significance of decarbonization of the power sector.

1.2. The need for energy storage

Figure 1.2 depicts the dynamics of installed power capacity growth in years 2014 – 2022 using the Polish electric power system as an example [8]. During those years, the amount of power capacity installed in RES increased by more than 5.5 times.

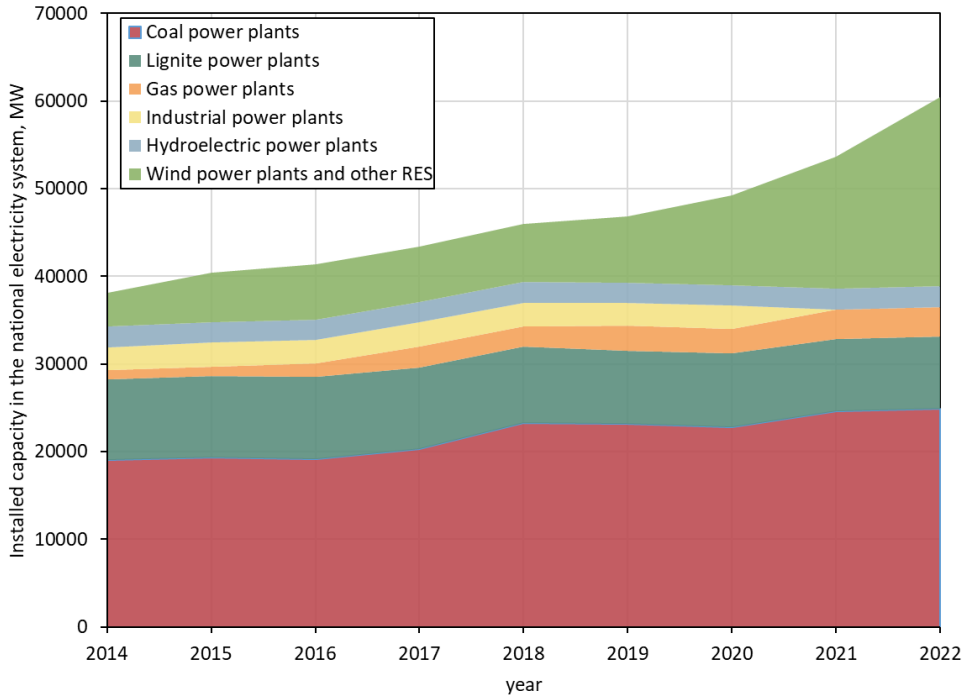

Figure 1.2 Growth dynamics of installed capacity in the Polish power system in 2014-2022 [9]

The advantages of renewable energy sources include reduction of greenhouse gas emissions, however, several unfavorable aspects, such as energy production unpredictability, lack of continuity of energy supply or terrain conditions, are associated with the use of RES installations. Due to the intermittent character of RES, installations of this type are characterized by a variable amount of produced electricity (Fig. 1.3), which depends mostly on the prevailing weather conditions and the variable activity of electricity consumers during the day [10]. Further increase of renewable energy installations installed capacity may inconveniently affect the stability of energy systems [11]. The power grid should always maintain a balance of supply and demand. As the share of renewable energy sources is constantly growing, the need for a dependable power system to meet electricity demand becomes more critical, especially given the fluctuating nature of renewable sources. That clarifies

the rapidly increasing need for power system flexibility implementation. In the period of dynamically conducted energy transformation, it is necessary to ensure the introduction of energy storage systems, as well as to maintain on the market stable energy sources based on the use of fossil fuels, provided that their combustion will be carried out in the most ecological way possible.

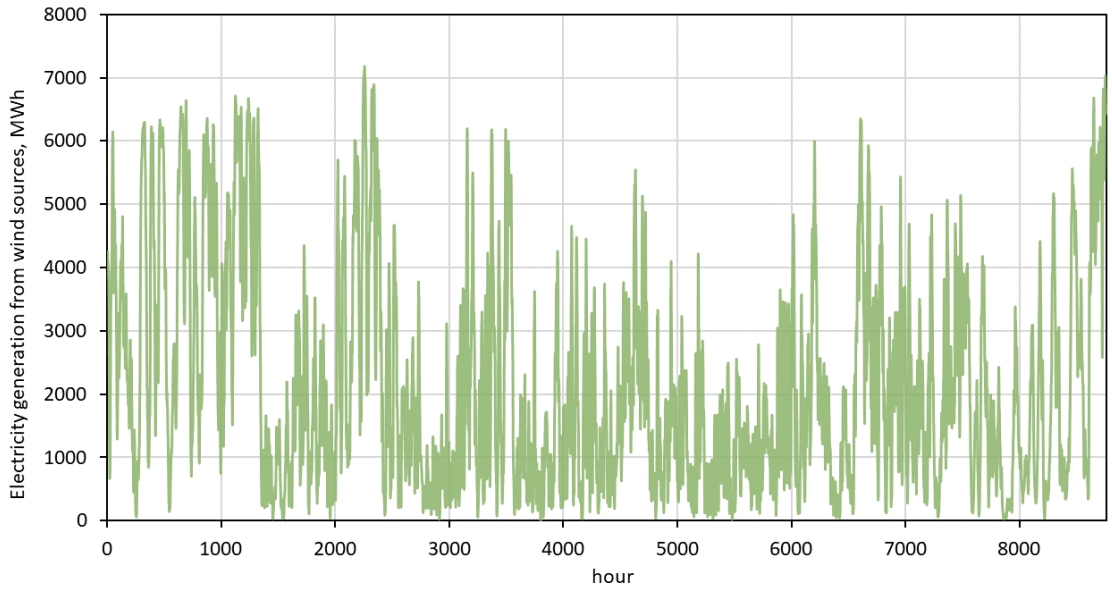

Figure 1.3 Electricity production from wind sources in Poland in 2022 [9]

The primary role of energy storage installations is the collection and storage of surplus electricity during its excess in power systems. The stored energy is dispatched to the grid when its current demand is higher than the possible production. With the appropriate use of the capabilities of installations dedicated to energy storage, the amount of electricity generated by conventional sources does not have to be adapted to the specific instantaneous demand in the power grid. It enables effective use of both conventional power plants with limited flexibility of regulation, and the renewable energy sources installations under the same power systems [12].

Energy storage allows for more efficient use of energy obtained from intermittent renewable sources. It not only solves the problem of renewable energy cooperation with the power system, but it also provides a security measure in the case of a system failure and supports the development of a more flexible and reliable conventional energy production system. In general, the idea behind energy storage is that surplus energy produced in demand valleys is stored and can be released when demand increases. Energy can be stored when production exceeds consumption and

used when consumption exceeds production. As a result, this technology ensures more efficient energy use and enables adaptation of energy production from renewable energy sources, which initially demonstrated problematic.

Among larger scale energy storage technologies Compressed Air Energy Storage (CAES), Pumped Hydroelectric Energy Storage (PHES) and Power to Gas (PtG) can be distinguished. Figure 1.4 depicts the capacity dependence of various energy storage technologies as a function of discharge time. It can be seen that power to gas (hydrogen, synthetic natural gas) technology is characterized by the highest storage capacity.

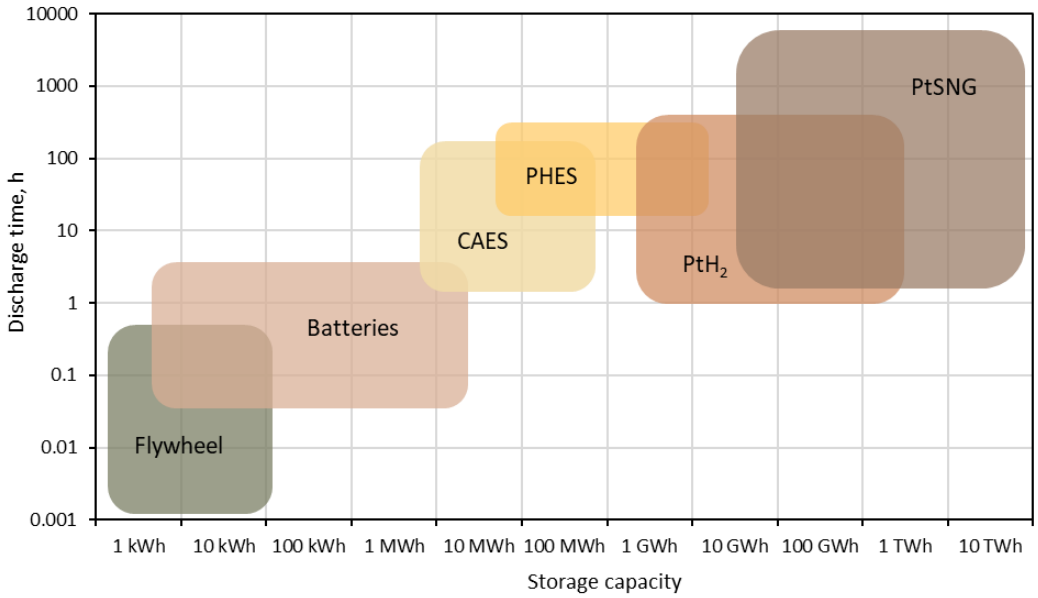

Figure 1.4 Energy storage technologies with reference to their capacity and discharge time [13]; where CAES – Compressed Air Energy Storage, PHES – Pumped Hydroelectric Energy Storage, PtH_2 – Power to H_2, PtSNG – Power to SNG

Power to hydrogen technology (PtH_2) is a process of producing hydrogen from electricity generated by renewable energy sources such as wind or solar power. The PtH_2 technology involves the electrolysis of water, where electricity is used to split water molecules into oxygen and hydrogen. Development of renewable hydrogen production and hydrogen infrastructure is one of the key elements in achieving the goals of the European Green Deal and Europe's clean energy transition. The integration of hydrogen generation systems with electricity generation systems can be additionally considered. It leads to the development of power to H_2 to power (PtH_2tP) systems enabling the effective use of hydrogen generated in a quantity

higher than market needs. Importantly, access to oxygen as a by-product of the electrolysis process can in this case economically justify the construction of such systems and improve their efficiency [14–16].

Hydrogen has a great potential to complement this strategy as a carrier for renewable energy storage, ensuring backup for seasonal fluctuations and connecting production locations to more distant demand centres. The only product of hydrogen utilisation is water vapor, making it a zero-emission fuel. As a result, hydrogen is an appealing option for lowering greenhouse gas emissions and air pollution. Hydrogen has a high energy density, meaning that it contains a large amount of energy per unit of weight or volume. It can be used in a variety of applications, including transportation, power generation, and heating. However, the process of producing hydrogen through electrolysis is energy-intensive and expensive, which makes it less economically viable compared to traditional fossil fuels. Nevertheless, with the increasing demand for clean energy, PtH_2 technology is expected to play a significant role in the transition towards a more sustainable energy system.

Hydrogen blending into natural gas grids could increase decarbonization while preserving the use of natural gas infrastructure, which can accept some fraction of hydrogen in the feedstock without causing significant problems. However, hydrogen blending into natural gas grids is limited to a certain volume level (which varies depending on country regulations) or is not regulated legally yet. Transporting hydrogen through pipelines is considered difficult because of its low density and high reactivity and flammability. Liquefied and compressed hydrogen are two common methods for storing and transporting hydrogen. Liquefied hydrogen is 4 times less dense than liquid gasoline, and it must be cryogenically cooled and greatly compressed just to reach a liquid state. Compressed hydrogen (pressure up to 700 bar) can be stored at lower temperatures than liquefied hydrogen, and it is less energy-intensive to produce. However, compressed hydrogen requires a significant amount of space, making it difficult to use in some applications. Finding a method for economically viable hydrogen transport and storage is a significant barrier to the widespread use of H_2 as a gaseous fuel.

Various ways of making the currently planned investments in power to H_2 systems more flexible should be considered. Such an increase in flexibility can be

achieved by subjecting hydrogen e.g. to the methanation process. While hydrogen production development is a long-term goal, a more mid-term goal of EU policy targets proposed within the REPowerEU plan [6] is synthetic or bio-methane production development. Synthetic natural gas (SNG) or bio-SNG/bio-methane (named like that when produced based on biomass sources) is considered as a good alternative over hydrogen because its more flexible in terms of utilization. Synthetic natural gas is characterized by similar composition, calorific value and range of Wobbe index to conventional natural gas [17,18], which indicates that it can be used within the existing infrustructure and injected into natural gas grid almost without any limitations.

Currently, the prices of hydrogen-based synthetic fuels are relatively high compared to traditional fossil fuels such as gasoline and diesel. However, due to the advancing development of technology, these prices can be expected to fall in the future. Technological advances and an increase in the scale of production may contribute to lower production costs for synthetic fuels. It can be hypothesized that the price of traditional fossil fuels will rise in the future, as the amount of fossil fuels in the world is limited and the costs of extracting and processing them are becoming higher. Therefore, as the demand for alternative energy sources increases, synthetic fuel prices may become more competitive [19].

2. Motivation and scope of the thesis

2.1. Motivation

As the share of electricity produced from renewable energy sources in the power grid is constantly increasing, consequently, there is a need for the development of energy storage technologies in high-capacity accumulators. The possible fluctuations in the amount of produced energy cause the necessity of balancing such sources for the stable operation of the power grid. Power to SNG (PtSNG) installations can be an important element in the process of storing surplus energy in electric power systems.

This dissertation evaluates the viability of using electrolysis and oxygen gasification of biomass for the production of synthetic natural gas. Biomass gasification and methanation technologies, in conjunction with electrolysis, could play a significant role as a seasonal storage, allowing SNG grid injection and storage. The main benefit of such a method is the production of a fuel that, in contrast to pure hydrogen, has greater potential for use in current energy systems, can be easily transported through current transmission networks, and is significantly simpler to store. The various configurations of proposed power to SNG systems studied within the scope of this dissertation are in line with the direction of research into new energy storage systems.

2.2. Scope and goals of the thesis

The primary objective of the dissertation was to numerically and experimentally investigate the potential of using the electrolysis and oxygen gasification process of solid fuels to produce synthetic natural gas by methanation in a polygeneration system. The proposed solution makes it possible to utilize:

- excess renewable electricity generation to produce hydrogen in electrolyzers for further use in SNG production,
- oxygen as a by-product of hydrogen generation in the oxygen gasification process,
- the gasification process to generate gas containing carbon monoxide and carbon dioxide used in the methanation process.

By developing mathematical models of the individual components of the proposed power to SNG system, it was possible to perform thermodynamic and economic analysis of the integrated system.

The experimental work additionally allowed determining the influence of selected parameters on the course and values of thermodynamic evaluation of the methanation process, as well as to optimizing the operational parameters of the process.

The main result of the work was the development of characteristics of individual sub-processes and guidelines for the parameters of these processes. The technical and economic parameters associated with the potential implementation of the proposed power to SNG systems were also determined.

The dissertation involved research on methanation process based on two main parts - experimental and techno-economic analysis. Experiments were conducted to broaden understanding of the methanation process under various operating conditions and to collect data relevant to research on PtSNG applications. The goal was to develop a methanation reactor with main aim of being effective, simple, and inexpensive (in terms of capital and operation costs) at the same time, as well as to evaluate the influence of the main process conditions on the effectiveness of methane production. Preliminary tests carried out on the constructed methane generator plant were previously published [20], and in this thesis the initial results were enriched with a new measurement campaign and the entire process is described in Chapter 4. Besides the experimental part, mathematical modeling of power to SNG systems was performed and aimed at carrying out the techno-economic analysis in order to assess diferent cases for SNG production. A number of systems based on power to SNG technology have been analyzed, and the results have been published in the following publications [12,14–16,21]. The most important results obtained are described in Chapters 5 and 6.

The primary goal required the dissertation accomplishment of several subgoals, including:

Experimental part:

– development of methanation installation lab stand,

– experimental analysis of the influence of selected parameters on the methanation process and thermodynamic evaluation indicators.

Techno-economic analysis:

– development of mathematical models for the proposed system's individual components, principally: biomass gasification system and methanation installation,

– detailed thermodynamic analysis of individual unit processes,

– integration of unit processes into the system for synthetic natural gas production based on electrolysis and gasification processes,

– determining the streams of substances and energy generated and used within the system (hydrogen, oxygen, water/steam, carbon monoxide, carbon dioxide, heat flux, etc.) and their potential for improving process efficiency,

– assessing the necessity of the use of Shift conversion reactor and separation systems to enhance the properties of the produced SNG,

– techno-economic analysis of the selected system structures.

3. Power to Synthetic Natural Gas

Power to gas is a technology that involves converting excess renewable electricity into a gas that can be stored and used as a fuel. The process involves using renewable electricity, typically from wind or solar power, to electrolyze water (or steam) into hydrogen and oxygen. Power to synthetic natural gas can be considered a development of the power to gas concept as it is also based on electrolysis process. Power to SNG involves a two-step process. Hydrogen resulting from electrolysis process is then combined with carbon feedstock to produce synthetic natural gas using a methanation process (Fig. 3.1). The resulting synthetic natural gas can be used for heating, electricity generation, or transportation. Power to SNG has the advantage of producing a gas that is very similar in composition to natural gas, making it easier to integrate into existing natural gas infrastructure. It can also help to reduce the carbon footprint of the gas industry, as the CO_2 used in the process can be sourced from industrial emissions or captured from the atmosphere.

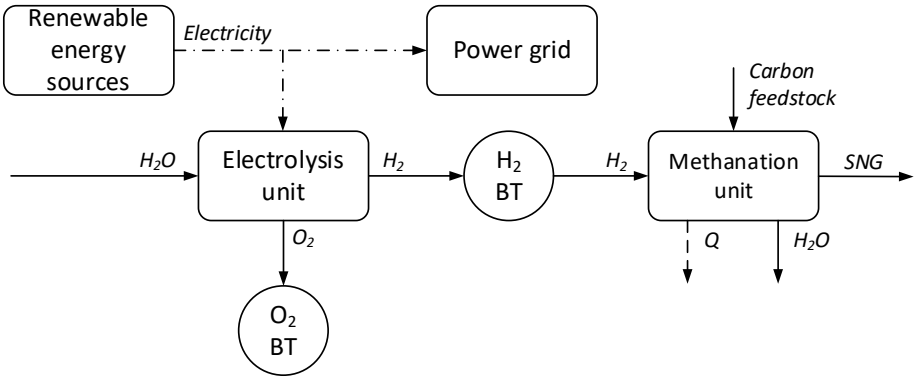

Figure 3.1 Simplified flowchart of power to SNG process; where BT is buffer tank

3.1. Electrolysis process

Electrolysis process in an emission-free electrochemical technology for hydrogen production. The basic reaction for water electrolysis is as follows (3.1):

$$2H_2O \rightarrow 2H_2 + O_2 \quad (3.1)$$

The reaction of decomposition of H_2O into H_2 and O_2 is endothermic. Energy called enthalpy of reaction ΔH is needed for the reaction which corresponds to the enthalpy of the formation of water. The standard enthalpy of the reaction is equal to 285.8 $kJmol^{-1}$ (237.3 $kJmol^{-1}$ of electricity and 48.6 $kJmol^{-1}$ of heat) [22,23]. In the

gaseous state (beyond 100 °C) the total energy demand for H_2O electrolysis process increases with higher temperatures but the free energy of the reaction decreases. This provides the opportunity to use more heat for the H_2O decomposition at higher temperatures. In the most general way, electrolyzers can be divided into high-temperature and low-temperature ones. Chosen characteristic parameters based on analyzes of the operation of low-temperature alkaline electrolyzers (AEL), anion exchange membrane (AEM) electrolyzers and polymer electrolyte membrane (PEM) electrolyzers and high-temperature solid oxide electrolyzers (SOE) described in [23–25] are presented in Table 3.1.

Table 3.1 Chosen parameters of alkaline, anion exchange membrane, proton exchange membrane and solid oxide electrolysis process [23–25]

	AEL	AEM	PEM	SOE
State of development	mature	R&D	commercial	R&D
Electrolyte	Alkaline solution; KOH/NaOH	DVB polymer support with KOH/NaOH	Solid polymer membrane	Yttria stabilized Zirconia (YSZ)
Charge carrier	OH^-	OH^-	H_3O^+/H^+	O^{2-}
Cell temperature, °C	40-90	40-60	20-100	800-1000
Cell voltage, V	1.8-2.4	1.4-2.0	1.8-2.2	0.91-1.3
System power consumption, kWh/Nm^3H_2	4.5-7.0	4.8	4.5-7.5	2.5-3.6

Alkaline water electrolysis is the most mature technology. An AEL cell consists of two electrodes: positive anode and negative cathode, separated by a diaphragm (mainly asbestos). When the electrodes are connected to a direct current, hydrogen is produced at the cathode and oxygen at the anode. The setup is immersed into a liquid electrolyte of which the most common is a KOH solution. The main drawback of this type of electrolyzers is corrosive character of the electrolyte [25]. In the alkaline electrolysis cell the following reactions (3.2,3.3) take place:

$$\text{Anode: } 4OH^- \rightarrow O_2 + 2H_2O + 4e^- \quad (3.2)$$

$$\text{Cathode: } 4H^+ + 4e^- \rightarrow 2H_2 \quad (3.3)$$

Anion exchange membrane water electrolysis is a developing technology. It is similar to conventional AEL technology with the same reactions taking place on the anode and cathode side. The main difference is the replacement of the diaphragm with an anion exchange membrane. AEM electrolyzer technology offers several advantages over AEL technology but still more investigation and improvements on the subject are needed.

Contrary to alkaline water electrolyzers, PEM electrolyzers do not require any liquid electrolyte. In this technology, the electrolyte is a solid polymer membrane and the most commonly used is Naflon [25]. In the PEM cell, the following reactions (3.4,3.5) take place:

$$\text{Anode: } H_2O \rightarrow \tfrac{1}{2}O_2 + 2H^+ + 2e^- \quad (3.4)$$

$$\text{Cathode: } 2H^+ + 2e^- \rightarrow H_2 \quad (3.5)$$

The biggest advantage of high-temperature electrolyzers is the lower demand for electricity compared to low-temperature devices. This is possible due to the use of heat as part the of energy source necessary for the process, so the temperature of the steam transported to the SOE electrolyzers has a big influence on their efficiency [25]. The reactions taking place during the electrolysis process at the anode (3.6) and the cathode (3.7) of the SOE electrolyzer can be written as [26]:

$$\text{Anode: } O^{2-} \rightarrow \tfrac{1}{2}O_2 + 2e^- \quad (3.6)$$

$$\text{Cathode: } H_2O + 2e^- \rightarrow H_2 + O^{2-} \quad (3.7)$$

3.2. Hydrogen storage

Hydrogen storage is an essential component of hydrogen-based energy systems because it allows hydrogen to be transported and distributed for a variety of applications, including transportation and energy generation. It is known that the storage of hydrogen is a challenging subject due to its low volumetric density [27]. There are several methods of hydrogen storage, including compression, liquification, liquid-organic carriers, and solid state method [28].

One of the most common methods for storing hydrogen in a gaseous form are high-pressure tanks. This technique, in addition to being a well-developed

technology, provides high rates of H_2 filling and release. Furthermore, no energy is required for the release of hydrogen. However, storing hydrogen at high pressure results in a significant loss of 13-18% of its heating value, which affects the overall operation cost [28]. Also, materials used for the development of storage tanks cannot interact with hydrogen [29].

Storage of hydrogen in a liquid form requires cryogenic temperatures. Since liquid hydrogen has a much higher density than gaseous hydrogen, its volumetric energy density significantly increases. If hydrogen is to remain liquid, it must be liquefied at 253 °C (the average boiling point of H_2) [28]. It needs to be kept in special storage units that can maintain this very low temperature. These containers are usually made of materials that minimize heat transfer, such as stainless steel, aluminum, or carbon fiber.

Despite continuous development of those technologies [30], hydrogen storage is still problematic, expensive and also poses a challenge for the transport and utilization infrastructures. These issues are being addressed through the research and development of new storage technologies, such as solid-state hydrogen storage, which may provide a more efficient and cost-effective solution for hydrogen storage [29].

Alternative way of hydrogen storage is its further conversion into many different chemical compounds or synthetic fuels. Hydrogen-derivative substances mainly comprise [31]:

- liquid derivatives (e-kerosene, e-gasoline, and e-diesel),
- methanol (MeOH), ammonia (NH_3),
- e-gases, such as synthetic natural gas.

3.3.Methanation process

There are two types of technologies to convert hydrogen and carbon oxides to methane, which are biological and thermochemical (catalytic) methanation [17]. These technologies differ in the reaction catalysts used and the process conditions. For biological methanation, methanogenic microorganisms are used to catalyze the methanation reaction. The biological reactors are operated at temperatures from 35 °C

to 65 °C and pressures of 1 to 15 bar to achieve optimal growth conditions for these microorganisms [17].

In the catalytic methanation process, carbon dioxide (3.8) and/or carbon oxide (3.9) react with hydrogen at elevated temperature and pressure in the presence of a catalyst to form methane and water vapour. The standard enthalpy of the reaction is equal to 165.1 $kJmol^{-1}$ for the CO_2 hydrogenation and 206.3 $kJmol^{-1}$ for the CO hydrogenation [32]. One of the main reactions during the synthesis is also water gas shift reaction (3.10).

$$CO_2 + 4H_2 \leftrightarrow CH_4 + 2H_2O \quad (3.8)$$

$$CO + 3H_2 \leftrightarrow CH_4 + H_2O \quad (3.9)$$

$$CO + H_2O \leftrightarrow CO_2 + H_2 \quad (3.10)$$

Side reactions (3.11-3.15) of the methanation process are as follows:

$$2CO + 2H_2 \leftrightarrow CH_4 + CO_2 \quad (3.11)$$

$$2CO \leftrightarrow C + CO_2 \quad (3.12)$$

$$CO + H_2 \leftrightarrow C + H_2O \quad (3.13)$$

$$CO_2 + 2H_2 \leftrightarrow C + 2H_2O \quad (3.14)$$

$$CH_4 \leftrightarrow C + H_2 \quad (3.15)$$

Figure 3.2 presents the Gibbs free energy (ΔG) of selected reactions taking place during the methanation process. The equilibrium of the reaction is shifted towards products in the case of $\Delta G < 0$, which is shown in the graph with the shaded area. It can be seen that the production of methane from carbon dioxide (I) and carbon monoxide (II) is favoured to temperature around 600 °C and around 650 °C, respectively. In the case of the water-gas shift reaction (III) up to about 800 °C, the production of carbon dioxide is favoured, while when this temperature is exceeded, carbon monoxide is formed. Accordingly, the process should be multistage to keep the reaction temperature low to support the production of the desired gases.

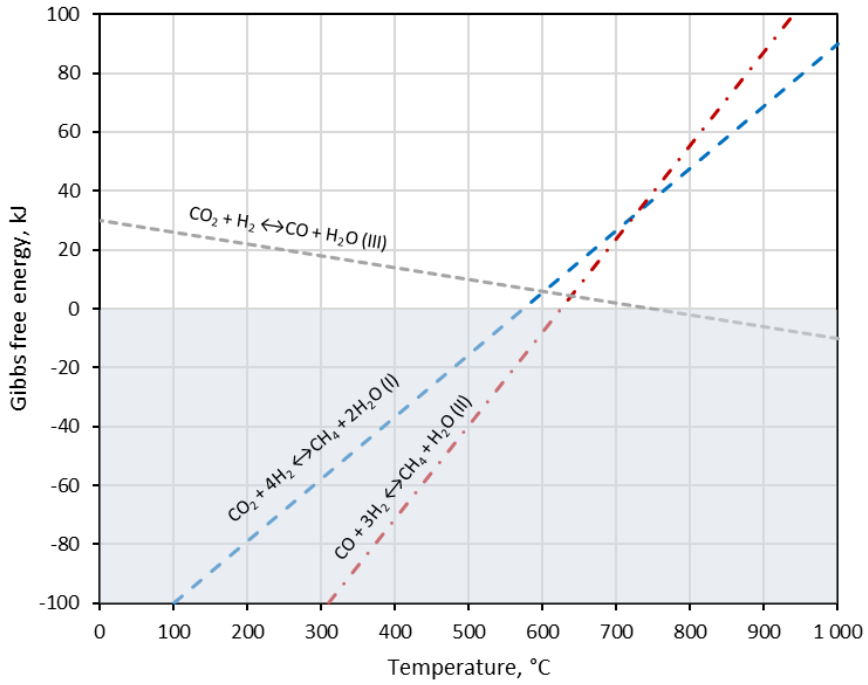

Figure 3.2 Gibbs free energy of selected reactions as a function of temperature

The thermochemical methanation reaction is strongly exothermic, therefore thermodynamic equilibrium turns the reaction towards products at low temperature and high pressure [32]. Figure 3.3 presents the mole fractions methanation reaction products in thermodynamic equilibrium depending on the temperature of the methanation process for atmospheric pressure (solid line) and for 20 bar pressure (dashed line) for initial molar composition of feedstock gases of 80% H_2 and 20% CO_2. In can be stated that the CH_4 yield increases with the decreasing reaction temperature and increasing reaction pressure.

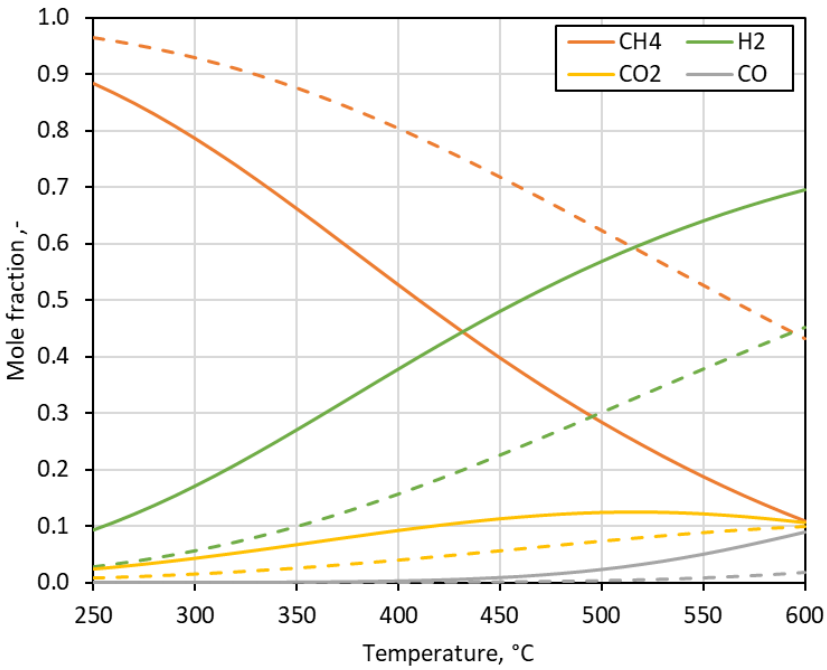

Figure 3.3 Mole fraction of methanation reaction products in thermodynamic equilibrium in a function of reaction temperature (solid line for 1 bar and dashed line for 20 bar)

3.3.1. Catalysts

The selection of a suitable catalyst is a very important factor for an efficient methanation process operation. The catalysts used may consist of different types of active metal (e.g. Rh, Ru, Ni) with different support (e.g. Al_2O_3, SiO_2, ZrO_2) [33]. The support material also affects the activity of the metal. The most commonly used in this process is nickel with the support of Al_2O_3 due to its high activity and relatively low cost (about 13.27 €/kg) [34,35]. Among active metals for the catalyst, nickel (Ni) is frequently used because of its high activity and CH_4 selectivity with relatively low cost. Catalyst based on ferrum (Fe) or cobalt (Co) shows lower activity and selectivity than achieved on nickel. Also, ruthenium (Ru) presents high activity and CH_4 selectivity, but the disadvantage is higher price (about 8047 €/kg) [34]. Good methanation performance can also be achieved on rhodium (Rh) catalyst, but the price of it is extremely high (about 441 500 €/kg) [34]. The least satisfying results among noble metals used for methanation is on palladium (Pd) catalyst. Chosen examples of various methanation process catalysts are summarized in Table 3.2.

Table 3.2 Examples of catalysts used for the methanation process [32]

Active metal	Support
Ni	Al_2O_3, CeO_2, ZrO_2, La_2O_3, MgO, SiO_2, TiO_2, Zeolites
Ru	Al_2O_3, CeO_2, TiO_2
Rh	Al_2O_3
Co	SiO_2
Fe	Al_2O_3, SiO_2
Mn	Al_2O_3
Cu	Al_2O_3

The order of active metals in terms of their reactivity is as follows [36]:

Ru > Fe > Ni > Co > Rh > Pd > Pt

3.3.2. Reactors and technologies

There are five main types of reactors used for catalytic methanation proposed in the literature: adiabatic fixed bed reactor (AFBR), cooled fixed bed reactor (CFBR), fluidised bed reactor (FBR), structured reactor (SR) and three-phase reactor (3PR). A short description of each is presented in Table 3.3.

Table 3.3 Types of methanation reactors [37,38]

Reactor type	Description
Adiabatic fixed bed reactor (AFBR)	It is the most mature reactor type for the methanation process (TRL = 9). Feed gases are reacting while passing through a packed catalyst bed located in the reactor. In this case, a series of adiabatic fixed bed reactors are used with inter-stage cooling. The main challenge for this approach is the complexity of the process that requires the integration of many heat exchangers and product recycle loop. Also, large amount of heat released during the reaction can lead to the formation of so-called hot-spots that can result in damaging the catalyst.
Cooled fixed bed reactor (CFBR):	Cooling agent in this type of reactors can be based on air, water or oil. It is used in order to avoid high temperature gradients within the catalytic bed and unify the temperature distribution. This type of methanation reactor can be available in a number of different forms:

Heat exchanger type reactor	Feed gas enters catalyst tubes from the top of the reactor and the heat generated during the reaction is transferred to a shell side fluid.
Multi-stage fixed bed reactor	A catalyst bed is divided into several sections with intersection cooling. Feed gas enters from the top and flows downstream the reactor.
Multi-quenched fixed bed reactor	A catalyst bed is divided into several sections within the reactor and the gas feed enters them in divided portions to maintain the uniform temperature of the reaction
Tube-cooled converter	Gas feed enters the tubes at the bottom of the reactor and is preheated as it flows upwards. Preheated gas leaves the tubes and goes downwards through the catalyst bed.
Fluidised bed reactor (FBR)	Based on fluidisation of solid catalyst particles in feed stream of the reactant gases. These types of reactor come in many different ratios between the amount of catalyst and volume of gas fed into the reactor.
Structured reactor (SR):	Feed gas flows through small channels covered with catalyst. This type of reactor is characterized by high heat transfer. Most popular structures are microchannel, monolith and honeycomb.
Three-phase reactor (3PR)	Catalyst is suspended in an inert liquid phase and feed gas bubbles through it. The liquid phase is characterized by high heat capacity in order to control the reaction temperature.

The conditions of methanation process performance vary depending on the type of reactor used, primarily the temperature and pressure of the reaction, the number of stages, and the load, usually defined as the gas hourly space velocity (GHSV) index (described in more detail in Chapter 4, as equation 4.1), which expresses the ratio of substrate volumetric flow to reactor volume. Main key parameters of operation (range of temperature and pressure, possible reactants load, typical GHSV and number of stages) of different types of reactors used for catalytic methanation are presented in the Table 3.4.

Table 3.4 Chosen parameters of catalytic methanation reactors [38]

	AFBR	CFBR	SR	FBR	3PR
Temperature, °C	250-700	250-500	250-300	300-400	300-350
Pressure, bar	5-100	5-100	1-20	1-12	20
Load range, %	40-100	30-100	30-100	50-100	20-100
GHSV, h^{-1}	<5000	<6000	<3000	<60,000	<1000
CH_4 content, %			>90		
Number of stages	2-7	1-2	1-2	1-2	1-2

There are various technologies available on different types of the methanation reactors. Suppliers, whose technology is based on adiabatic fixed-bed reactors, include Air Liquide (formerly Lurgi) with Lurgi methanation, Haldor Topsøe with TREMP methanation, Johnson Matthey (Davy Technologies) with HICOM methanation, Outetec methanation and the Ralph M. Parsons Company with RMP methanation [39–41]. The representative companies developing methanation technologies based on cooled fixed-bed reactors are Etogas with steam cooling, Linde with internal contorted heat exchanger and MAN with molten-salt cooling [39]. An example of technology based on fluidized-bed reactor is Comflux process based on isothermal fluidized-bed reactor. With the heat released from the reaction, highly pressurized stream can be produced.

Lurgi methanation is based on two adiabatic fixed-bed reactors with inter section cooling and gas recycle loop (Fig. 3.4). The Lurgi methanation process occurs at high temperature (around 350-500 °C) and pressure (around 20-30 bar). A typical catalyst is chromium oxide on an alumina support [39–41].

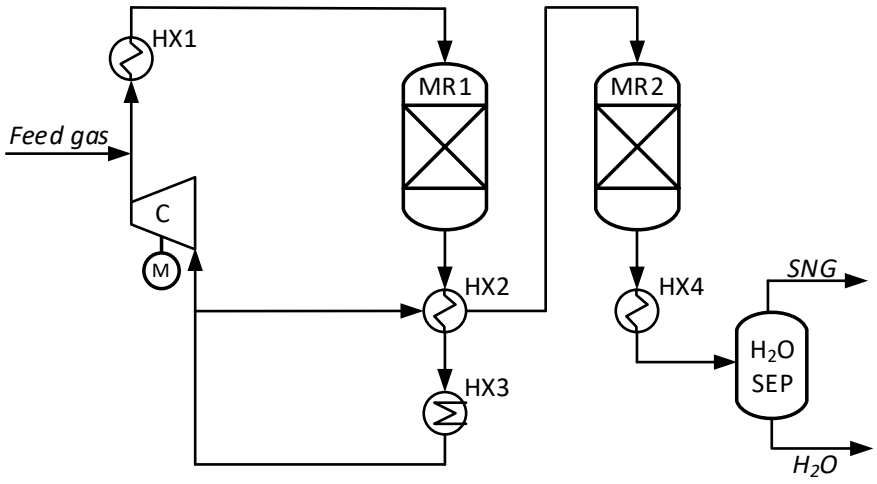

Figure 3.4 Lurgi process [40]; where: MR – methanation reactor, HX – heat exchanger, C – compressor, M – motor, SEP - separator

TREMP methanation was developed to maximize the process efficiency. TREMP methanation is based on three adiabatic fixed bed reactors (Fig. 3.5). The heat of the reaction causes a significant temperature increase (the temperature behind the first reactor can even reach 700 °C), which is controlled by recycle in the first methanation reactor. A part of the feed gas is recycled and in subsequent reactors temperature is lower in order to maximize the conversion. TREMP process is optimized for minimum recycle to reduce energy consumption. This is possible due to the exceptional high-temperature stability of MCR (Methanation Catalyst Reduced) nickel-based methanation catalyst developed by Haldor Topsoe. TREMP technology ensures efficient heat recovery. Up to 85% of the heat released during methanation reactions can be recovered as high-pressure superheated steam [42].

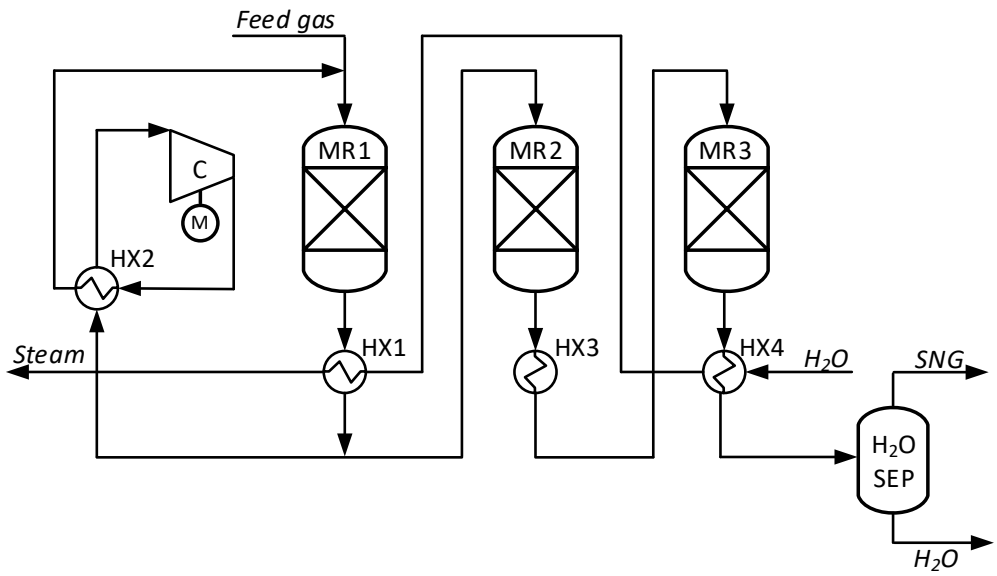

Figure 3.5 Haldor Topsøe TREMP™ process [40]; where: MR – methanation reactor, HX – heat exchanger, C – compressor, M – motor, SEP - separator

In HICOM process the syngas passes through a series of adiabatic fixed-bed reactors (Fig. 3.6). Typical parameters of HICOM methanation are temperature of 300-450 °C, pressure of 20-30 bar. the reaction is typically carried out over a nickel-based catalyst on a high-surface-area support material, such as alumina or silica [39–41]. Also, part of the gas from first stages is recycled and part passes through next methanation reactors at lower operating temperature. Heat recovered from the final product gas cooling is used for heating the feed gas in the saturator before the first methanation stages.

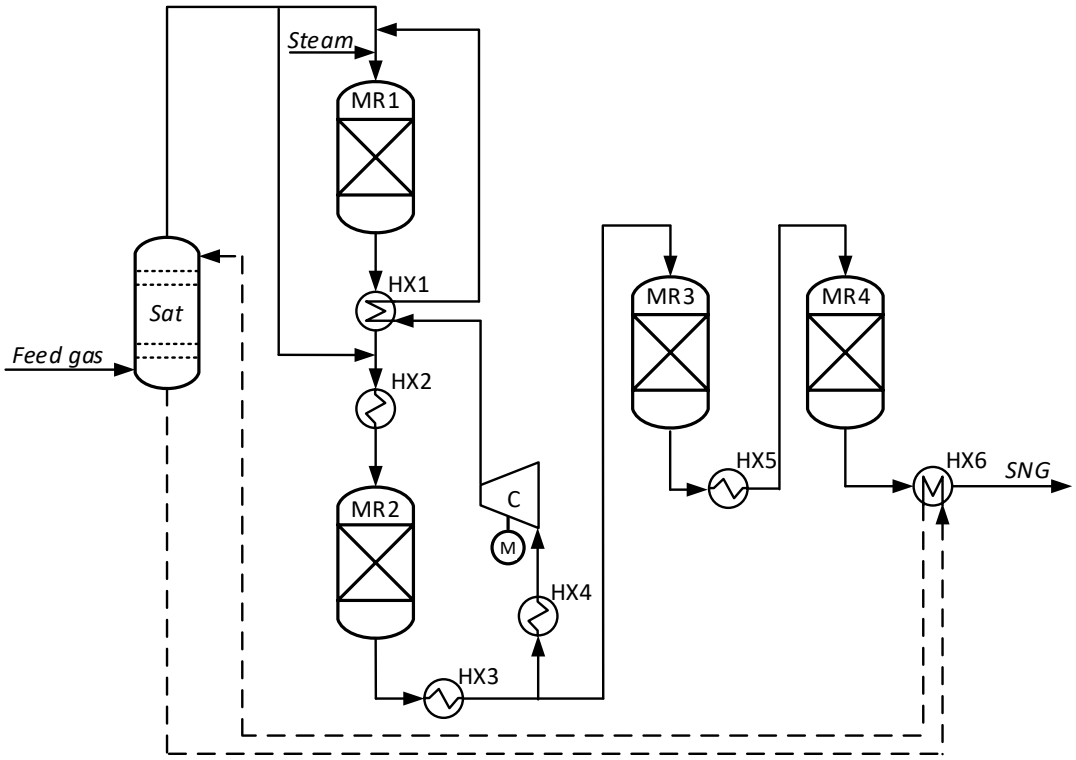

Figure 3.6 HICOM process [40]; where: MR – methanation reactor, HX – heat exchanger, Sat – saturator, C – compressor, M - motor

The RMP methanation process is based on a number of adiabatic fixed-bed reactors with a series of interstage cooling but without gas recycle (Fig. 3.7). The methanation reaction is typically carried out at temperatures between 200 °C and 400 °C, at pressures of 10-30 bar and with the use of nickel based catalyst [39–41]. Number of methanation stages is usually equal to 4-6 reactors.

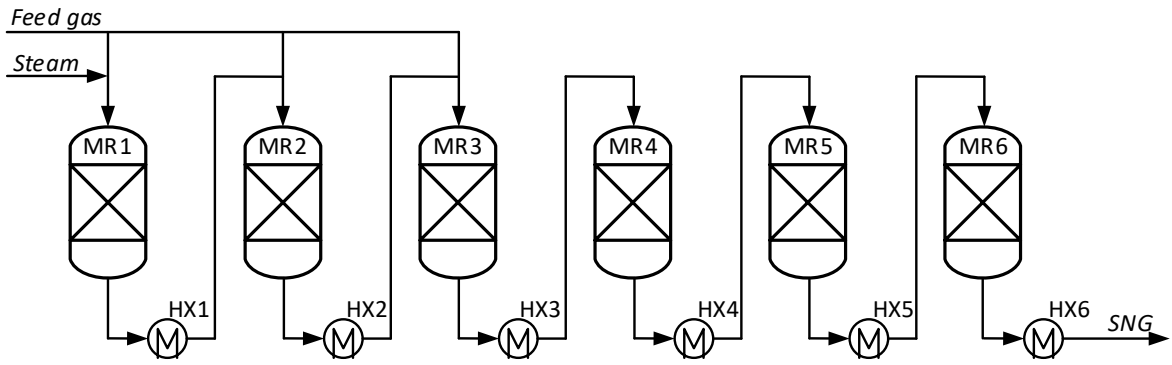

Figure 3.7 RMP process [40]; where: MR – methanation reactor, HX – heat exchanger

3.4. Syngas from biomass gasification as a carbon feedstock source for methanation

There are different ways to produce SNG in terms of used carbon feedstock. The most common method is using gases resulting from processing of solid fuels, such as coal and biomass [40]. Solid fuels can be converted to process gas through e.g. gasification or combustion. The resulting gas can then be used as a feedstock for methanation. Biomass is a more promising fuel used for this type of process than coal, because it is considered a renewable energy source. Using gas from biomass as a carbon feedstock for methanation process allows for a closed cycle of carbon, as combustion of SNG from biogenic sources causes CO_2 emissions equal to CO_2 absorbed during growth of biomass. In the case of using biomass for the production of carbon oxides for the methanation process, the methods of biomass conversion also differ depending on the considered biomass type. Figure 3.8 presents the possible methods of obtaining a carbon source for the production of SNG.

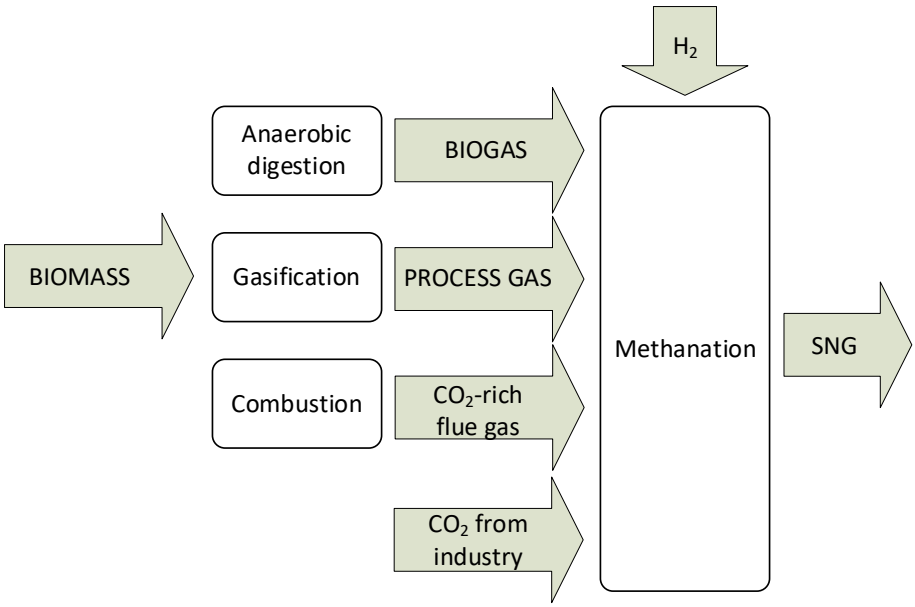

Figure 3.8 Selected methods of obtaining a carbon feedstock for the production of synthetic methane

One of the ways of producing carbon oxides is biomass gasification, a thermochemical process which results in obtaining the process gas. Depending on the gasification agent used (air, oxygen, steam), process gas has a different composition. Air biomass gasification is a relatively simple and cost-effective process, but the process gas contains a significant amount of nitrogen and other non-combustible gases, which reduce its heating value. Oxygen biomass gasification eliminates the nitrogen and other non-combustible gases found in air, producing a gas with a higher heating value. The absence of nitrogen also reduces the need for downstream gas cleaning, making the process more efficient. However, oxygen biomass gasification requires the use of pure oxygen, which can be expensive to produce. The process also requires higher temperature and pressure, which can increase the cost of the gasifier [43].

Carbon oxides can also be obtained in the anaerobic digestion of biomass [44]. Biogas is produced from organic matter, such as agricultural waste, municipal solid waste, and wastewater and it is composed mainly of carbon dioxide and methane. Then biogas can be further upgraded and subjected to the methanation process [45], or the carbon dioxide can be separated and used as a feedstock for the process.

Another option to obtain a carbon feedstock for methanation process is considering gases from industrial installations, such as carbon capture and storage

(CCS) or from post-combustion exhaust streams [46]. Carbon feedstock for methanation process based on CO_2 separation from flue gases can be obtained not necessarily only from biomass combustion, but also assuming the use of fossil fuels.

In this thesis, the carbon feedstock source considered for methanation process is process gas from biomass gasification process. The main types of gasifiers are: updraft and downdraft fixed-bed gasifiers, entrained-flow gasifiers, bubbling fluidized-bed gasifiers, circulating fluidized-bed gasifiers, dual-fluidized bed gasifiers and plasma gasifiers. A short description of each type is presented in the Table 3.5.

Table 3.5 Types of gasifiers [47]

Gasifier type	Description
Updraft fixed-bed gasifier	Feedstock is fed from the top of the gasifier. Air, oxygen or steam inlet is from the bottom part. Part of char burns and provides heat. Process gas leaves from the top of the gasifier, and ash is collected at the bottom.
Downdraft fixed-bed gasifier	Feedstock is fed from the top of the gasifier. Air, oxygen or steam inlet is also from the top. Part of the feedstock is burned and form a reaction zone which the gases have to pass through. Process gas leaves at the bottom of the gasifier and ash is collected at the base.
Entrained-flow gasifier	Fined feedstock is injected with pressurized gasifying agent (oxygen and/or steam). Fast combustion of part of the feedstock at high temperature provides large amount of heat and high quality process gas is produced. Ash melts on the walls and is discharged as a slag.
Bubbling fluidized-bed (BFB) gasifier	Gasifier's bed is filled up with fine inert material. Air, oxygen or steam streams are introduced upwards through the bed. Feedstock is fed from the side part of the gasifier. Process gas leaves the gasifier from the top part.

	Temperature below 900 °C is used for the process to avoid melting of ash.
Circulating fluidized-bed (CFB) gasifier	Gasifier's bed is filled up with fine inert material. Air, oxygen or steam streams are introduced upwards through the bed, causing the suspension of the material within the gasifier. Feedstock is fed from the side part, partially combusts to provide heat and partially synthesizes to produce process gas. Bed particles are separated from the process gas in a cyclone and are recirculated to the gasifier's bed. Temperature below 900 °C is used for the process to avoid melting of ash.
Dual fluidized-bed (DFB) gasifier	Consists of two fluidized-bed chambers, one for gasification, second for combustion. Feedstock is fed into a gasification chamber together with steam as a gasifying agent. Part of char is combusted in combustion chamber to provide heat for the gasification part. Nitrogen-free process gas is produced. Temperature below 900 °C is used for the process to avoid melting of ash.
Plasma gasifier	Feedstock is fed into the gasifier and comes into contact with the plasma. Temperature of the process is from 1500 to 5000 °C. Process gas is produced from organic matter and inorganic matter creates inert slag.

Chemical reactions that occur in the gasification reactor are strongly dependent on the gasification process parameters (temperature, pressure) but also on the type of the feedstock. In the initial phases of the process, gasification involves the thermal decomposition and the feedstock in order to produce volatile matter and char. This process is followed by char gasification. Partial combustion also occurs within the gasification, as the process typically uses one-fifth to one-third of the stoichiometric oxidant. The heat of partial oxidation of the feedstock provides the energy to drive the endothermic gasification process. The composition of the process gas after biomass gasification depends on many factors, such as the type of biomass, the temperature of the process, the ratio between the feed and the gasifying agent, the

duration of the process and type of gasifier [47]. Table 3.6 presents the composition of syngas from wood gasification using different types of oxidizers and gasifiers [48].

Table 3.6 Influence of the oxidizer in the final syngas composition [48]

Oxidizing agent	Composition (% vol, dry basis)				
	H_2	CO	CO_2	CH_4	N_2
Air (downdraft)	17	21	13	1	48
Air (updraft)	11	24	9	3	53
O_2 (downdraft)	32	48	15	2	3
Air (BFB)	9	14	20	7	50
Air (CFB)	14	19	15	3	47
Steam (BFB)	52	23	18	7	n.d.
Steam (CFB)	34	27	23	11	5

n.d. – not definied

3.5.Power to SNG installations performance and costs

The configuration of a power to SNG system can vary depending on the type of electrolyzer, carbon feedstock source, and methanation reactor adopted to the integrated system. Depending on the scale of the installation, the efficiency of the overall system and the price of SNG will also be diversified. Table 3.7 summarizes SNG production process performance presented in the studies found in the literature for different plant configurations using biomass as fuel. Looking at the values reported in the table, efficiency values of the SNG production process vary significantly for different cases. For the plant configurations based on biomass gasification, electrolysis and methanation the values of efficiency (explained in more detail in Chapters 5 and 6) varies from 44.4 to 69.0%, for the cases based on biogas methanation with renewable hydrogen the values are ranging from 52.2 to 84.3%, for the cases of the source of carbon feedstock for the methanation coming from CCS, the reported value is 72.6% and for the methanation of syngas from biomass gasification (without any additional source of hydrogen for the process) the efficiency values range from 53.1 to 71.1%. Within similar configurations of SNG production systems, efficiency values vary depending on the type of fuel used, the efficiency of the various technology components used, and the definition of efficiency itself.

Table 3.7 SNG production efficiencies and costs from different plant configurations of studies found in literature

Source	Plant configuration	Efficiency	Output (SNG)	Cost, €/MWh_{SNG}	Ref. year
[49]	gasification+electrolysis+methanation	n.s.	100 MW	65-133	2015
[50]	gasification+electrolysis+methanation	54.8-62.2%	62.5 MW	n.s.	2016
[51,52]	gasification+(PEM)electrolysis+methanation	69%	319 MW	42-126	2017
[53]	gasification+electrolysis+methanation	57.67-63.43%	50 MW	n.s.	2019
[54]	gasification+electrolysis+methanation	44.4%	20.8 MW	n.s.	2022
[24]	gasification+electrolysis+methanation (heat and O_2 utilisation)	n.s.	n.s.	72-102	2050
[51,55]	biogas+electrolysis+methanation	80.7-81.5%	13.2 MW	230-250	2019
[51,56]	biogas+(PEM)electrolysis+methanation	52.2%	n.s.	107-143	2020
[57]	biogas+electrolysis+methanation	84.3%	500 kW	420	2021
[58]	CCS+electrolysis+methanation	n.s.	n.s.	70-125	2018
[51,59]	CCS+electrolysis+methanation	72.6%	50.4 MW	115	2020
[60]	CCS+electrolysis+methanation	n.s.	4.1 MW	42.32-85.12	2030
[50,61]	gasification+methanation	70.3%	n.s.	n.s.	2010
[50,62]	gasification+methanation	53.1%	105 MW	n.s.	2011
[63]	gasification+methanation	68%	884 kW	n.s.	2012
[50,64]	gasification+methanation	64.8-71.1%	100 MW	n.s.	2016

n.s. – not specified

In the literature, the calculated value of the levelised cost of SNG production varies significantly depending on the specific proposed case of the plant and the assumptions made. Hannula [49] presented a cost range of SNG of about 65-133 €/MWh_{SNG} (calculated for the year 2015) depending on the configuration of the plant, and for the case considering a hybrid approach (chemical synthesis of process gas with hydrogen), the levelised production cost of SNG was equal to 81.7 €/MWh_{SNG}. In another study [51,52], where the SNG production plant based on biomass gasification, PEM electrolysis and methanation is presented, calculated SNG price ranged from 42 to 126 €/MWh_{SNG} (2017 was the reference year). Gotz [24] presented the range of levelised cost of SNG production values from 40 to 600 €/MWh_{SNG} varying for different years assumed for the analysis, different

configurations of the plant, especially on the side of carbon feedstock and different plant loads. For the case of the SNG production plant for the year 2050 assuming biomass gasification as the source of carbon oxides for the methanation and also heat and O_2 utilisation, Gotz [24] showed the values of SNG production costs on the level of 72-102 €/MWh_{SNG}. In another study, Guilera [58] presented the costs of SNG as 70-125 €/MWh_{SNG} (price depending on the specific country) calculated for the year 2018 and for the case assuming post-combustion CO_2 capture as the source of carbon feedstock for the methanation. Another examples of studies referring to CCS as a carbon oxides feedstock for the methanation presented SNG prices equal to 115 €/MWh_{SNG} for the year 2020 [51,59] and 42.32-85.12 €/MWh_{SNG} predicted for the year 2030 [60]. For different studies analyzing configuration of SNG production plant based on biogas methanation (with additional renewable hydrogen feed) [51,55–57] the calculated SNG prices ranged from 107 to 420 €/MWh_{SNG}.

3.6. Existing methanation plants and pilot projects

Depending on the feedstocks used for the methanation process, existing installations can be divided into those based on syngas methanation, biogas methanation or CO_2 methanation (each of which can additionally be performed in the presence of an additional hydrogen source or not). This subsection presents examplary existing methanation plants and projects.

Among power to SNG installations based on syngas methanation, projects like GAYA, GOBIGAS, BioSNG and DemoSNG can be distinguished (Tab. 3.8).

Table 3.8 Methanation projects based on biomass gasification [65]

Project name	Location	Capacity	Technology
BioSNG (EU project)	Gussing, Austria	1 MW_{SNG}	PSI
GAYA (Engie)	Saint Fons, France	400 kW_{SNG}	Not specified
GOBIGAS (Goteborg Energi)	Gothenburg, Sweden	20 MW_{SNG}	TREMP
DemoSNG (EU project)	Koping, Sweden	50 kW_{SNG}	KIT (honeycomb)

The first plant producing SNG from biomass gasification was BioSNG plant launched in 2008 in Gussing, Austria [39]. For the gasification fast internally

circulating fluidized bed (FICFB) process was chosen and syngas is produced from biomass feedstocks such as wood chips and agricultural residues. For methanation a fluidized-bed reactor was designed by PSI, with an output of SNG produced equal to 1 MW.

The GAYA project started in 2010 and the coordinator is GDF-SUEZ [66]. For the gasification process the same technology as in BioSNG project was developed. It is assumed that the final product of methanation (with the assumed output of 400kW_{SNG}) will be injected into natural gas grid.

The target of methane output in GOBIGAS project is for approximately 65% of the amount of waste wood biomass feed energy [66]. For the methanation unit development, TREMP technology is considered in the project. GOBIGAS project assumes SNG output of 20 MW.

Within the DemoSNG project a new reactor concept has been developed by DVGW-Forschungsstelle at the Engler-Bunte Institute (DVGW-EBI) and Karlsruhe Institute of Technology [67], where Gas Natural Fenosa is responsible for hydrogen production through PEM electrolysis, KIT for biomass gasification and KTH Royal Institute of Technology is in charge of syngas cleaning. This project assumes the use of a single reactor with a honeycomb catalyst and output of 50 kW_{SNG}.

An example of PtSNG plant based on methanation of CO_2 from CCS is ETOGAS-Audi e-gas (6 MWe) with SNG output equal to 325 Nm^3/h [67]. It is located in Wertle, Germany and has been working since 2013. The type of used methanation reactor is a fixed-bed isothermal reactor cooled with molten salt (MAN methanation technology). Hydrogen is produced by three alkaline electrolyzers powered by an offshore wind farm, and carbon feedstock for the reaction is carbon dioxide captured from biogas by amine absorption.

Another example of pilot scale methanation installation is $RENERG^2$ project developed by the Paul Schrerrer Institute in Switzerland. Bubbling fluidized bed methanation reactor (GanyMeth) is tested between 1 and 12 bar of operating pressure and producing up to 160 kW of SNG [67]. Primarily experimental tests were performed on bottled gasses with the intention of exchanging them for real ones.

An example of biogas upgrading methanation installation is El-opgraderet biogas project with a pilot plant at Foulum, Denmark. The project was launched in

2013. As a hydrogen source, the 40 kW_e SOEC electrolyser was assumed and methanation technology was developed by Haldor Topsoe

Another example of biogas upgrading methanation is a Spanish pilot plant RENOVAGAS. The plant capacity is up to 2 Nm^3/h of SNG production. The pilot installation comprises a 15 kW alkaline electrolyser and a modular multichannel reactor with oil-based cooling.

Other PtSNG project is HELMETH [67] led by the Karlsruhe Institute of Technology (KIT) and Sunfire. The project assumes the integration of high-temperature electrolysis with CO_2 methanation. Hydrogen is produced by a 10 kW SOEC and the methanation process is performed in two reactors placed in series at 300 °C and 30 bar, with intersection water removal and producing up to 5.4 m^3/h (20 - 60 kW) of SNG.

A pilot scale experimental facility for the research on the CO_2 methanation process has been developed at ENEA Casaccia Research Center [41]. The reactor is a multi-tubular fixed-bed type, that can work in cooled or under adiabatic conditions. A diathermic oil is used as a cooling medium. The installation can work at 1-5 bar and the nominal methane flow in SNG is in the range of 0.25 to 1 Nm^3/h. For the experimental test including the Ru-based catalyst bed, high methane content (up to 67%) has been achieved for temperatures in the range of 300–330 °C and pressure of 5 bar [67].

The methanation plants described above are mostly medium to small scale. Problems related to the operability of CO_2 methanation plants are mainly related to process temperature control and the possibility of the appearance of so-called hot spots in the catalyst bed contributing to catalyst degradation and deterioration of process efficiency. In addition, when it comes to syngas methanation, there is the challenge of composition of the syngas produced from different feedstocks, which can vary widely, and impacts the efficiency and selectivity of the methanation process. The presence of impurities, such as sulfur and nitrogen compounds, can also impact the performance of catalysts used in the process. Moreover, the concentration of methane achieved in the aforementioned projects is often not very high (and often the composition of the gas is not documented), and further SNG purification steps (separation of unreacted CO_2 and/or H_2) are required. Before scaling up to larger

installations, bench-scale and pilot plants can help identify any operational issues and refine the process. The work on the methanation installation carried out within the framework of this dissertation is part of research aimed at determining the optimal operating conditions of the methanation reactor to maximize the share of methane in SNG.

4. Methane generator lab stand at Silesian University of Technology

4.1. Description of the lab installation

The lab-scale methanation installation used for the experimental research was funded by the Polish National Science Centre and developed within the framework of the OPUS project entitled: *Utilization of electrolysis and oxygen gasification processes for the production of synthetic natural gas in a polygeneration system* (no. 2017/27/B/ST8/02270). The installation (Fig. 4.1) has been built at the Silesian University of Technology in the Department of Power Engineering and Turbomachinery. The manufacturer of the methanation installation was the Czylok company, however, the originator of the reactor design was a research team from the Silesian University of Technology.The main idea while designing this installation was to develop the reactor which will aim to be effective, simple and inexpensive (in capital and operation cost) at the same time. The goal of experimental study was to assess the influence of the main process parameters on the effectiveness of methane production. Preliminary study on the methane generator was presented in [20] and this chaper has been enhanced with an additional measurement campaign.

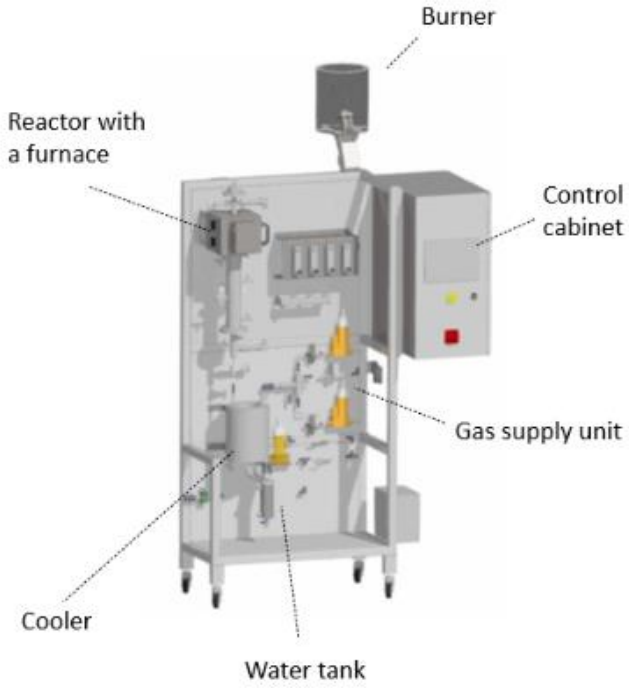

Figure 4.1 General representation of the methanation installation build at the Silesian University of Technology

The technical drawing of the reactor prepared by the Czylok company is presented in Figure 4.2. Nickel powder was used as a reaction catalyst in the first reactor type. The catalyst bed diameter is about 32.3 mm, while its length reaches 500 mm, which gives a total volume of the catalyst bed equal to 0.41 dm^3.

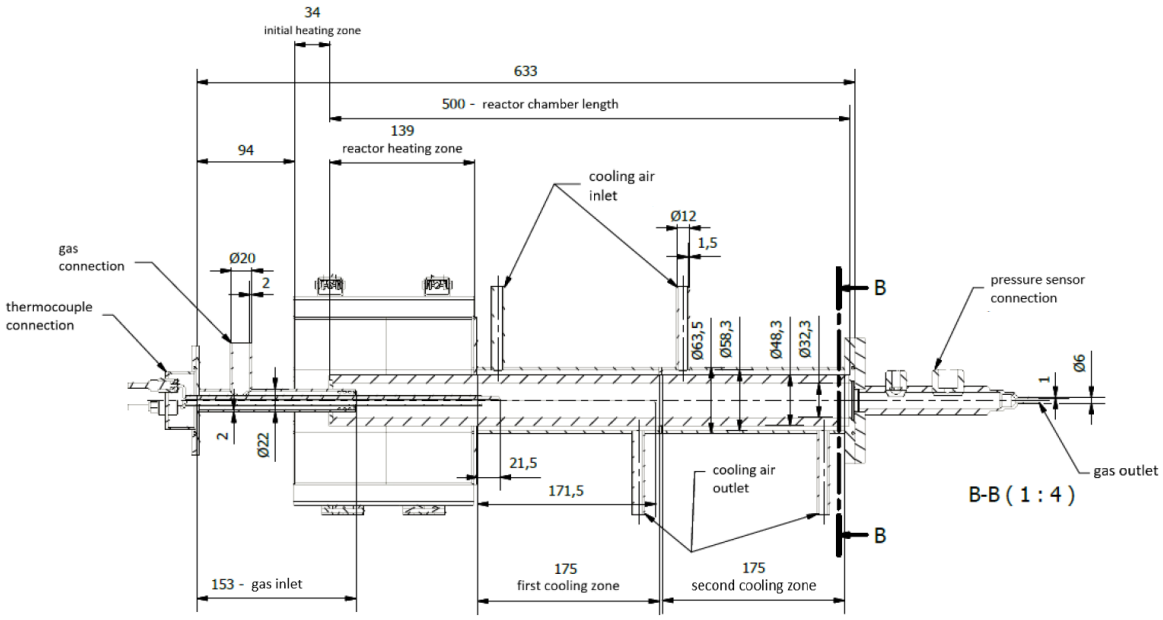

Figure 4.2 Technical drawing of a methanation reactor

The methane generation laboratory installation is equipped with three solenoid valves for each process gas separately - carbon dioxide, hydrogen and nitrogen. The flow of two of these gases - carbon dioxide and hydrogen is controlled automatically by mass flow regulators (with the possibility of setting the accuracy of the flow equal to 0.1 dm^3min^{-1}), while the flow of the third gas, nitrogen, is manually controlled by a rotameter valve - this gas is used to flush the installation. At the reactor inlet, there is a PC-28 pressure transducer to measure the pressure and a thermocouple to measure the temperature of the gas. There are three PPT-K-I-KSek-K4 thermocouples installed in the reactor to measure the temperature at the beginning (160 mm from the inlet), in the middle (310 mm from the inlet) and at the end (460 mm from the inlet) of the catalyst bed. The maximum calculated measurement uncertainty (eq. 4.1) for the pressure value was 1154.70 Pa, while for the measured temperature was 4.62 °C (Table 4.1). The upper part of the reactor is heated by a furnace with one control thermocouple.

$$u(x) = \frac{\Delta x}{\sqrt{3}} = \frac{a \cdot b}{\sqrt{3}} \tag{4.1}$$

where:

a – class of the measuring device;

b – range of the measuring device.

Table 4.1 The results of the calculations of the type B uncertainties for thermocouples and pressure sensors

	Pressure sensor	Thermocouple
Type	PC-28	PPT-K
Range	Up to 1 MPa	from -40 to 800 °C
Class	0.2	1
Uncertainty	1154.70 Pa	4.62 °C

Experimental studies were carried out in two stages, for the first and second type of methanation reactor (after modernization) .The first reactor was designed with air-cooled sections around the reactor's bed. At the reactor outlet, there is another thermocouple, a second pressure transducer and a manual needle valve to set the pressure in the system. Behind the reactor's outlet a cooler, connected to the water separator, is built. The cooler has one cooling zone, thermocouples are installed at its inlet and outlet, and the air flow in the cooling zone is controlled manually using a rotameter. Behind the cooler and the water separator, there is the last thermocouple, the mass flow meter for the produced methane and the outlet for taking a gas sample for analysis. The entire system is connected to the burner where the resulting gas is burnt. The entire apparatus (except for manual rotameters) of the methane generator is connected to a control cabinet with a control panel (Fig. 4.3), displaying process parameters.

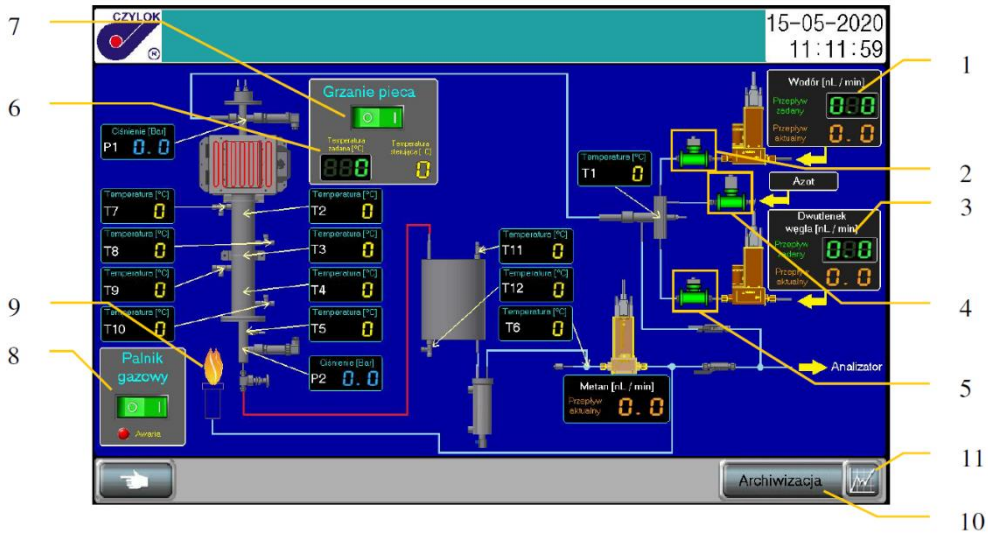

Figure 4.3 Control panel of the methane generator installation (1,2 – hydrogen inlet; 3,5 – carbon dioxide inlet; 4 – nitrogen inlet; 6,7 – furnace temperature setting; 8,9 – starting the burner; 10,11 – measurement logging)

The produced gases are partially burnt and partially introduced to VARIOluxx gas analyzer of MRU air Emission Monitoring Systems [68]. The data about accuracy of the gas composition measurement with the analyzer was taken from the manufacturer's manual and are presented in Table 4.2.

Table 4.2 Accuracy of gas analyzer

Gas	Range	Resolution	Absolute accuracy
CO	0-10%/ 100%	0.01 Vol%	±0.5% Vol
CO_2	0-10%/ 100%	0.01 Vol%	±0.5% Vol
CH_4	0-10%/ 100%	0.01 Vol%	±0.5% Vol
H_2	0-10%/ 100%	0.1Vol%	3%
O_2	0-25 Vol%	0.01 Vol%	±0.5% Vol

It allows for the measurements of carbon dioxide, carbon monoxide, methane and oxygen with an absolute accuracy of +/- 0.5 Vol%, and for the measurements of hydrogen with an absolute accuracy equal 3% [68]. For hydrogen content measurement the thermal conductivity detector is used and for carbon dioxide, carbon monoxide, methane and oxygen content measurements the infrared sensors.

The reactor that was primarily constructed was working on nickel powder catalyst (diameter of particles in the range of micrometres). That powder was characterized by extensive inertia and led to significant pressure drops between the

reactor's inlet and outlet. It also contributed to a high temperature gradient within the reactor length, and significant temperature differences appeared between three thermocouples located in the beginning, the middle and the end of the catalyst bed. Results of the experimental tests on first type of the methanation reactor are presented in the section 4.3.1. of the thesis.

Thus, to accelerate the process and improve the temperature distribution in the reactor, it was decided to develop a new design of the reactor without air-cooled sections. In the second phase of methane generator development, a system of additional reactor heating was added. A second furnace was built along the length of the reactor. It was also decided to change the catalyst. The second reactor was filled up with 3.2 mm pellets of 0.5 wt. % Ru/(Al_2O_3). Results of the experimental tests on second type of the methanation reactor are presented in the section 4.3.2. of the thesis. Figure 4.4 presents the modernized installation of the methane generator after the second phase of development.

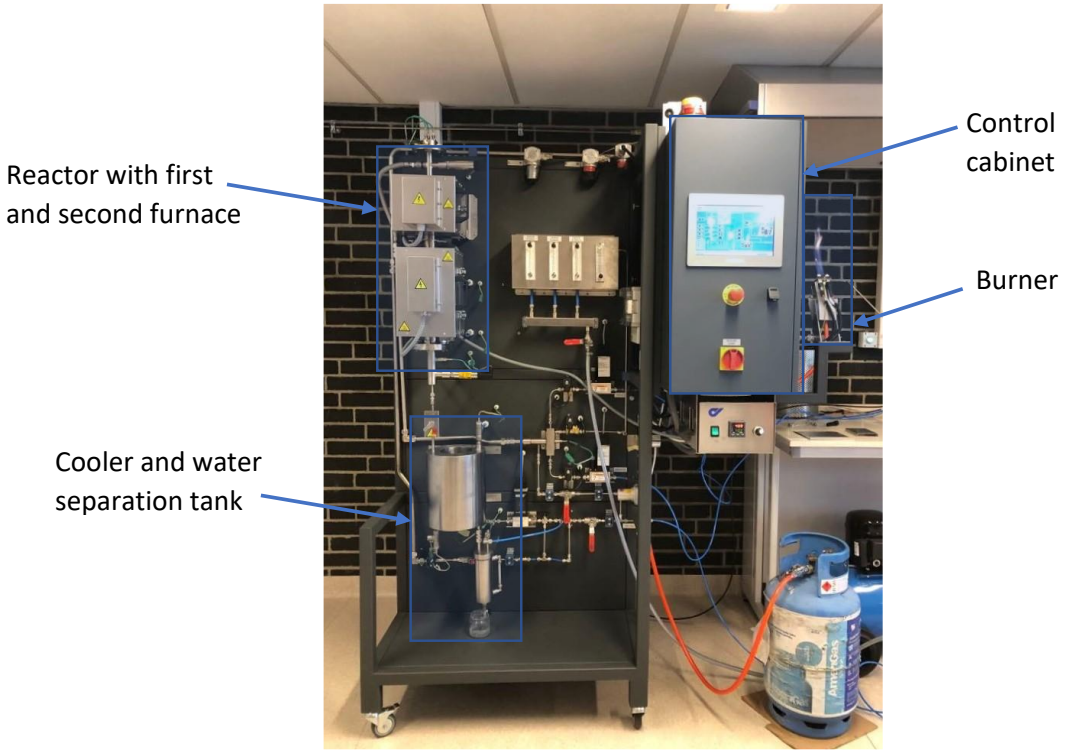

Figure 4.4 Methane generator installation (after modernization)

4.2.Key performance indicators of the methanation process

Based on the knowledge of the reactor's volume and the manually set volumetric flow of carbon dioxide and hydrogen mixture, such performance indicator

as gas hourly space velocity (GHSV) can be calculated as presented by formula (4.2). Also, knowing the mass of the catalytic bed, the weighted hourly space velocity (WHSV) can be calculated from (4.3). These quantities enable comparison of the results for various measurement series, catalysts and reactors.

$$GHSV = \frac{\dot{v}_{\text{in}}}{V_{\text{R}}} \tag{4.2}$$

where:

$\dot{v}_{\text{in}}$ is a volumetric stream of inlet gases to the reactor, $\text{Ndm}^3\text{h}^{-1}$,

V_{R} is a catalytic bed volume of the reactor, dm^3.

$$WHSV = \frac{\dot{m}_{\text{CO}_2\text{in}}}{m_{\text{cat}}} \tag{4.3}$$

where:

$\dot{m}_{\text{CO}_2\text{in}}$ is the inlet carbon dioxide mass flow, gh^{-1},

m_{cat} is the catalyst bed mass, g.

The gas outlet stream was calculated by knowing the inlet streams, the chemical reaction and the outlet gas composition read on the analyzer. Based on the obtained results, it is possible to estimate the conversion of carbon dioxide to methane, x_{CO2}. This coefficient describes how much carbon dioxide was converted during the reaction and it can be calculated from equation (4.4):

$$x_{\text{CO}_2} = \frac{\dot{n}_{CO_{2\text{in}}} - \dot{n}_{CO_{2\text{out}}}}{\dot{n}_{CO_{2\text{in}}}} \tag{4.4}$$

where:

$\dot{n}_{CO_{2\text{in}}}$ is the mole flow of CO_2 in the inlet gas, molh^{-1},

$\dot{n}_{CO_{2\text{out}}}$ is the mole flow of CO_2 in the outlet gas, molh^{-1}.

4.3.Results of experimental tests

A measurement campaign was conducted to identify the most effective parameters for methanation reactor operation. Each series of measurements included:

a catalytic bed heating phase, a catalytic bed activation with a hydrogen phase and a reaction phase. In the reaction phase, the reactor was fed with a stream of H_2 and CO_2 mixed in the stoichiometric ratio of 4:1. The goal of the performed tests was to check the influence of a given range of inlet flows of the reactants on the methanation reaction parameters (temperature of the catalyst bed, SNG composition) in different reaction operating pressure for two designs of methanation reactor.

During the tests, the temperature in three zones of the catalyst bed of the reactor was measured continuously with a time step of 30 s (T_1 - 160 mm from the inlet, T_2 - 310 mm from the and T_3 - 460 mm from the inlet). The temperatures mentioned correspond successively to the following thermocouples, marked in Figure 4.3 as T_2, T_3 and T_4. The system also measured the gauge pressure at the inlet and outlet of the reactor with a time step of 30 s. The main focus of the conducted measurements was on the produced gas composition as the aim was to produce SNG with the highest possible methane content.

4.3.1. First phase of methanation reactor development

First campaign of the experimental test was performed with the use of initial design of the methanation reactor filled with the powder of nickel catalyst. The heating process lasted about 9 hours and temperatures of the catalyst bed achieved at the end of this process were: T_1 = 216 °C, T_2 = 120 °C, T_3 = 64 °C. The activation of the catalyst bed with a hydrogen stream took about 1 hour and temperatures achieved at the end of this process were: T_1 = 255 °C, T_2 = 130 °C, and T_3 = 62 °C. After heating and activation, carbon dioxide was introduced to the reactor and the methanation process started. During the methanation reaction temperature within the catalyst bed increased insignificantly and the large differences between the temperature measured by the thermocouples at the 3 points of the reactor remained as presented in the Figure 4.5 (T_1 marked with a dashed black line, T_2 marked with a dashed red line, and T_3 marked with a dashed blue line). The uneven temperature distribution within the catalyst bed was due to high thermal resistance of nickel powder used in the primarilly developed reactor. Too thin catalyst granulometry led also to a significant pressure drop between the inlet and outlet of the methanation reactor. As a result, during tests on the first reactor filled with nickel powder, an inlet gauge pressure (represented in Fig. 4.5 with continuous blue line) of about 5 bar was

maintained and the outlet gauge pressure was equal to 0 bar. The difficult controllability was also manifested by problems in setting the desired values of the hydrogen and carbon dioxide volumetric flows. The determined values were 1 dm^3min^{-1} of carbon dioxide and 4 dm^3min^{-1} of hydrogen, however, the actual values were variable and depended on the resistance caused by the catalyst bed. For this reason, it was impossible to determine the GHSV and WHSV values for the performed tests.

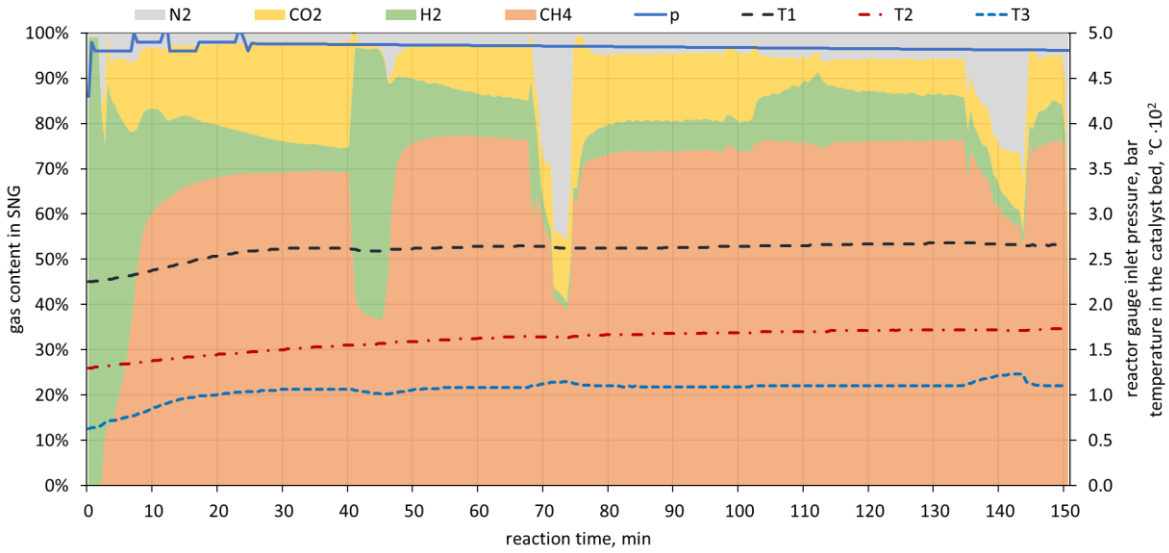

Figure 4.5 Results of methanation reaction operation conditions and SNG composition performed on the first reactor type (Appendix A)

The differences in temperature distribution between the three thermocouples located at different heights of the catalyst bed were significant but fairly constant during the whole reaction time. At the final phase of the reaction they were the highest and reached T_1 = 268 °C, T_2 = 173 °C, and T_3 = 123 °C. Despite the differences in temperature distribution the methane content in the produced SNG (dry basis) was rather high and achieved up to 76.3% (orange shaded area) followed by 11.7% of carbon dioxide (yellow shaded area) and 9% of hydrogen (green shaded area). Also, for the considered case, the CO_2 conversion was determined and it was over 80% for the whole reaction time.

The methane content ‘valleys’ visible in Fig. 4.5 were caused by the attempts of changing the set volumetric flows of reactant gases. As this measurement series were performed on nickel powder, too thin granulometry of the catalyst particles caused that changing the flow rate of one component affected the flow rate of the

other component uncontrollably, and it was difficult to align these flows in time. For example, around the 40th minute of the reaction, the H_2 stream was increased and the effect could be observed after approximately 15-20 minutes (when it was possible to set the streams). A similar trend can be noticed around the 70th minute of the reaction when the CO_2 stream was increased. It can be noted that the nitrogen content detected on the gas analyzer increased during this time, but this was due to the same reason, since the nitrogen content of the analyzed gas is calculated as the difference of the content of all other compounds from 100%.

4.3.2. Second phase of methanation reactor development

For the experimental test on ruthenium catalyst, measurements were performed, corresponding to hydrogen inlet flows from 3.6 Ndm^3min^{-1} to 8.0 Ndm^3min^{-1}, and according to stoichiometric conditions, carbon dioxide inlet flows from 0.9 Ndm^3min^{-1} to 2.0 Ndm^3min^{-1}. These values correspond to the values of GHSV from 663 h^{-1} to 1474 h^{-1}. Greater space velocity implies a shorter contact time between gas and catalyst. For the performed experimental tests it was 5.4 s for the lowest GHSV value equal to 663 h^{-1}, and 2.4 s for the highest GHSV value of 1474 h^{-1}. The mass of the catalyst used in the reactor was 385.9 g, so the WHSV values were in the range of 0.277 – 0.616 $g_{CO2}\, g_{cat}^{-1}\, h^{-1}$. All performance indicator values are summarized in Table 4.3.

Table 4.3 Inlet streams of reagents used in the tested measurement series with calculated performance indicators

no:	m_{H2in}	m_{CO2in}	GHSV	WHSV	t
	Ndm^3min^{-1}	Ndm^3min^{-1}	h^{-1}	$g_{CO2}\, g_{cat}^{-1}\, h^{-1}$	s
1	3.6	0.9	663	0.277	5.4
2	4.0	1.0	737	0.307	4.9
3	4.4	1.1	811	0.338	4.4
4	4.8	1.2	885	0.369	4.1
5	5.2	1.3	958	0.400	3.8
6	5.6	1.4	1032	0.430	3.5
7	6.0	1.5	1106	0.461	3.3
8	6.4	1.6	1179	0.492	3.1
9	8.0	2.0	1474	0.615	2.4

For each test performed, the reactor was heated up (temperature of both furnaces was set to 400 °C) for about 30 minutes with additional nitrogen flow to improve heat transport in the catalyst bed and purge the installation with inert gas. Temperatures of the catalyst bed achieved at the end of heating process were: T_1 = 125 °C, T_2 = 263 °C, T_3 = 155 °C (for the case of GHSV = 737 h^{-1}). After that, the catalyst bed was activated with a hydrogen stream for another 15 minutes, and temperatures of the catalyst bed were respectively T_1 = 199 °C, T_2 = 309 °C, T_3 = 177 °C (considering the case of GHSV = 737 h^{-1}). After activation, carbon dioxide was introduced to the reactor and the methanation process started. From this moment, furnaces were turned off and the methanation reactor operation was considered self-sufficient according to reaction heat transferred to the catalyst bed.

Measurements were made to investigate the reactor's operational capabilities and the effects of different reactant flow inlet streams, temperature and process pressure on the composition of the SNG produced. Last two measurement performed (GHSV = 1179 h^{-1} and GHSV = 1474 h^{-1}) for chosen catalyst were consider not optimal for the size of methanation unit. Volumetric streams set for the reactor were too high, which resulted in shorter residence time of the reactant gases in the catalyst bed and following lower methane content in generated SNG. Also, reaction heat was higher in reference to other tests on lower volumetric streams of reactant gases, which

resulted in rapid increase of the temperature in the first zone of the reactor, that was difficult to control. Results from those two tests were thus rejected from this study.

Seven charts are presented in Figure 4.6 showing the results of dry SNG composition and catalyst bed temperature measurements over time while increasing the reaction pressure for different cases of GHSV tested at the methanation plant: a) 663 h^{-1}, b) 737 h^{-1}, c) 811 h^{-1}, d) 885 h^{-1}, e) 958 h^{-1}, f) 1032 h^{-1} and g) 1106 h^{-1}. The shaded layers of the graph represent the shares of methane (orange), hydrogen (green) and carbon dioxide (yellow) in the SNG produced. Dashed plots rempresent the three temperatures measured inside the reactor (T_1 marked with a dashed black line, T_2 marked with a dashed red line, and T_3 marked with a dashed blue line). During the reactor work, in order to assess the influence of the pressure on the operation of the reactor, the pressure was gradually increased by manually closing the needle valve downstream of the reactor (blue continuous plot represents the gauge pressure behind the reactor).

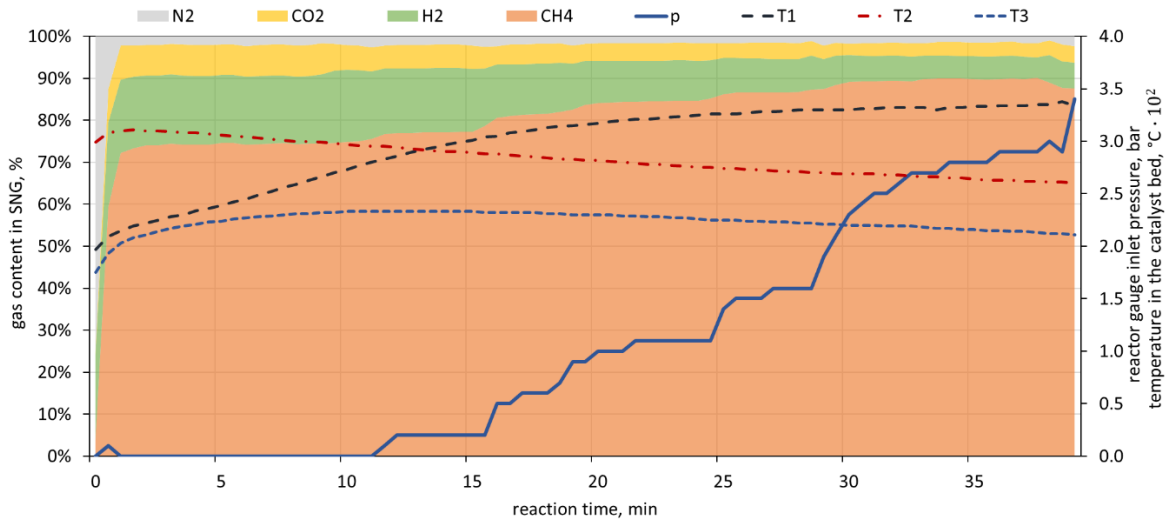
N2
CO2
H2
CH4
p
T1
T2
T3
gas content in SNG, %
reactor gauge inlet pressure, bar
temperature in the catalyst bed, °C · 10²
reaction time, min

a)

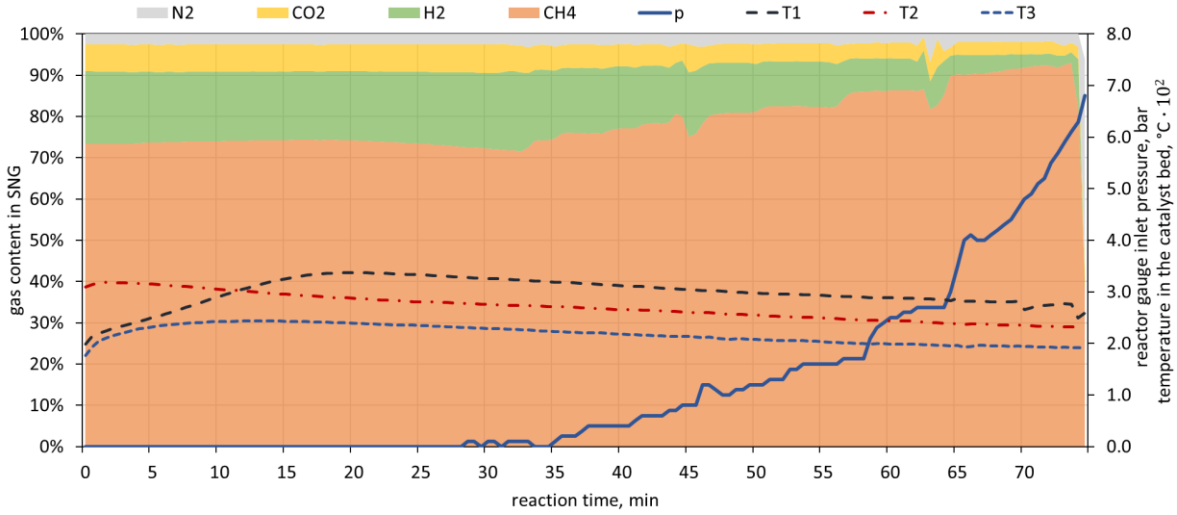
N2
CO2
H2
CH4
p
T1
T2
T3
gas content in SNG
reactor gauge inlet pressure, bar
temperature in the catalyst bed, °C · 10²
reaction time, min

b)

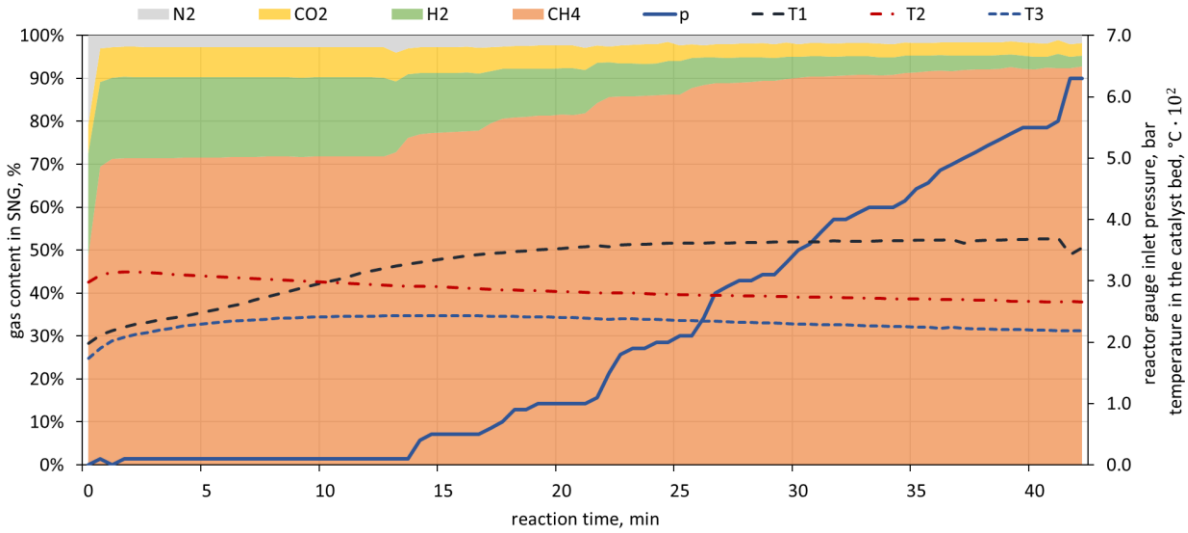
N2
CO2
H2
CH4
p
T1
T2
T3
gas content in SNG, %
reactor gauge inlet pressure, bar
temperature in the catalyst bed, °C · 10²
reaction time, min

c)

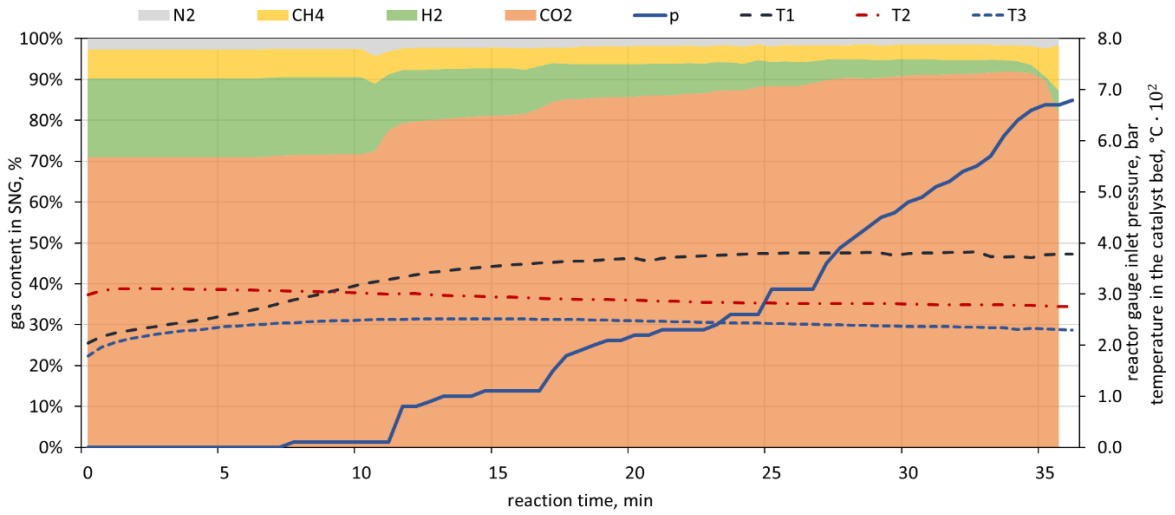
N2
CH4
H2
CO2
p
T1
T2
T3
gas content in SNG, %
reactor gauge inlet pressure, bar
temperature in the catalyst bed, °C · 10²
reaction time, min

d)

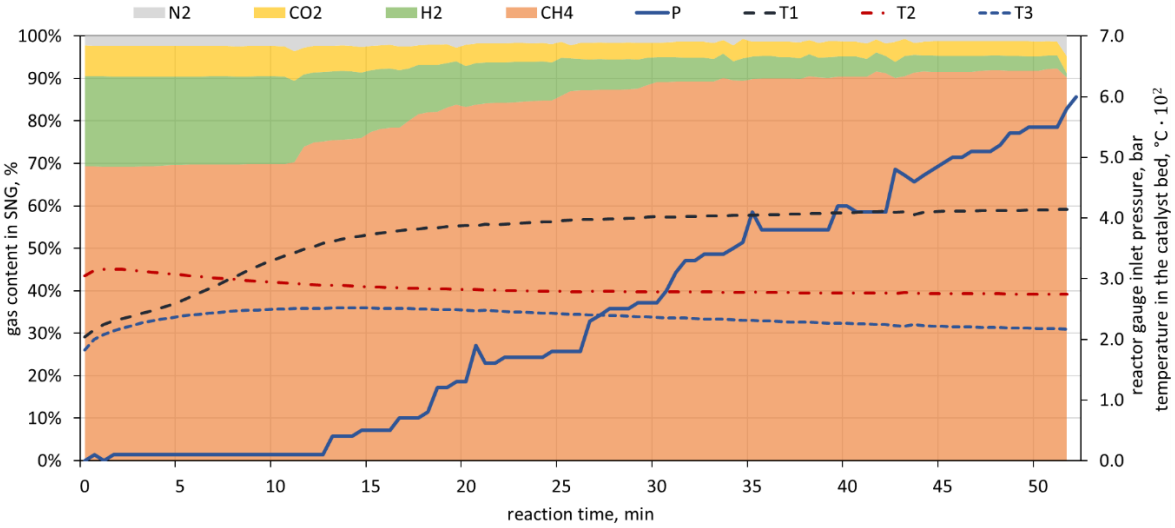
N2
CO2
H2
CH4
P
T1
T2
T3
gas content in SNG, %
reactor gauge inlet pressure, bar
temperature in the catalyst bed, °C · 10²
reaction time, min

e)

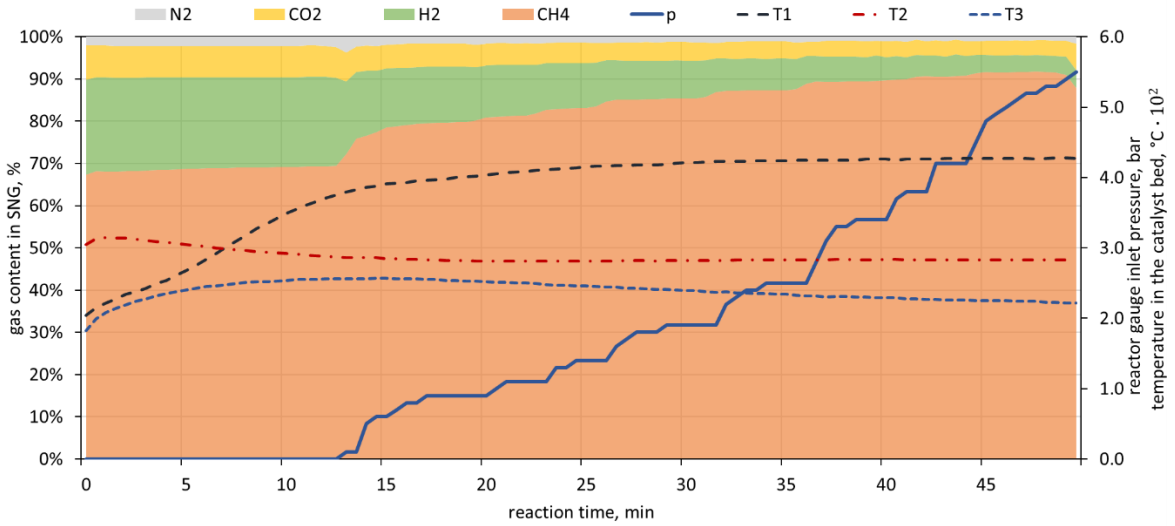
N2
CO2
H2
CH4
p
T1
T2
T3
gas content in SNG, %
reactor gauge inlet pressure, bar
temperature in the catalyst bed, °C · 10²
reaction time, min

f)

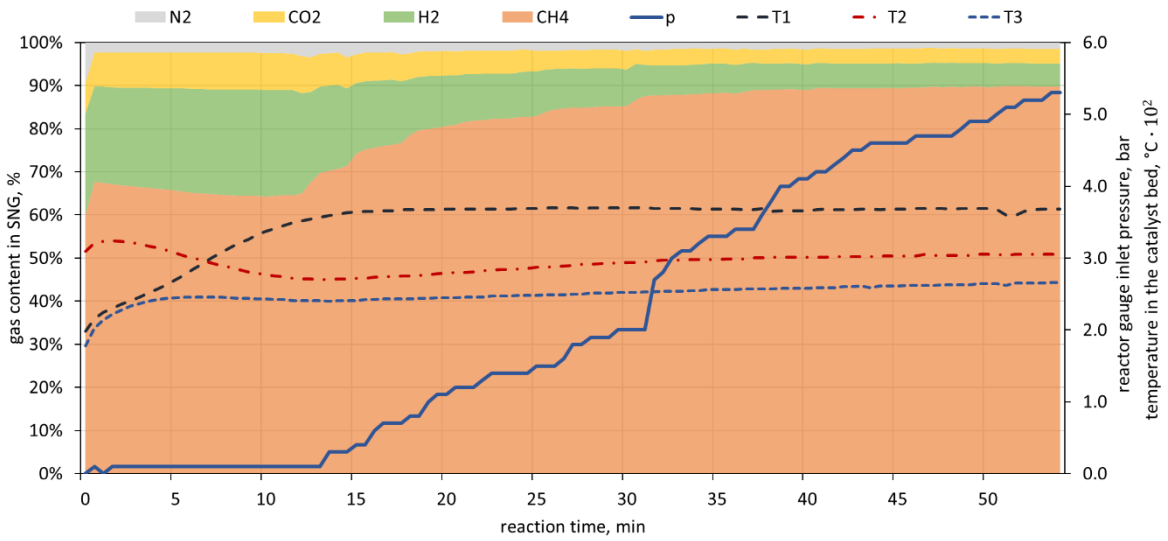

g)

Figure 4.6 Results of SNG composition and catalytic bed temperature while increasing the operation pressure (p) for GHSV equal to a) 663 h^{-1}, b) 737 h^{-1}, c) 811 h^{-1}, d) 885 h^{-1}, e) 958 h^{-1}, f) 1032 h^{-1} and g) 1106 h^{-1} (Appendix B)

During experimental tests, it was found, that a very problematic issue is the control of the catalyst bed temperature. The temperature results from the energy balance and is determined by the combined effect of generated heat flow due to the exothermal reaction, heat flow fed to the reactor (by external heaters) and heat loss to ambient. The most even temperature distribution (the smallest temperature difference between T_1 and T_2 and T_2 and T_3) occurring stably throughout the reaction phase was achieved for the test at GHSV = 737 h^{-1}, where the highest point temperatures were equal to T_1 = 337 °C, T_2 = 288 °C, T_3 = 240 °C. Then, those temperatures began to gradually but steadily decrease over time, which could indicate that the heat of reaction was not sufficient to support the uniform temperature of the bed, and at the final stage of the reaction were respectively: T_1 = 271 °C, T_2 = 231°C, T_3 = 192 °C. For the measurement series with GHSV higher than 737 h^{-1}, the differences in catalyst bed measured temperatures were more significant, but they remained stable during the reaction, so it can be considered that these cases were more self-sufficient in terms of heat balance. Different temperature distributions were obtained at the three measurement points along the length of the reactor, depending on the different reactants flow set. However, no significant effect of those discrepancies between the temperature values on the methane content of SNG was observed in tested series.

As the pressure in the reactor is set manually by closing the valve downstream of the reactor, the time of each measurement series shown in Fig 4.6 is different. Methanation reaction is favoured by higher pressure, because increasing the reaction pressure causes a decrease in volume and, at the same time, an increase in concentration, i.e. an increase in the number of moles of gas in a given volume. Increasing the concentration allows the gas particles to meet more often, which increases the rate of the chemical reaction. Increasing the reaction pressure leads to a shift in the chemical equilibrium of the methanation reaction towards the products. The effect of pressure on the process, in the range from atmospheric pressure to about 6.0 bar of gauge pressure in the reactor, was studied, although due to the installation limitations, higher pressure was not always possible to achieve. For the operation of methanation reaction under atmospheric conditions, the highest content of CH_4 in the produced SNG was equal to 75.5% for GHSV value of 663 h^{-1}. With increasing pressure in the reactor, the share of methane in the produced gas increases. It was possible to achieve methane content in SNG up to 93.3% (GHSV = 737 h^{-1}) at 6.0 bar of reactor gauge pressure. Results of methane content in SNG in every test performed are presented in the Fig. 4.7. Error bars presented in the Figure 4.7 indicate the uncertainty of the CH_4 measurement and were calculated based on the absolute accuracy of methane registered by the gas analyzer (data presented in Table 4.2).

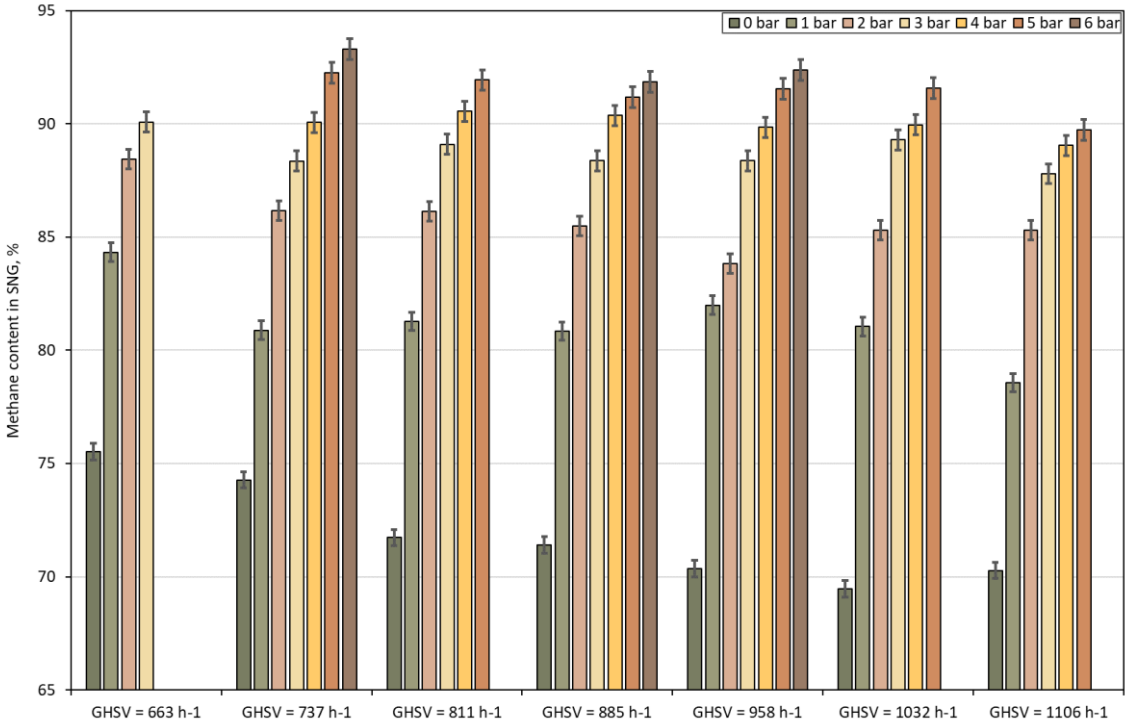

Figure 4.7 Methane content in produced SNG

Table 4.4 presents the calculated carbon dioxide conversion rates for performed tests. The values of the x_{CO_2} coefficient for the methanation reactor operation in atmospheric conditions are from 84.37% to 88.47%. Carbon dioxide conversion to methane is kinetically boosted by raising the pressure. For the case of gauge pressure in the methanation reactor of 6 bar, CO_2 conversion parameter is equal to 94.36 – 95.83%. For the operation under atmospheric conditions, the higher the GHSV value (so the higher the inlet flows of the reactants), the lower CH_4 content in SNG. Higher inlet flow translates into a shorter residence time, which could lead to uneven distribution of the reaction in the catalyst bed between performed tests. This could contribute to the appearance of a temperature gradient within the catalyst bed, leading to a higher temperature increase in the upper part of the reactor and lower temperatures downstream of the reactor. The hypothesis was stated, that in the case of a longer residence time, the reaction could occur mainly in the upper part of the catalytic bed and in the case of a slightly shorter residence time, the reaction could spread downstream the catalyst bed (because the reactants flowed through the reactor faster). And because there is a lower temperature downstream of the catalyst bed it favours the methanation reaction, so the rest of H_2 and CO_2 may react to CH_4. Probably in the case of longer residence time and lower volumetric flow, there is

more time for the rest of H_2 and CO_2 to synthesize downstream of the catalyst bed, which results in a better general conversion and higher methane content in produced SNG. This can also apply for the higher operating pressure of the reaction, although the higher the pressure, the more unified the results between the different GHSV parameter values of the series.

Table 4.4 Carbon dioxide conversion rate (x_{CO_2}) calculated for different values of gauge pressure in methanation reactor

p, bar	x_{CO_2}						
	GHSV						
	663 h^{-1}	737 h^{-1}	811 h^{-1}	885 h^{-1}	958 h^{-1}	1032 h^{-1}	1106 h^{-1}
0	88.47	86.98	85.46	86.92	85.42	84.72	84.37
1	92.07	91.14	89.83	91.06	90.99	90.02	88.33
2	94.53	93.02	91.64	92.71	91.33	91.81	92.06
3	94.18	94.00	94.12	93.75	93.68	93.43	93.09
4	-	94.23	94.45	94.21	93.58	93.53	93.83
5	-	94.68	94.68	94.05	93.77	93.80	93.93
6	-	95.83	-	94.16	94.36	-	-

Calculated chemical energy of produced SNG achieved for performed tests is presented in the Fig. 4.8. We were able to achieve values from 0.81 kW_{SNG} (GHSV = 663 h^{-1}, p_g = 0 bar) to 1.44 kW_{SNG} (GHSV = 1106 h^{-1}, p_g = 5 bar)

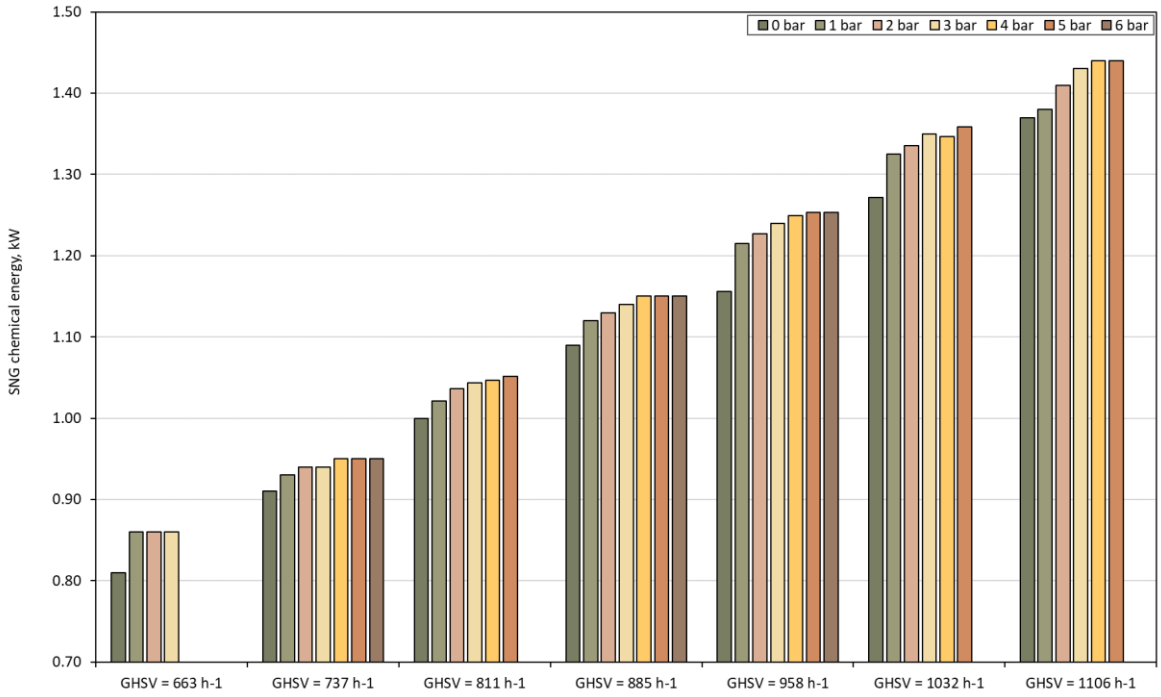

Figure 4.8 Results of SNG chemical energy

4.4.Discussion

For both considered methanation reactors construction, not only the structure of the reactor was different (i.e., the additional furnace and no cooling in the second reactor) but also operation conditions (temperature and pressure of the process) differed significantly. The catalyst, crucial for the reaction, was also different in these two cases. However, some conclusions and guidelines for further studies can be drawn from the conducted tests. The main differences between the two reactors are presented in Table 4.5.

Table 4.5 The main differences in operating conditions of the methane generator for nickel powder catalyst bed and Ru/(Al_2O_3) catalyst bed

	Ni (first reactor)	Ru/(Al_2O_3) (second reactor)
heating time	9 h	1 h
gauge pressure in reactor's bed	about 5 bar (caused by catalyst)	0 – 6 bar (set manually)
H_2:CO_2 ratio	not possible to set desired volume streams of gases	4:1
CH_4 content in SNG	up to 82.7% (p_g = 5 bar)	up to 75.5% (p_g = 0 bar) up to 92.3% (p_g = 5 bar) up to 93.3% (pg = 6 bar)
CO_2 conversion	>80%	>90%

The most difficult to obtain for the first reactor's design were uniform operating temperatures within the catalyst's bed. Differences in temperatures were significant and equalled approximately 100 °C between the first and second zone of the reactor and 60-70 °C between the second and third zone of the reactor. In the second reactor type it was possible to achieve more even temperature distribution during the methanation process by replacing the catalyst with pellet shaped one. The change of the catalyst also had a direct impact on better control over the process, in particular, the control of the pressure in the reactor and the determination of the flow of hydrogen and carbon dioxide.

From the results it can be seen how the implemented changes contributed to the achievement of better results in the technological process. In the case of using the new catalyst, Ru/(Al_2O_3) in the form of the pellets, its high reactivity and satisfactory results of methane content in generated SNG and CO_2 conversion higher than in the case of using a nickel catalyst powder can be observed. The reactor heating time was also much shorter and the reaction itself was faster. A possible parameter for further optimization and better control of the methanation process is the temperature of the catalytic bed, the uniform distribution of which is hindered by the heat of reaction generated in the upper part of the reactor for higher inlet flows of the reactants. Unifying the temperature distribution of the catalytic bed, in this case, would require

additional complicated cooling or a different structure, which may translate into higher investment costs.

5. Initial thermodynamic analysis of SNG production systems

One of the main goals of the thesis was the techno-economic analysis of the power to SNG system as a whole. This required first modeling of the system's individual systems (validation of the models, determination of the impact of selected parameters) and then their integration. Before analyzing selected structures of synthetic natural gas production systems, the initial studies on methanation and gasification processes were performed.

5.1. Initial study of methanation process modelling

This subsection describes the first attempt to the sensitivity analysis of methanation process for various carbon feedstocks types. The influence of methanation operating temperature, recycled ratio and pressure was studied. Every case assumed the additional flow of hydrogen introduced to the methanation unit in order to achieve full utilization of carbon oxides.

The initial study assessed six different carbon feedstocks compositions for methanation process, four resulting from biomass gasification (PG-1, PG-2, PG-3, PG-4). Simulations incorporating a water-gas shift reactor unit upstream of the methanation unit were also considered for different process gas compositions. However, the impact of the additional shift reactor was considered negligible for the assumed methanation model, so it was dropped from further simulations [21]. Composition of the process gas from gasification depends on many factors (e.g. gasifying agents, gasifying temperature and pressure) and may change over time. In order to study the effect of syngas from different biomass on the methanation process operation, process gas compositions from the following sources were adopted [69–72].

5.1.1. Methodology and assumptions

The model of methanation process was designed in Aspen Plus software [73]. Base method used for simulations was Redlich-Kwong-Soave equation of state with modified Huron-Vidal mixing rules. The considered methanation unit consists of three stages of adiabatic methanation reactors with interstage cooling and process gas recirculation, which enabled the mapping of reactor zones that can operate at different temperatures. In the model, depending on the composition of the process gas used,

the demand for hydrogen is controlled, so that the stoichiometric ratios of the compounds participating in the reaction remain adequate. The methanation process was simulated using RGibbs reactor, which assumes multiphase equilibrium based on Gibbs free energy minimization. In order to improve the conversion, diluting the inlet gas is used through a recycle loop, whereby the temperature is lowered [74]. The recirculation loop begins after the first stage of methanation process. A simplified layout of the reaction is presented in the Fig. 5.1.

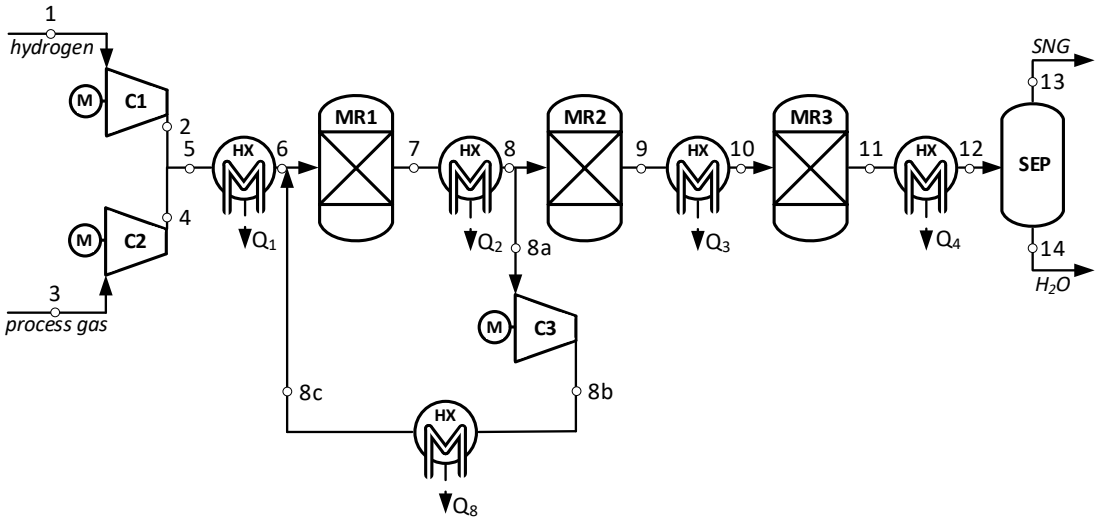

Figure 5.1 Flowsheet of methanation process; where MR – methanation reactor, HX – heat exchanger, C – compressor, M- motor, SEP separator, Q – heat stream

In Table 5.1 all assumptions used to build thermodynamic models in the Aspen Plus software are summarized. Reference was made to the numbering of the streams used in Fig. 5.1.

Table 5.1 Main assumptions for the thermodynamic analysis of methanation process

Point number (Fig. 5.1)	Parameter	Value
1	hydrogen temperature at the inlet to methanation unit	20 °C
1	hydrogen pressure at the inlet to methanation unit	5 bar
3	process gas temperature at the inlet to methanation unit	25 °C
3	process gas pressure at the inlet to methanation unit	1.5 bar
C1, C2, C3	isentropic efficiency of compressors	88%
C1, C2, C3	mechanical efficiency of compressors	99%

	pressure drop in methanation reactors (MR)	0.1 MPa
	pressure drop in heat exchangers (HX)	0.1 MPa
6, 8, 8c, 10	temperature behind heat exchangers (HX)	200 °C
12	temperature of gas separation process	25 °C

All process gases come from a different type of biomass. Simulations were conducted for dry syngas and for two moisture content in syngas - 15 and 30% (respectively *a*, *b* and *c* for each syngas case). Mole fractions of considered process gas feedstock are presented in Table 5.2. Lower heating value for each case was also calculated.

Table 5.2 Process gas compositions for methanation process simulation

	PG-1 [69]			PG- 2 [70]			PG- 3 [71]			PG- 4 [72]		
	a	b	c	a	b	c	a	b	c	a	b	c
H_2, %	48.40	41.14	33.88	34.21	29.07	23.94	55.71	47.41	39.05	4.75	4.04	3.33
CO_2, %	28.88	24.55	20.22	27.64	23.49	19.35	3.31	2.82	2.32	32.99	28.03	23.09
CH_4, %	6.46	5.49	4.52	7.87	6.69	5.51	0.08	0.07	0.06	7.94	6.75	5.56
H_2O, %	0.00	15.00	30.00	0.00	15.00	30.00	0.00	15.00	30.00	0.00	15.00	30.00
CO, %	16.26	13.82	11.38	29.24	24.85	20.46	40.76	34.69	28.57	54.36	46.18	38.04
N_2, %	-	-	-	1.06	0.90	0.74	0.07	0.06	0.05	-	-	-
LHV, MJ/kg	11.14	9.56	7.95	10.11	8.86	7.54	17.85	14.56	11.52	7.36	6.68	5.89

The efficiency of the system was defined according to formula (5.1). The heat recovered downstream of the methanation reactors was treated as a potential manageable effect (the heat flux needed to heat the gases upstream of the first reactor has already been subtracted from this value). On the other hand, the energy of the compressors was treated as the system's auxiliaries and subtracted from the 1 MW of SNG produced.

$$\eta_{\mathrm{PtSNG}} = \frac{E_{\mathrm{ch,SNG}} - E_{\mathrm{el,C}} + Q_{\mathrm{met}}}{E_{\mathrm{ch,PG}} + \frac{E_{\mathrm{ch,H_2}}}{\eta_{\mathrm{HG}}}} \tag{5.1}$$

where:

$E_{\mathrm{ch,SNG}}$ SNG chemical energy, MWh,

$E_{\mathrm{el,C}}$ compressors electricity consumption, MWh,

Q_{met} heat recovered after the methanation reactors, MWh,

$E_{ch,PG}$ chemical energy of process gas from biomass gasification, MWh,

E_{ch,H_2} hydrogen chemical energy, MWh,

η_{HG} efficiency of hydrogen generators, 58.86%, [41].

5.1.2. Results and discussion

On the example of the first composition of the process gas (PR-1 case *a*), the effect of temperature and pressure in the methanation reactors and the recirculated stream ratio on the composition of the obtained SNG was analysed. For this purpose, sensitivity analysis of the impact of these parameters on the composition of produced SNG were performed. The gas inlet temperature to each methanation reactor was varied in the range of 200-300 °C, which corresponds to the operation temperatures of the Ni(Al_2O_3) catalyst. Figure 5.2 presents the results of this simulation. The chart presents the dependence of the composition of produced SNG and the conversion rate as a function of the reaction initial temperature. Conversion factor was calculated according to the equation (4.4).

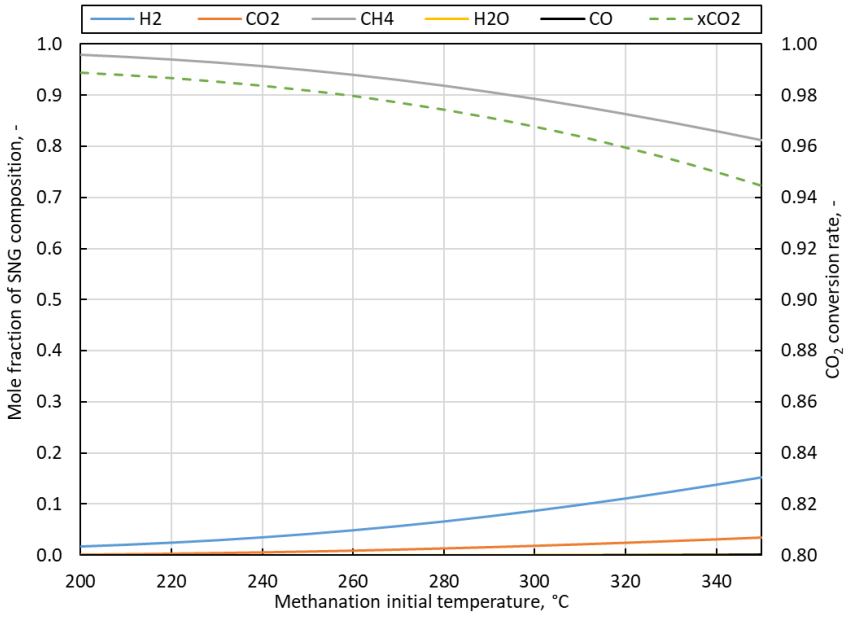

Figure 5.2 Dependence of SNG composition and conversion rate on the methanation reaction initial temperature, for a pressure of 10 bar

The dependence of methane content in the final gas product decreases as the reaction initial temperature increases. The produced SNG contains more unreacted hydrogen and carbon dioxide, which means that the conversion rate is lower than

when the reaction occurs at lower temperatures. In addition, Table 5.3 presents the results of the molar composition of gas in individual process stages and heat stream recovered in the heat exchangers outside the adiabatic reactors ($\dot{Q}_{\mathrm{met}}$) for reaction temperatures of 200, 250 and 300 °C. The conversion factor ($x_{\mathrm{CO_2}}$) relates to the individual reactors (MR1-MR3) for the points downstream of the reactors (7, 9 and 11, respectively), while in the case of point 13, which already corresponds to the final product, the conversion was calculated for the whole system. The most preferred SNG composition and conversion factor was obtained for the temperature of 200 °C, which is in line with the adopted calculation methodology, because in the case of equilibrium simulations of the considered reactions, the lowest possible initial temperatures of the process are desirable, so that the chemical equilibrium is directed towards the products. The outlet temperature in the case of an adiabatic process is not controlled, hence the division into reactor intersections. However, as shown in Figure 3.2, temperatures up to the range of about 550 °C do not have a very negative effect on the methanation process itself, because the chemical equilibrium in this range favours the production of products. Nevertheless, in the case of a real process, it will have an important impact, for example due to the catalyst used, which limits the methanation process operation to the temperatures at which it is active. The process initial temperature equal to 200 °C was used in further calculations for the rest of the assumed gas compositions of carbon feedstock.

Table 5.3 Gas composition at highlighted process points (in relation to Figure 5.1) and heat stream from the methanation reactors ($\dot{Q}_{met}$) for reaction temperatures of 200, 250 and 300 °C

	3	6	7	9	11	13	$\dot{Q}_{\mathrm{met}}$, kW
T, °C	25	200	488	337	234	25	
H_2	0.4840	0.3452	0.1597	0.0433	0.0115	0.0275	
CO_2	0.2888	0.0669	0.0373	0.0098	0.0019	0.0044	
CH_4	0.0646	0.2424	0.3371	0.3912	0.4056	0.9644	297
H_2O	0.0000	0.3206	0.4634	0.5556	0.5808	0.0036	
CO	0.1626	0.0247	0.0022	0.000	0.000	0.000	
x_{CO_2}	-	-	0.61	0.76	0.80	0.99	
T, °C	25	250	521	397	304	25	
H_2	0.4840	0.3689	0.1979	0.0785	0.0295	0.0680	
CO_2	0.2888	0.0719	0.0450	0.0185	0.0064	0.0143	
CH_4	0.0646	0.2310	0.3186	0.3750	0.3974	0.9139	293
H_2O	0.0000	0.3020	0.4336	0.5276	0.5665	0.0036	
CO	0.1626	0.0260	0.0046	0.000	0.000	0.000	
x_{CO_2}	-	-	0.54	0.64	0.66	0.97	
T, °C	25	300	553	451	370	25	
H_2	0.4840	0.3943	0.2382	0.1235	0.0614	0.1338	
CO_2	0.2888	0.0763	0.0521	0.0292	0.0143	0.0303	
CH_4	0.0646	0.2183	0.2984	0.3542	0.3829	0.8320	285
H_2O	0.0000	0.2823	0.4024	0.4919	0.5411	0.0036	
CO	0.1626	0.0285	0.0087	0.0009	0.0000	0.0002	
x_{CO_2}	-	-	0.47	0.53	0.53	0.95	

Figure 5.3 presents the dependence of the SNG composition and conversion rate on the recirculated gas fraction in the first stage of methanation process. Recycled ratio was defined as the split fraction of recycled gas in the loop. Values from 0.2 to 0.9 were used for the sensitivity analysis. The higher the recycled ratio, the more favourable the SNG composition and conversion rate values. However, increasing the proportion of recirculated gas affects the energy consumption of the gas compressor in the recirculation loop. The recirculation ratio value of 78% was adopted for the calculations because it was considered the limit value, after which the share of methane in SNG did not increase significantly enough to make it profitable to increase the system's own electricity expenditure. The recirculation ratio factor is, however, a value for further optimization in the case of calculations for a specific gas example.

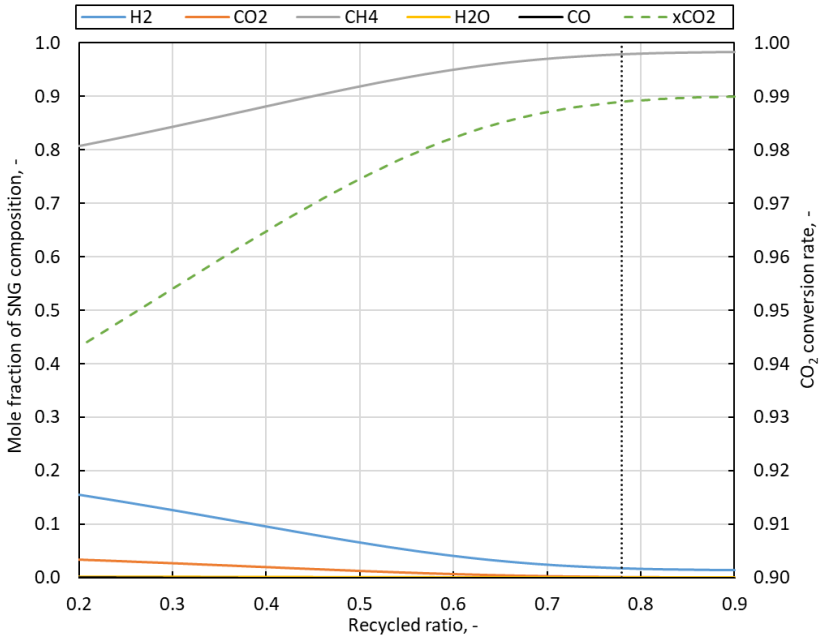

Figure 5.3 Dependence of SNG composition and conversion rate on the methanation process recycle ratio, for initial temperature of 200 °C

Sensitivity analysis was also carried out for various levels of pressure in the methanation process. Within the assumed range of compressors ($C_{1\text{-}3}$) outlet pressure (10-20 bar), the final SNG composition differs slightly in favour of the highest pressure. The results of the molar gas composition at individual points are presented in Table 5.4. The content of methane produced at lowest pressure assumed was about 96%, and highest pressure assumed the content was about 98%. The table also contains another simulation result - the demand for electricity (E_{elC}) to drive the compressors ($C_{1\text{-}3}$).

Table 5.4 Gas composition at highlighted process points (in relation to Figure 5.1) and compressors electricity demand (E_{elC}) for compressors (C_{1-3}) outlet pressure of 10, 15 and 20 bar

	3	6	7	9	11	13	E_{elC}, kW
p, bar	1.5	9.9	9.8	9.6	9.4	9.3	
H_2	0.4840	0.3453	0.1598	0.0433	0.0116	0.0275	
CO_2	0.2888	0.0670	0.0373	0.0098	0.0019	0.0044	
CH_4	0.0646	0.2424	0.3371	0.3912	0.4057	0.9645	26
H_2O	0.0000	0.3206	0.4635	0.5556	0.5809	0.0036	
CO	0.1626	0.0248	0.0023	0.0000	0.0000	0.0000	
x_{CO_2}	-	-	0.61	0.76	0.80	0.99	
p, bar	1.5	14.9	14.8	14.6	14.4	14.3	
H_2	0.4840	0.3340	0.1415	0.0322	0.0086	0.0206	
CO_2	0.2888	0.0643	0.0331	0.0071	0.0012	0.0027	
CH_4	0.0646	0.2476	0.3456	0.3963	0.4070	0.9744	35
H_2O	0.0000	0.3296	0.4779	0.5644	0.5832	0.0024	
CO	0.1626	0.0246	0.0018	0.0000	0.0000	0.0000	
x_{CO_2}	-	-	0.65	0.80	0.83	0.99	
p, bar	1.5	19.9	19.8	19.6	19.4	19.3	
H_2	0.4840	0.3263	0.1290	0.0257	0.0071	0.0170	
CO_2	0.2888	0.0624	0.0302	0.0055	0.0008	0.0018	
CH_4	0.0646	0.2512	0.3515	0.3992	0.4077	0.9793	43
H_2O	0.0000	0.3357	0.4878	0.5696	0.5844	0.0018	
CO	0.1626	0.0245	0.0015	0.0000	0.0000	0.0000	
x_{CO_2}	-	-	0.67	0.83	0.85	0.98	

As the pressure of the methanation process increases, the demand for electricity increases. However, the increase in the process pressure is not meaningly reflected in the increase in the share of methane in SNG (for 10 bar, the share of methane in SNG is high and amounts to over 96%), therefore, a pressure of 10 bar was assumed for further calculations for the rest of the assumed gas compositions of carbon feedstock to perform a comparative quantitative analysis.

In order to compare the methanation process for various carbon feedstock compositions (according to table 5.2), simulations were carried out assuming that

1 MW of SNG was the output. Figure 5.4 presents the demand for hydrogen produced in electrolysis process and the mass flow of generated SNG depending on the carbon feedstock used in the simulation.

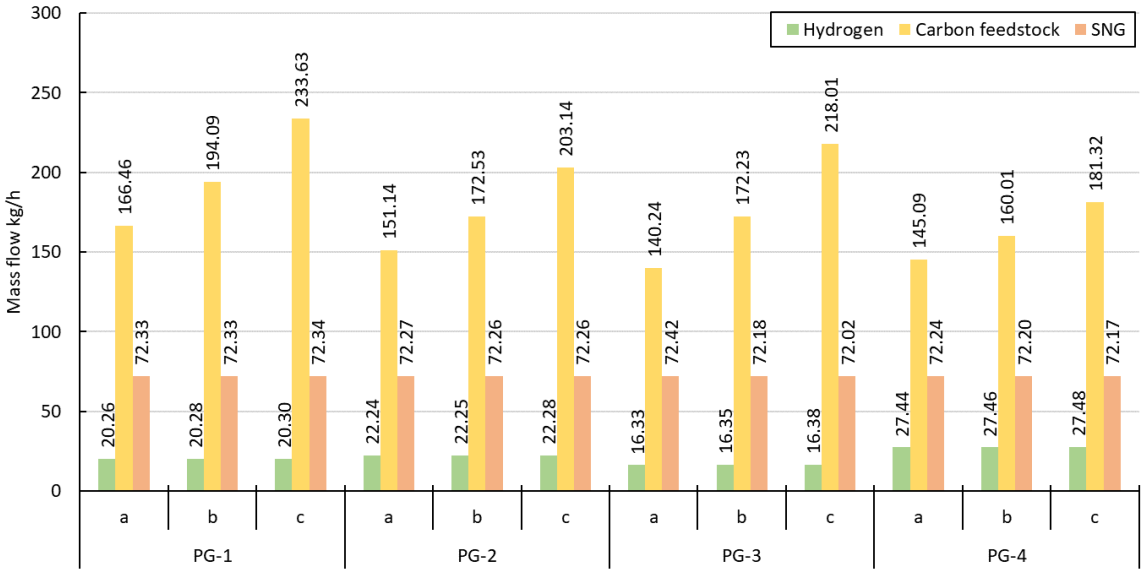

Figure 5.4 Feedstock gases streams for the production of 1 MW of SNG for various compositions of carbon feedstock used in methanation process simulation

Depending on the gas used at the inlet to the methanation process the demand for process gas and hydrogen for the production of 1 MW of SNG varies. The amount of hydrogen needed for the process depends on the hydrogen content of the gas from biomass processing. PG-3 contains a large share of hydrogen, so a relatively smaller stream of hydrogen produced in the electrolysis process is fed to the methanation process compared to the case of PG-1 and PG-2. PG-4 in its composition contains the least amount of hydrogen among other gases, so the process requires the largest stream of hydrogen from electrolysis. Lower demand for process gas was observed in the cases with lower moisture content in the feeding gas, which is obvious due to the dilution of the process gas by water vapor. However, it has to be underlined that the system has to be treated as a whole – thus, it may be more profitable in terms of overall energetic effect to use wet gas, instead of drying it, accepting, e.g., lower quality of resulting SNG gas.

Table 5.5 presents the molar composition of SNG produced for each of the gas compositions used in the simulation. In addition, the calculated LHV of each gas and the conversion rate (x_{CO_2}) are summarized in the table. The high conversion rate of

CO_2 and CO to CH_4 in all considered cases is obtained due to the adopted equilibrium simulation method. In cases of gas compositions obtained from biomass gasification the slight differences appear in the composition of the product gas, the share of methane in the produced SNG is similar and is in the range of 93-96%. What directly affects LHV, but also in the case of gases obtained by this technology, the values are similar and equal to approximately 48-49.5 MJ/kg. The influence of the moisture content in each of the analyzed gases is an individual matter and depends on the considered fuel. In most of the studied cases, this parameter did not affect the composition of the produced SNG and its calorific value, however, the greatest importance of this parameter was noted in the case of PG-3 gas.

Table 5.5 Comparison of the molar composition of the SNG produced from different carbon feedstocks

	SNG composition (% vol, dry basis)					
	PG-1			PG-2		
	a	*b*	*c*	*a*	*b*	*c*
H_2	0.0275	0.0276	0.0283	0.0293	0.0290	0.0290
CO_2	0.0044	0.0044	0.0045	0.0041	0.0041	0.0041
CH_4	0.9645	0.9644	0.9635	0.9474	0.9478	0.9478
H_2O	0.0036	0.0036	0.0036	0.0036	0.0036	0.0036
CO	0.0000	0.0000	0.0000	0.0000	0.0000	0.0000
N_2	-	-	-	0.0153	0.0153	0.0153
x_{CO_2}	0.99	0.98	0.98	0.99	0.99	0.98
LHV, MJ/kg	49.46	49.46	49.46	48.17	48.18	48.18
	PG-3			PG-4		
	a	*b*	*c*	*a*	*b*	*c*
H_2	0.0523	0.0465	0.0421	0.0347	0.0340	0.0332
CO_2	0.0064	0.0048	0.0038	0.0044	0.0042	0.0040
CH_4	0.9362	0.9435	0.9489	0.9573	0.9582	0.9591
H_2O	0.0036	0.0036	0.0036	0.0036	0.0036	0.0036
CO	0.0000	0.0000	0.0000	0.0000	0.0000	0.0000
N_2	0.0014	0.0014	0.0014			
x_{CO_2}	0.99	0.99	0.99	0.99	0.99	0.99
LHV, MJ/kg	49.27	49.44	49.55	49.52	49.55	49.57

Table 5.6 presents the results of the efficiency calculations of the considered system.

Table 5.6 Calculated efficiency values of the considered power to SNG system cases

		$\eta_{PtSNG.}$ %
PG-1	a	76.49
	b	76.57
	c	76.51
PG-2	a	75.11
	b	75.19
	c	75.11
PG-3	a	80.50
	b	80.62
	c	80.53
PG-4	a	69.34
	b	69.38
	c	69.34

The degree of moisture in the process gases from biomass gasification is of marginal importance. However, the efficiencies differ with regard to the different fuel compositions considered for the methanation process. In the performed analysis, among gas compositions from biomass gasification, the highest efficiency of the system was obtained for PG-3.

5.2. Initial study on an integrated system on SNG production based on biomass gasification and electrolysis processes

This subsection describes the first attempt of analyzing integrated system of SNG production based on biomass gasification and electrolysis processes. The influence of different biomass gasification parameters was studied in terms of the composition of syngas as a carbon feedstock for the methanation process. Different levels of availability of hydrogen were considered and two stages of the operation of the SNG production plant were proposed [12].

Figure 5.5 presents the conceptual layout of a considered power to SNG installation. The analyzed system consists of a module of hydrogen production in the electrolysis process and a module of SNG production in the methanation process.

Electricity from renewable energy installations in the night energy demand valleys powers hydrogen generators, where hydrogen and oxygen are produced in the electrolysis process. The process products are stored in buffer tanks. The installation for the production of SNG is fed with hydrogen produced in the electrolysis process and a feedstock of carbon oxides. As a source of carbon oxides for methanation, the use of process gas produced in biomass gasification was assumed. Depending on the gasification agent used (air, oxygen, steam), syngas from biomass gasification has a different composition. The synthesis gas derived from air biomass consists mainly of hydrogen, carbon monoxide, carbon dioxide, nitrogen, methane and water vapour [71]. It is a simple and cost-effective process, but the syngas contains a significant amount of nitrogen and other non-combustible gases, which reduce its heating value. Oxygen biomass gasification eliminates the nitrogen and other non-combustible gases found in air, producing a gas with a higher heating value. Using steam as a gasifying agent increases the amount of hydrogen in the process gas from biomass gasification. The use of steam and oxygen (which is a product of electrolysis) as gasifying agents, assumed as part of the considered power to SNG system, allows to avoid the presence of nitrogen appearing when air is used as a gasification oxidizer. The SNG generated in the process is dried and the condensed water can be reused in the electrolysis process.

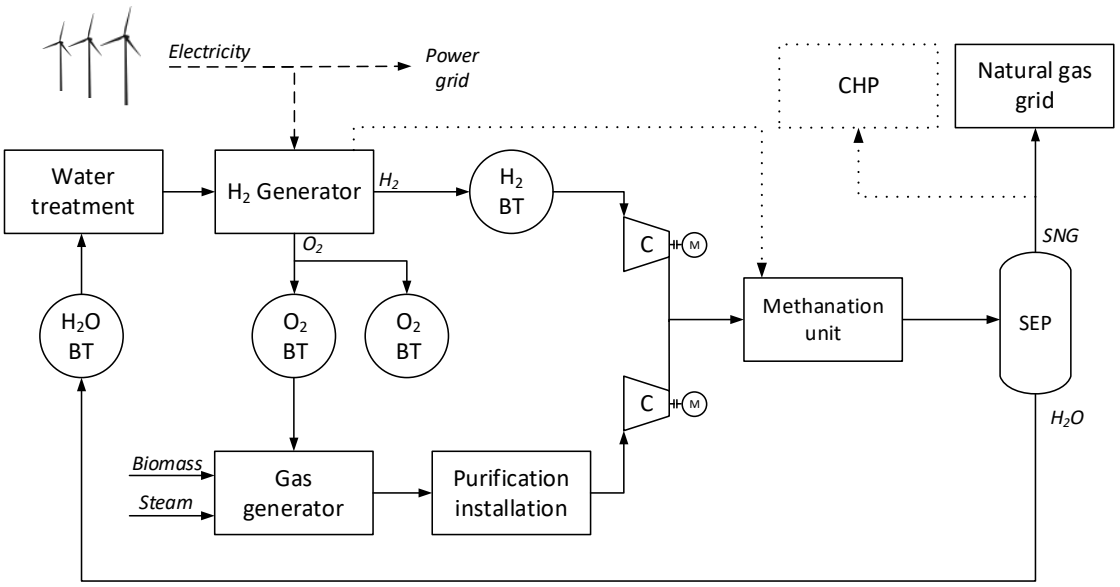

Figure 5.5 Schematic representation of a power to SNG installation; BT – buffer tank, C – compressor, M – motor, SEP – gas/liquid separator, CHP – combined heat and power unit; dotted lines indicate alternative routes of products

The primary goal of such installation is to store energy in the form of chemical energy of SNG. In this system hydrogen is produced in the electrolysis process at night, during reduced demand for electricity. Hydrogen generators are powered by energy from renewable energy sources, in this case, wind farms were assumed. The SNG produced in the methanation process is injected directly into the gas network that is used for storage. In order to extend the operation time of difficult-to-control system elements, such as the biomass gasification unit and the methanation unit, it is proposed that the process gas should also be methanized when there is no access to hydrogen produced in the electrolysis process. This produces a synthesis gas consisting mainly of methane and carbon dioxide in various proportions, depending on the conditions of the gasification process. The resulting SNG, however, contains less methane than in previous case, so it cannot be stored in the gas grid as its composition would not meet the requirements for network gas parameters. Thus, in this case it is proposed to use the gas in the CHP unit to produce electricity and heat.

Two operating states of the system were proposed that differ with hydrogen availability from RES (first case assumed the use of additional hydrogen stream which was not available in the second operation case) . In the first case, which assumed the production of energy from renewable sources and the availability of hydrogen from the electrolysis process, biomass gasification is focused on the

production of an appropriate proportion of carbon oxides and hydrogen in the process gas for methanation (the gasifying agents are oxygen and steam), the produced SNG gas is rich in methane and can be injected into the gas network. In the second state which assumes no production of energy from renewable sources, hydrogen is not generated in the electrolysis process.

5.2.1. Methodology and assumptions

As part of the calculations, simulations of biomass gasification and methanation were carried out using Aspen Plus software [73]. For the purposes of this thesis, the equilibrium approach of simulating the biomass gasification and methanation processes, as presented by the authors of the works [75–77] was considered. The mathematical models used were validated for the data available in the given literature.

The model predicts the process gas resulting from biomass gasification for different types of biomass. The biomass gasification process was considered to be comprised of three stages. The dry fuel was directed to the decomposition stage of the gasification process, which was simulated by the yield reactor (RYield). In this stage, biomass was converted into individual components of carbon, nitrogen, oxygen, hydrogen and ash, by assuming the yield distribution according to the biomass analysis. To simulate the next stage of the gasification process the equilibrium reactor (RGibbs) was used. At this stage, a part of the process gas was oxidized and also, partial decomposition occurred. Then, a solids separator was used to separate the resulting ash from the gas mixture. The last stage of the gasification process is also performed by the Gibbs reactor. In this stage, oxygen is introduced to the process as gasification agents and the final composition of the gasification gas is calculated. After this stage, the gas-liquid separator is introduced to the process. The scheme of the simulation model of the biomass gasification process is presented in Figure 5.6.

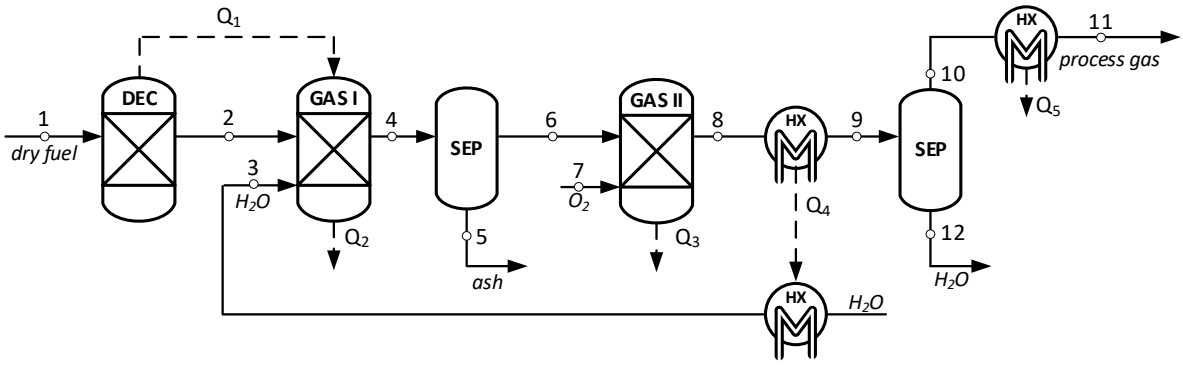

Figure 5.6 Simulation model of biomass gasification process: DEC – biomass decomposition unit, GAS – gasification unit, SEP – solid and liquid separator, HX – heat exchanger, Q - heat

The main assumptions for the biomass gasification simulation model are given in Table 5.7. The pressure drop in particular components was assumed as zero and the tar formation was not considered. Biomass and ash were considered non-conventional solid streams and HCOALGEN and DCOALIGT options were used to calculate their properties. For calculations of the properties of conventional components the Redlich-Kwong-Soave equation of state with Boston-Mathias alpha function was used.

Table 5.7 Main assumptions for the thermodynamic analysis of biomass gasification process

Parameter	Value
Biomass pressure	1.1 bar
Biomass temperature	25 °C
Decomposition pressure	1.1 bar
Decomposition temperature	500 °C
Gasification pressure	1.1 bar
Steam pressure	3 bar
Steam temperature	300 °C
Oxygen pressure	1.1 bar
Oxygen temperature	15 °C

The use of the process gas produced after gasification of wood residue was assumed for further calculations. The composition of the assumed fuel [78] used in the simulation is presented in Table 5.8.

Table 5.8 Elementary composition of biomass fuel (dry basis) assumed for calculations

Parameter	Value
Ultimate analysis (wt. %, d.b.)	
Carbon	49.90
Hydrogen	6.72
Nitrogen	0.16
Oxygen	42.66
Proximate analysis (wt. % d.b.)	
Ash	0.36
Volatile matter	81.81
Fixed carbon	17.83

In the case of using the process gas produced in local power systems, process optimization is usually conducted to obtain the maximum calorific value of the produced gas. However, when the purpose of the process is to generate gas for further synthesis, such as the production of SNG, the optimization criteria may be different, for example, it may be maximizing the content of certain components (such as carbon monoxide or hydrogen), in the generated gas. For that reason, the influence of various parameters (and above all the amount of gasifying agents - oxygen and steam) on the composition of the resulting process gas was assessed. The behaviour of individual components of the process gas for different values of the supplied streams of gasification agents, i.e. steam and oxygen, were also investigated.

The resulting process gas together with the buffered hydrogen are directed to the methanation system, which consists of three equilibrium reactors (RGibbs) with a heat exchanger behind each of them and a process gas recirculation loop located after the first stage of the methanation reactor (model was previously described in section 5.1.1). Then the separator model was used and gas generated in the process was dried and the condensed water could be reused in the electrolysis process. The scheme of the simulation model of the methanation process is presented in Figure 5.7.

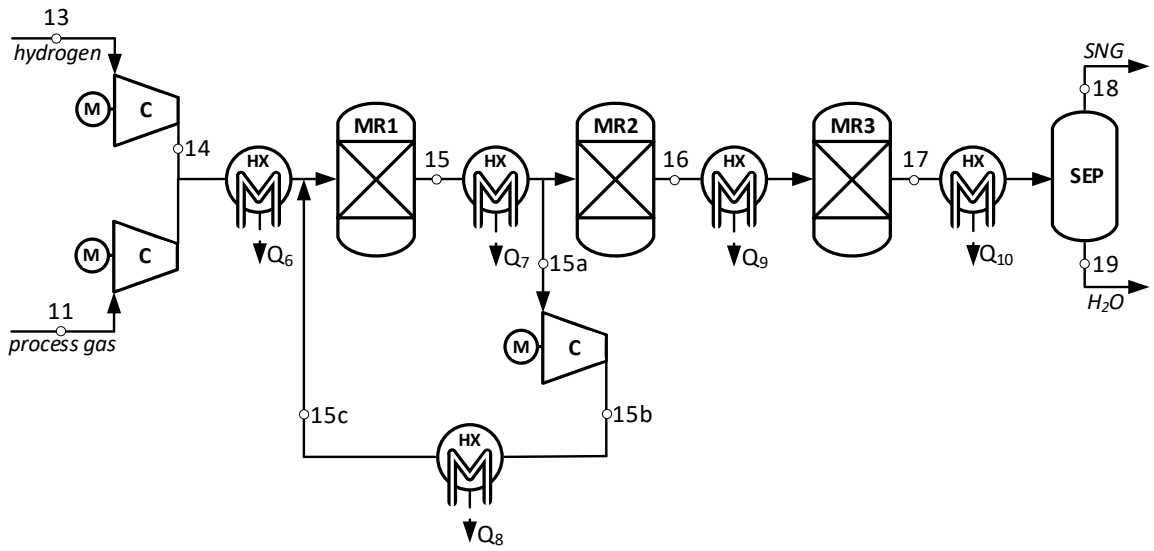

Figure 5.7 Simulation model of methanation process; C – compressor, HX – heat exchanger, MR – methanation reactor, SEP – gas/liquid separator, Q - heat

Table 5.9 presents the main data necessary to develop a thermodynamic model of the methanation process in Aspen Plus software. The base method used for simulations was the Redlich-Kwong-Soave equation of state with modified Huron-Vidal mixing rules.

Table 5.9 Main assumptions for the thermodynamic analysis of methanation process

Parameter	Value
Hydrogen inlet temperature	20 °C
Hydrogen inlet pressure	5 bar
CO_2:H_2 ratio	1:4
Compressors (C) outlet pressure	10 bar
Isentropic efficiency of compressors	88%
Mechanical efficiency of compressors	99%
Heat exchangers (HX) outlet temperature	200 °C

One of the basic elements of the power to SNG installation is the hydrogen generator which is responsible for the water electrolysis process. The products of this process are hydrogen and oxygen. It is assumed that the hydrogen generator in the calculation model is supplied in electricity with a renewable energy source – a wind farm. Hydrogen generator can work with variable power supply, which is determined by the variable power of the wind farm. The characteristics of the wind farm, as well as calculation model assumptions, are described in the article [79]. The hydrogen

generator is powered by a renewable source for eight hours per day, between 22:00 and 06:00. The calculation model assumed the nominal power of the wind farm equal to 30 MW. It was assumed that a constant stream of hydrogen is supplied to the methanation unit. In order to improve the cooperation between the wind farm, the hydrogen generator and the gas tank, a bypass allowing the direct connection of the generator with the methanation reactor was implemented into the system. This variant allows the use of energy generated by the wind farm when the hydrogen buffer tank installed in the presented system is full. The nominal power of hydrogen generator, resulting from the demand for hydrogen in the methanation reactor, were calculated using the universal algorithm widely described by the authors in [80].

In the case of power to SNG systems, being a storage solution, the efficiency should be calculated taking into consideration annual amounts of streams. Definitions of local efficiency for the considered operating states of the system are presented by formulas 5.2 and 5.3.

1st case of operation state:

$$\eta_{\mathrm{PtSNG}} = \frac{E_{\mathrm{ch,SNG\_grid}} + Q}{E_{\mathrm{ch,b}} + E_{\mathrm{ch,H_2}} + E_{\mathrm{el,C}}} \tag{5.2}$$

2nd case of operation state:

$$\eta_{\mathrm{PtSNG}} = \frac{E_{\mathrm{ch,SNG\_CHP}} + Q}{E_{\mathrm{ch,b}} + E_{\mathrm{el,C}}} \tag{5.3}$$

where:

$E_{\mathrm{ch,SNG\_grid}}$ – chemical energy of SNG sent to the gas network, MWh,

$E_{\mathrm{ch,SNG\_CHP}}$ – chemical energy of the SNG used in the CHP unit, MWh,

$E_{\mathrm{ch,b}}$ – chemical energy of biomass feedstock, MWh,

$E_{\mathrm{ch,H2}}$ – hydrogen chemical energy, MWh,

$E_{\mathrm{el,C}}$ – compressors electricity consumption, MWh,

Q – amount of heat recovered from gasification and methanation processes, MWh.

It was assumed that the hydrogen generator works in an eight-hour night regime, while the gasification and methanation unit works continuously.

5.2.2. Results and discussion

The developed model of the biomass gasification process prior to connection with the methanation unit was validated for various biomass compositions [78,81–83]. Figure 5.8 presents the simulated compositions of process gas generated in the biomass gasification process. Calculations were performed for the gasification temperature of 700 °C. The share of hydrogen for individual fuel compositions is similar and amounts to over 50%. Process gases differ in the proportion of other components, such as carbon dioxide, carbon monoxide and methane. The share of carbon monoxide in the gas produced in all cases is over 20%, the share of carbon dioxide ranges from 15 - 22%, while the share of methane is negligible and amounts to less than 10%. The calculated results are in line with the literature data, therefore the model can be considered validated.

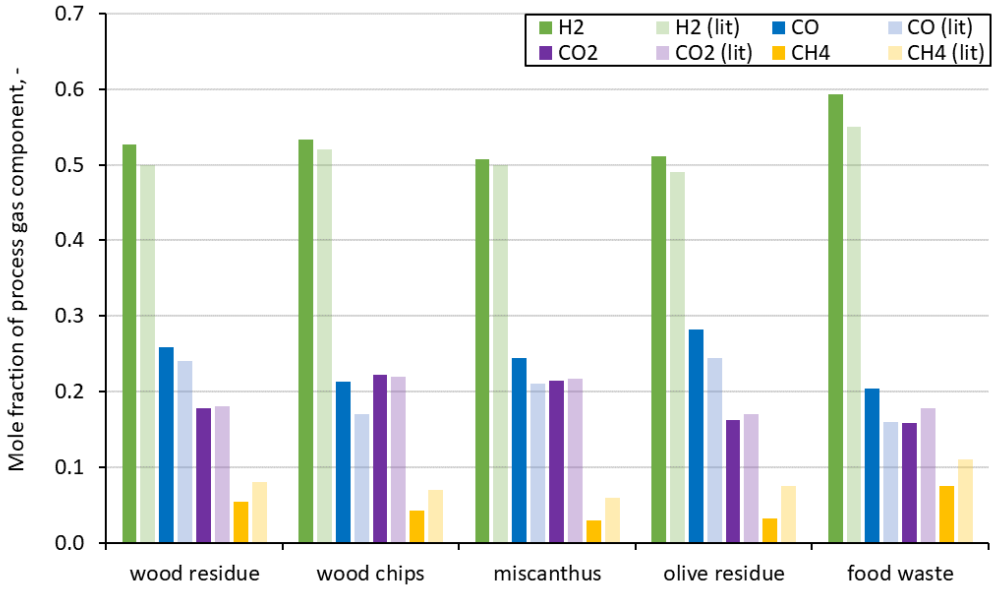

Figure 5.8 The composition of the process gas for different biomass feedstock obtained by the simulation model and compared with the literature (lit) data [79–82]

A sensitivity analysis of the effect of gasification process temperature on the composition of process gas after biomass gasification was performed. The main aim of this step was to analyse the gas composition for further simulations of the states of operation of the entire system. Figure 5.9 presents the validation of the syngas composition depending on the temperature of the gasification process. The

temperature was varied in the range of 500 - 900 °C and for this range, the trends for the individual components of the process gas remained consistent with the literature data [78]. For the gasification process temperature of 500 °C, the share of hydrogen was slightly over 30%, with the higher process temperature, this share increased, and for the temperature of 700 °C, it was over 50%. Then, the share of hydrogen decreased slightly with a further increase in temperature but remained at the level of over 50%. A similar trend could be observed for carbon monoxide. For the lowest process temperature, this share was about 8%, then, with the temperature increase, the share increased and was the highest for the highest process temperature, reaching over 30%. The trends of carbon dioxide and methane shares were opposite to the rest of the components. The share of carbon dioxide for the gasification process temperature of 500 °C was less than 40% and decreased with increasing temperature. This share was the lowest for the highest process temperature, below 15%. Similarly, for methane, this share was over 20% for the lowest process temperature and decreased with increasing gasification temperature, while after exceeding 700 °C it was negligible.

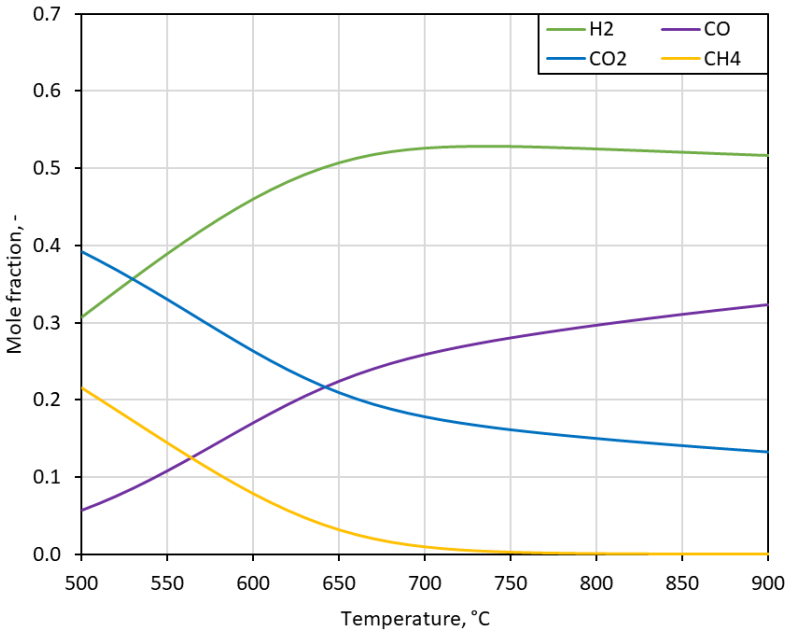

Figure 5.9 The composition of the process gas resulting from the gasification of wood residue

The simulations were carried out for two proposed cases of system operating states, with and without hydrogen availability from RES. The calculations assumed that the power generated in SNG equals 1 MW. The parameters of the other elements of the system (hydrogen generator power, hydrogen tank capacity) were selected to

ensure the highest energy efficiency of the power to SNG installation. The composition of biomass for the gasification process is constant, while the variability of the composition of the process gas results from differences in the supplied streams of gasifying agents (oxygen and steam), appropriate for the considered system operation cases (depending on the availability of hydrogen from the electrolysis process).

1st case of operation state (assuming renewable H_2 availability)

In the case of the first system operation, the focus is on examining the biomass gasification process in terms of different molar fractions of products in the process gas. For this state, a hydrogen stream from the electrolysis process necessary for complete methanation of carbon oxides from syngas is assumed.

Quantitative analysis of the reactants and products streams of methanation process was performed depending on the effect of steam to biomass ratio and oxygen to biomass ratio values assumed for biomass gasification. The results are presented in Figure 5.10. The graphs show the process gas and additional hydrogen mass streams from the electrolysis process to produce 1 MW of SNG depending on the gasification agent streams supplied to the biomass gasification process. The analysis was carried out for the steam to biomass ratio range of 0.1 - 1.0, the oxygen flux to biomass flux ratio of 0.1, 0.3 and 0.5 (figures *a* to *c*, respectively), and for different temperatures of the gasification process. The diagrams also show how the molar streams of hydrogen, carbon monoxide and carbon dioxide change depending on various parameters of the gasification process.

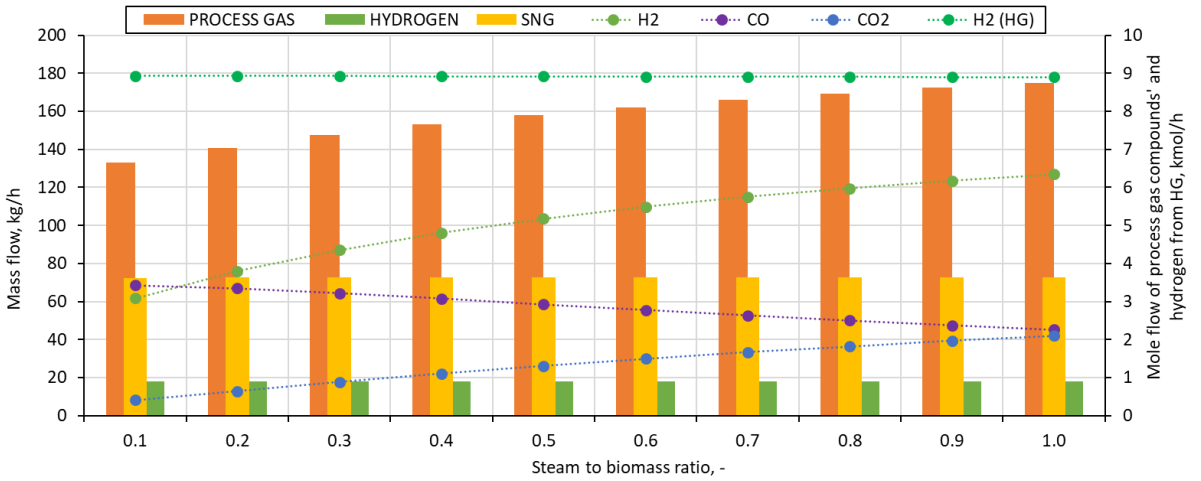

a)

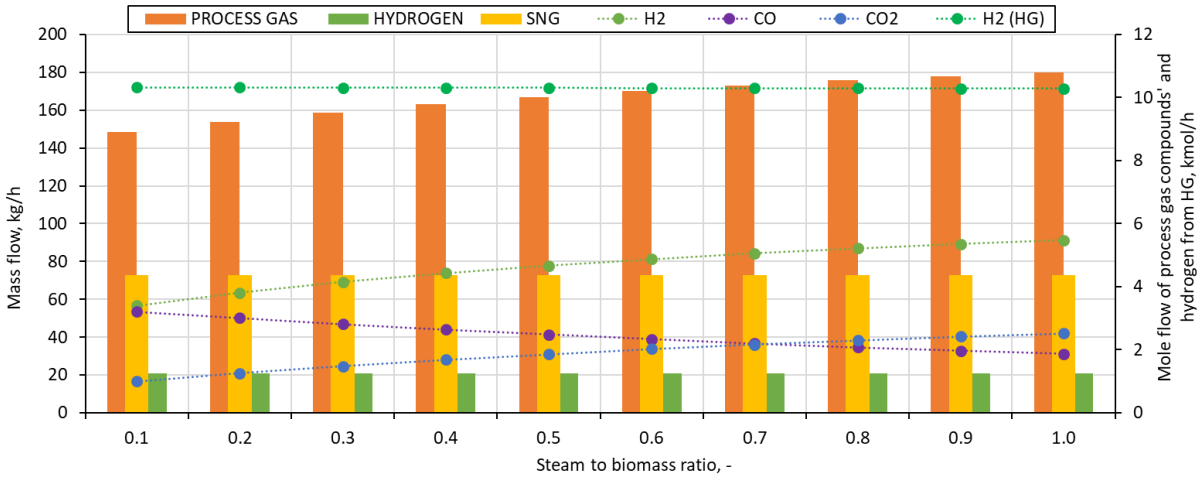

b)

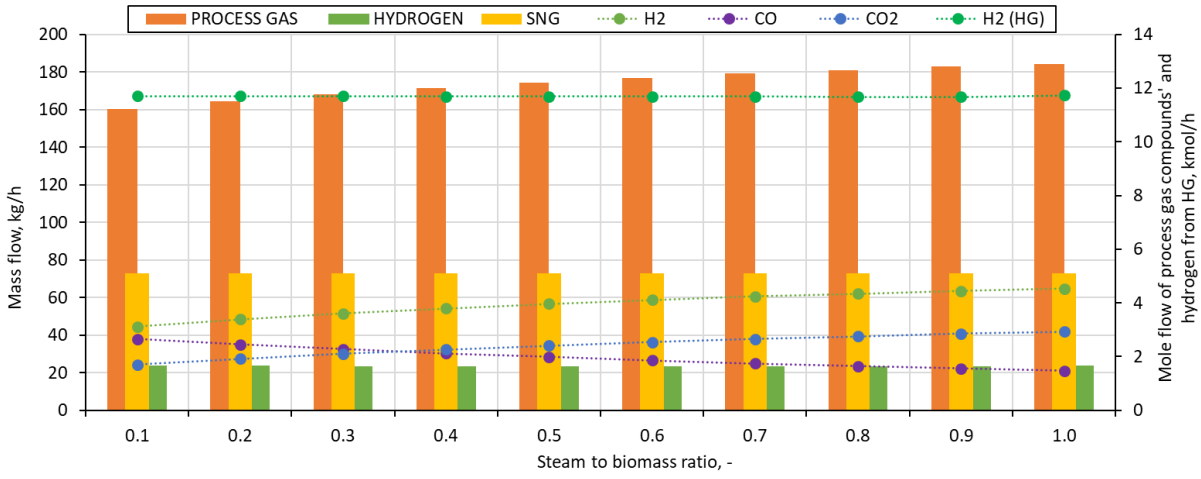

c)

Figure 5.10 Results of the quantitative analysis of the methanation process as a function of steam to biomass ratio for different amounts of oxygen supplied to the gasification process (a) 0.1, b) 0.3, c) 0.5) (Appendix C)

As presented in the Figure 5.10, the use of steam as a gasification agent supports the enrichment of hydrogen content in the process gas composition. A high proportion of hydrogen in the process gas is desirable for the methanation process as it introduces additional hydrogen into the reaction and can be a feature that allows manipulation of the hydrogen stream supply from the electrolysis process. As the stream of steam supplied to the gasification process increases, the share of hydrogen and carbon dioxide in the process gas increases, while the share of carbon monoxide decreases. In addition, the graphs also show the hydrogen stream fed to the methanation process from the electrolysis process, depending on the different compositions of the process gas. It remains at a similar level for a given case of the oxygen stream fed to the gasification process and increases with the increase of the oxygen stream and the resulting modification of the process gas composition. Additionally, the conversion of the methanation process was calculated and for each case, the result was over 99%.

Regardless the process gas composition obtained within the model, the mole fraction of methane in the resulting SNG is similar and is in the range of 0.94 - 0.95. However, the amount of process gas supplied to the methanation process differs, while the amount of hydrogen remains at a similar level for the various variants. A greater amount of process gas should be delivered to the methanation process in the case of gas composition with higher steam to biomass ratio. This is due to the greater proportion of water vapour and, thus, lower proportions of carbon oxides in the process gas. The stream of hydrogen needed by the methanation unit for the synthesis of the stream of carbon oxides obtained by the biomass gasification unit is more dependent on the stream of oxygen supplied to the gasification process, as it has a more significant impact on the amount of carbon oxides produced.

To estimate the size of the hydrogen generator for this case of power to SNG system operation, three hydrogen streams needed for the methanation process were assumed (for three values of oxygen to biomass ratio used in the biomass gasification process). Hydrogen stream required for the methanation process are equal, respectively, to 17.98 kg/h, 20.77 kg/h and 23.57 kg/h for the values of 0.1, 0.3 and 0.5 of the oxygen to biomass ratio. Based on those values, calculated hydrogen generator powers were equal to 1.23 MW, 1.42 MW and 1.61 MW. Efficiency at the nominal operating points for these three generators was equal to 0.72 [83].

2nd case of operation state (no additional H_2 production)

In order to increase the efficiency of the proposed system and prevent the need to shut down the gasifier and the methanation unit, which in practice may cause difficulties, it has been proposed to use a CHP unit when hydrogen from the electrolysis process is not available to be fed to the methanation system for the production of SNG. Therefore, the syngas was subjected to a methanation process. As a CHP unit, a gas engine was considered. It was assumed that it is possible to use the methanized process gas directly in the engine.

The model of the engine was built in the MS Excel environment, based on the methodology presented in **Błąd! Nie można odnaleźć źródła odwołania.**. Especially important was the adoption of proper characteristics when changing the fuel from nominal (usually natural gas) to the gas with different compositions and adopting the characteristic parameters (efficiencies) to the amount of gas that is fuelled to the engine. Detailed gas engine model description is presented in **Błąd! Nie można odnaleźć źródła odwołania.**. The analysis conducted here assumes that the heat generated in the cogeneration system is produced for the district heating (DH) system with a temperature characteristic at 90 °C/70 °C, which determines the amount of heat that can be usefully utilized. The simulation results are presented in Table 5.10.

Table 5.10 Results of the simulation of the methanation process for the process gas without the addition of hydrogen from the electrolysis process for the oxygen flux coefficients equal to a) 0.1, b) 0.3 and c) 0.5 of the supplied biomass stream value

	a	*b*	*c*
H_2	0.0016	0.0013	0.0010
CH_4	0.4980	0.4202	0.3411
CO	0.0000	0.0000	0.0000
CO_2	0.4975	0.5756	0.6551
LHV, MJ/kg	13.35	10.50	7.97

Three compositions of the process gas resulting from the biomass gasification process were analyzed for the oxygen flux coefficients equal to a) 0.1, b) 0.3 and c) 0.5 of the supplied biomass stream value. The higher the oxygen content in the process, the greater the amount of carbon dioxide in the final product, while the methane content decreases. To increase the share of hydrogen in the process gas fed

to methanation, simulations of the gasification process were carried out with an increased share of steam to biomass ratio (0.5-2.0). However, from the point of view of SNG produced in the methanation process, the share of steam did not significantly affect the composition of the final gas. The electric power produced in the engine system for the assumptions made is 393 kW. The value of the low-temperature heat flux equals 202.77 kW, while the high-temperature heat flux differs within the adopted assumptions and for the assumed cases equals: a) 305.25 kW, b) 342.47 kW and c) 397.52 kW, which is caused by the greater amount of gas stream supplied to the engine resulting from its lower calorific value.

Calculated values of power to SNG efficiency for two considered cases of system operation are presented in Table 5.11.

Table 5.11 The results of the local efficiency calculated for the considered 3 operating states of the system depending on the assumed oxygen to fuel ratio (a) 0.1, b) 0.3, c) 0.5)

	η_{PtSNG}, %	
	1st case	2nd case
a	68.77	43.80
b	62.84	31.19
c	57.62	20.56

The values for the analyzed cases are within the range of 57.62% – 68.77% for the first case assuming the hydrogen production from RES, and 20.56 – 43.80% for the second case without additional hydrogen production. The efficiency value of the system drops significantly with the increase in the share of the oxygen stream in the biomass gasification process, while in the case of different values of the steam to biomass ratio in the scope of the same oxygen to biomass ratio supplied to the system, the differences in calculated efficiency are negligible and have not been presented in the table. Supplying more oxygen also results in the need to supply more hydrogen to the methanation process from hydrogen generators. It is a reaction to a change in the composition of the process gas, and, more precisely, the amount of carbon oxides, which must be balanced so that the synthesis product is 1 MW of SNG. The higher values of the energy efficiency for the first case of operation is due to the calculated smaller size of the hydrogen generator needed to power the methanation unit.

6. Characteristics of the selected SNG production systems

The main goal of this analysis is to assess the thermodynamic and economic potential of three SNG production systems that integrates biomass gasification and syngas methanation processes. On the basis of preliminary analyses of individual elements, it was decided to compare two biomass gasification technologies (direct and indirect gasification) to perform a more detailed techno-economic analysis. The three cases analyzed assumed the following configurations: Case 1 - direct gasification (CFB), syngas methanation with hydrogen from electrolysis, Case 2 - indirect gasification (DFB), syngas methanation with hydrogen from electrolysis, Case 3 - indirect gasification (DFB), syngas methanation and CO_2 separation. In the Case 3 assuming methanation of syngas alone (without additional production of hydrogen from electrolysis), CO_2 separation from SNG was additionally assumed due to the required high proportion of CH_4 in the final product in order to inject SNG into the grid. Description of the considered systems is presented in the Table 6.1.

Table 6.1 Description of considered cases of SNG production based on different types of biomass gasification reactor

Case	Description
Case 1 (CFB+EL+M)	assumes a direct steam-oxy biomass gasifier based on circulating fluidised bed (CFB) and syngas fixed-bed methanation with an additional source of hydrogen
Case 2 (DFB+EL+M)	assumes an indirect steam-blown dual fluidised bed biomass gasifier and syngas fixed-bed methanation with an additional source of hydrogen
Case 3 (DFB+M+CCS)	assumes an indirect steam-blown dual fluidised bed (DFB) biomass gasifier consisting of fast internally circulating fluidised bed (FICFB), syngas fixed-bed methanation and CO_2 capture

The first and second cases are considered to be an energy storage options. Hydrogen generators were introduced to meet the hydrogen demands to completely utilize the CO_2 present in the syngas. The model assumes cooperation with hydrogen generators operating in an alkaline environment (AEM). The main assumptions are that the surplus energy from RES drives the water electrolysis unit, where hydrogen and oxygen are produced. These gases are stored in buffer tanks.

For each of the considered cases prior to the methanation reactor, the reactant gases are pressurized and pre-heated. The methanation process takes place in the fixed-bed reactor, where Ru/(Al_2O_3) [84] was assumed as a catalyst. Heat and water are recovered from the methanation step. Steam generated from heat recovery is also used in the gasification process. Moreover, water recovered after the methanation reaction can be purified and used in the electrolysis unit

6.1. Case 1

The first considered case (CFB+EL+M) of SNG production a direct steam-oxy biomass gasifier based on circulating fluidised bed (CFB) is assumed. This case assumes that oxygen, a by-product of the electrolysis process, will be used as a gasifying agent, which makes the flue gas free of nitrogen oxides. In this case the combustion reactions occur simultaneously with the gasification. Assuming CFB gasifier allows to exclude the additional emissions of CO_2 that are not posissible to omit in the case of DFB gasification. Then the syngas is cooled and the water is removed from the gas. Next, before methnation, there are some additional steps for syngas cleaning and removing such impurities as ash, dust, HCl, NH_3 and H_2S. The reactant gases are introduced to the methanation unit in different ratios of H_2:CO_2:CO in order to achieve the highest conversion of particular species to methane. The general flowsheet of this case is presented in the Fig. 6.1.

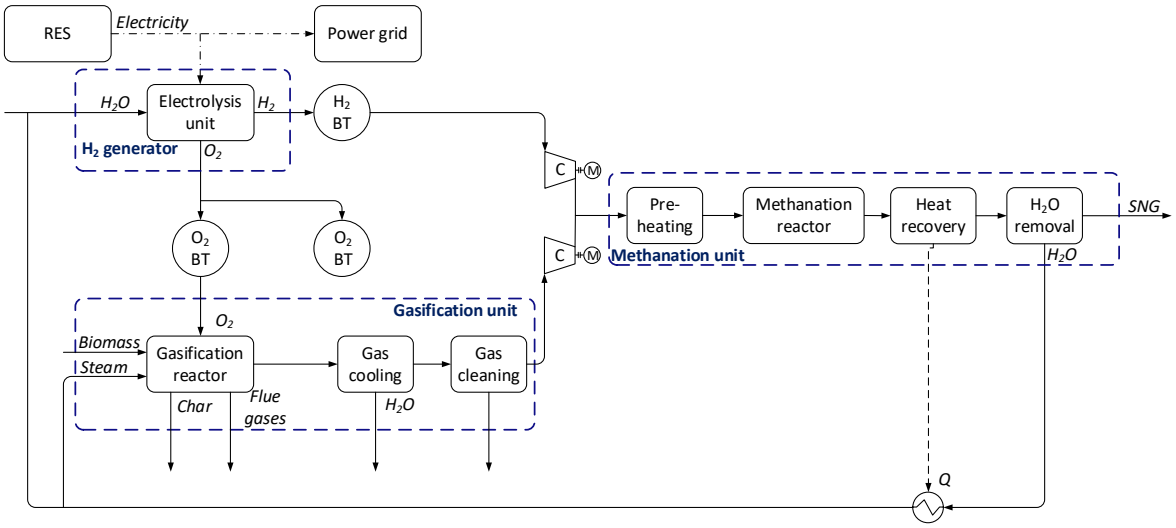

Figure 6.1 General outline of the third system (CFB+EL+M); BT – buffer tank, C - compressor

6.2. Case 2

For biomass gasification also DFB gasifier was assumed. The biomass gasifier used to produce the syngas in this simulation is modelled on the basis of an indirect steam-blown dual fluidised bed (DFB) gasifier consisting of fast internally circulating fluidised bed (FICFB) [81,85]. In this type of gasifier, obtained syngas is rich in H_2 and CO as the flue gas that is released from the combustion reactor is separated from the product gas. This prevents syngas dilution are also less number of gas cleaning equipment is required. While the endothermic process of steam gasification takes place in a bubbling bed, the exothermic combustion takes place in a fast-fluidised bed. The heated bed material is circulated between the two fluidised beds and transports heat from the exothermic to the endothermic process. The second system also assumes that oxygen, a by-product of the electrolysis process, will be used as a gasifying agent. Using pure oxygen instead of air makes the flue gas free of nitrogen oxides and mostly consists of CO_2 which can partly be recirculated to the combustion chamber. The general flowsheet of this case is presented in the Figure 6.2.

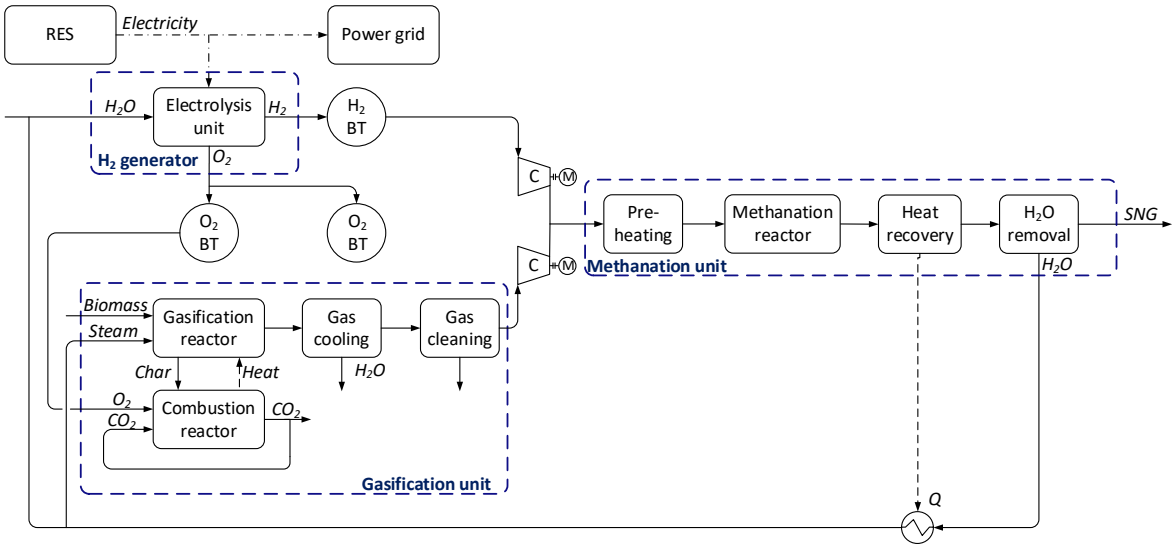

Figure 6.2 General outline of the second system (DFB+EL+M); BT – buffer tank, C - compressor

6.3. Case 3

In the third considered scenario of SNG production (DFB+M+CCS), the syngas obtained from biomass gasification is sent to the methanation reactor directly (Figure 6.3). In this case, H_2 content in syngas is a limiting reactant in the methanation reaction and therefore the remaining (unreacted) CO_2 is captured and sent for permanent storage to achieve negative emissions. Produced biomethane consists mainly of CH_4 and CO_2. The chemical absorption process using activated methyldiethanolamine (a-MDEA) is assumed for CO_2 capture. Activated methyldiethanolamine is a widely used effective solvent for capturing CO_2 at high purity (CO_2 purity > 99.4%) from industrial flue gases streams [86]. The process is characterized by high CO_2 absorption capacity, low energy requirement for solvent regeneration, and selective CO_2 absorption.

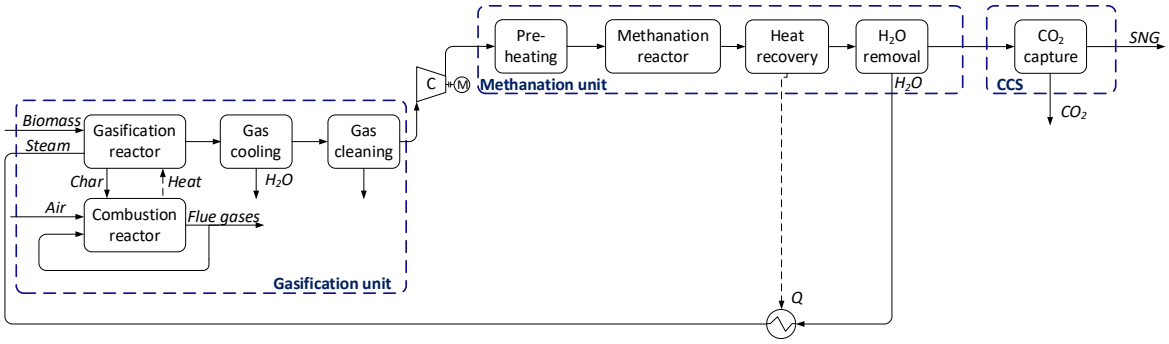

Figure 6.3 General outline of the first analyzed system (DFB+M+CCS) ; C - compressor

6.4.Evaluation of the operation of SNG production systems

6.4.1. Thermodynamic indicators

The overall efficiency of the considered SNG production system can be assessed according to key performance indicators such as cold gas efficiency (6.1), system efficiency (6.2) and carbon recovery (6.3), defined by following formulas:

$$\eta_{\mathrm{En}} = \frac{Ech_{\mathrm{SNG}}}{Ech_{\mathrm{biomass}} + Ech_{\mathrm{H2}}} \tag{6.1}$$

$$\eta_{\mathrm{En,Q}} = \frac{Ech_{\mathrm{SNG}} + Q_{\mathrm{m}}}{Ech_{\mathrm{biomass}} + Nel_{\mathrm{HG}} + \mathrm{E}el_{\mathrm{C}} + Q_{\mathrm{aMDEA}}} \tag{6.2}$$

$$CR = \frac{\dot{m}_{\mathrm{C,SNG}}}{\dot{m}_{\mathrm{C,biomass}}} \tag{6.3}$$

where:

$E_{\mathrm{ch_{SNG}}}$– SNG chemical energy, MWh,

Q_{m} – heat recovered from methanation process, MWh,

$E_{\mathrm{ch_b}}$ – process gas chemical energy, MWh,

$E_{\mathrm{ch_{H2}}}$ – hydrogen chemical energy, MWh,

$E_{\mathrm{el_C}}$ – compressors electricity consumption, MWh,

$N_{\mathrm{el_{HG}}}$ – hydrogen generators input power, MWh,

Q_{aMDEA} – the amount of heat needed for CO_2 capture process, MWh,

$\dot{m}_{\mathrm{C,SNG}}$ – carbon mass flow in SNG, kg_C/h,

$\dot{m}_{C,biomass}$ – carbon mass flow in biomass, kg_C/h.

The cold gas efficiency calculated using the first formula (6.1) refers only to the value of the chemical energy of the produced SNG, supplied hydrogen and biomass. The second definition of system efficiency (6.2) differs from the first one as it also considers that the heat generated in the methanation process is recovered to produce steam for the gasification process. The second formula also considers the energy demands of the methanation process, which are the electricity needed to power the compression system, and the amount of heat needed for the CO_2 capture process. It also does not consider only the chemical energy of hydrogen supplied to the methanation unit but the hydrogen generators input power. The third formula (6.3) defines carbon recovery as the ratio of the mass fraction of carbon in the SNG to the mass fraction of carbon in biomass.

6.4.2. Economic indicators

An economic analysis of the system was performed in order to calculate the SNG break-even price in the considered systems. The unit costs of production in the analysis were scaled using CEPCI (chemical engineering plant cost index) and the reference year was 2022 (CEPCI available for March 2022). The estimations were conducted using discount methods (in accordance with the guidelines of the United Nations Industrial Development Organization, UNIDO [87]), based on the calculation of the Net Present Value (NPV). Net Present Value is a sum of the cash flows realized during the time of analysis and discounted using a known value of the discount rate according to equation 6.4:

$$NPV = \sum_{t=0}^{t=n} \frac{CF_t}{(1+r)^t} \tag{6.4}$$

where:

CF – cash flows, €,

t – subsequent years of operation of the installation,

n – time of analysis, years,

r – discount rate, %.

Cash flows (CF) can be determined according to equation 6.5:

$$CF_t = [-J + S - C_{\text{op}} - T_{\text{in}} + A + L]_t \tag{6.5}$$

where:

J – investment costs, €,

S – revenue from sales, €,

C_{op} – operating costs, €,

T_{in} – income tax, €,

A – depreciation, €,

L – salvage value, €.

Capital investment expenditures (J) were determined by a unit investment cost index, expressed in monetary units and related to characteristic parameters of the sysem, such as power or flow. The total investment outlay can be determined from equation 6.6.

$$J = c_i Y \tag{6.6}$$

where:

c_{i} – unit investment cost, e.g. €/MW,

Y – characteristic parameter of the system.

In order to conduct an economic analysis of the proposed SNG production systems, it is necessary to assume appropriate capital expenditures (CAPEX) and operational expenditures (OPEX) of the proposed installations. One of the method of estimating the capital expenditures of the considered installation is through multiplying the unit investment cost indicator by the characteristic value of the installation, e.g., nominal power or flow.

The break-even price and the levelized cost of production are both important concepts in determining the profitability of a project. However, they are calculated and used in different ways.

The break-even price is the price at which a product generates enough revenue to cover all its costs, including fixed costs and variable costs. This means that at the break-even price, the project is neither making a profit nor a loss. Using the condition of zeroing the net present value (*NPV*=0), with the assumption that the investment costs are incurred in the year 0, it is possible to determine the break-even point of SNG production, defined by the break-even price of SNG sales (eq. 6.7). This price presents the minimum value of SNG sales produced by a given system, necessary to ensure the profitability of the investment after the assumed operation time.

$$C_{\mathrm{SNG}}^{\mathrm{b-e}} = C_{\mathrm{SNG}}(NPV = 0) \tag{6.7}$$

where:

C_{SNG} – SNG selling price, €,

b-e – break-even.

The levelized cost (*LC*) of production is the average cost of producing SNG over the lifetime of the project, taking into account all the costs involved, such as capital costs, operation and maintenance costs, and fuel costs. It was calculated in order to compare calculated values with the literature data on the basis of equation 6.8 [88].

$$LC = \frac{\sum_{t=1}^{n}(CAPEX_{\mathrm{t}} + FOM_{\mathrm{t}} + VOM_{\mathrm{t}}) \cdot (1+r)^{-t}}{\sum_{t=1}^{n}(SNG\ produced_{\mathrm{t}}) \cdot (1+r)^{-t}} \tag{6.8}$$

where:

FOM – fixed operation and maintenance costs, €,

VOM – variable operation and maintenance costs, €.

6.5. Thermodynamic analysis of the selected SNG production processes

6.5.1. Methodology and assumptions

To perform a thermodynamic analysis of the considered SNG production systems, a simulation of biomass gasification and methanation units was carried out using Aspen Plus [73]. The equation of state used for thermodynamic property estimations was the Peng-Robinson with Boston-Mathias modifications. Figures 6.4 - 6.6 presents the main assumptions for the design conditions at characteristic points

and chemical reactions implemented for gasification and methanation processes simulation.

The biomass gasification model predicts the syngas composition resulting from biomass gasification for different temperatures of the process. The biomass gasification process was modelled in three main stages. The dry fuel was directed to the decomposition (DECOMP) stage of the gasification process, which was simulated by the yield reactor (*RYield*). In this stage, biomass was converted into individual components of carbon, nitrogen, oxygen, hydrogen and ash, by assuming the yield distribution according to the biomass analysis. To simulate the next stage of the gasification process (GASIF) the equilibrium reactor (*RGibbs*) was used with specified gasification reactions (with a zero temperature approach set for each reaction). Gasifying agents used for the process are steam and oxygen (assumed steam to fuel ratio = 0.42 and oxygen to fuel ratio = 0.48 for gasification at 850 °C). In the case of CFB gasification (Figure 6.4) combustion takes place directly in the gasification reactors, so no additional reactor is assumed for this process. In DFB gasification (Figure 6.5) a fraction of carbon and ash from biomass goes to the combustion process (COMB), simulated by *RStoic* reactor with no specific reactions set, and the heat flux from the combustion process is coupled with the gasification section of the simulation. The main assumption is that the combustion step provides the needed amount of heat to the gasification process and the overall heat balance is equal to zero. The assumptions needed for the biomass gasification simulation model are as follows:

- biomass LHV = 19.09 MJ/kg (elementary composition: carbon = 51.19%, hydrogen = 6.08%, oxygen = 41.3%, nitrogen = 0.2%, sulphur = 0.02%, chlorine = 0.05%, ash = 1.16%) [81],
- pressure drops neglected,
- char is 100% carbon,
- fuel bond N_2 converted to NH_3, CL to HCl, S to H_2S,
- tar formation not considered.

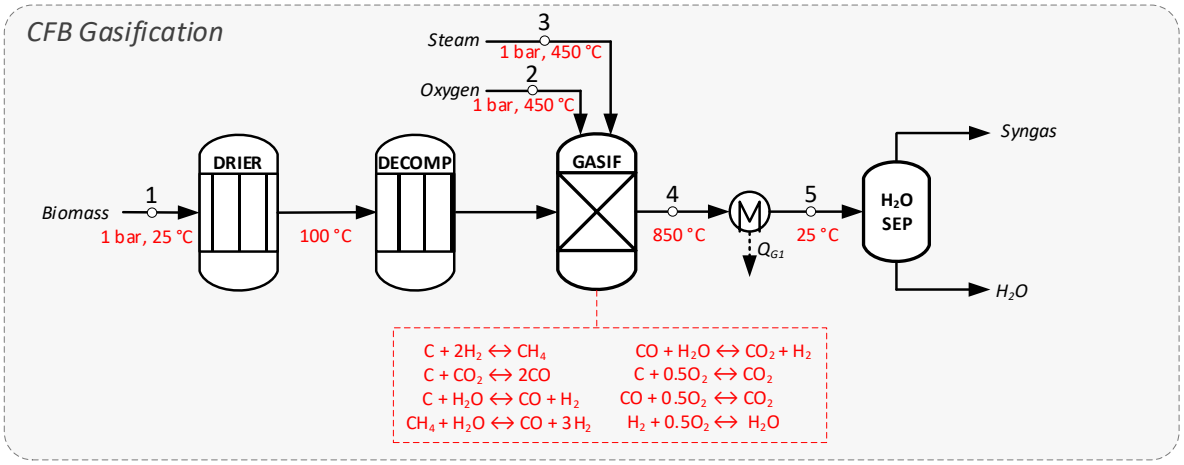

Figure 6.4 The main assumptions for the thermodynamic model of the CFB gasification process

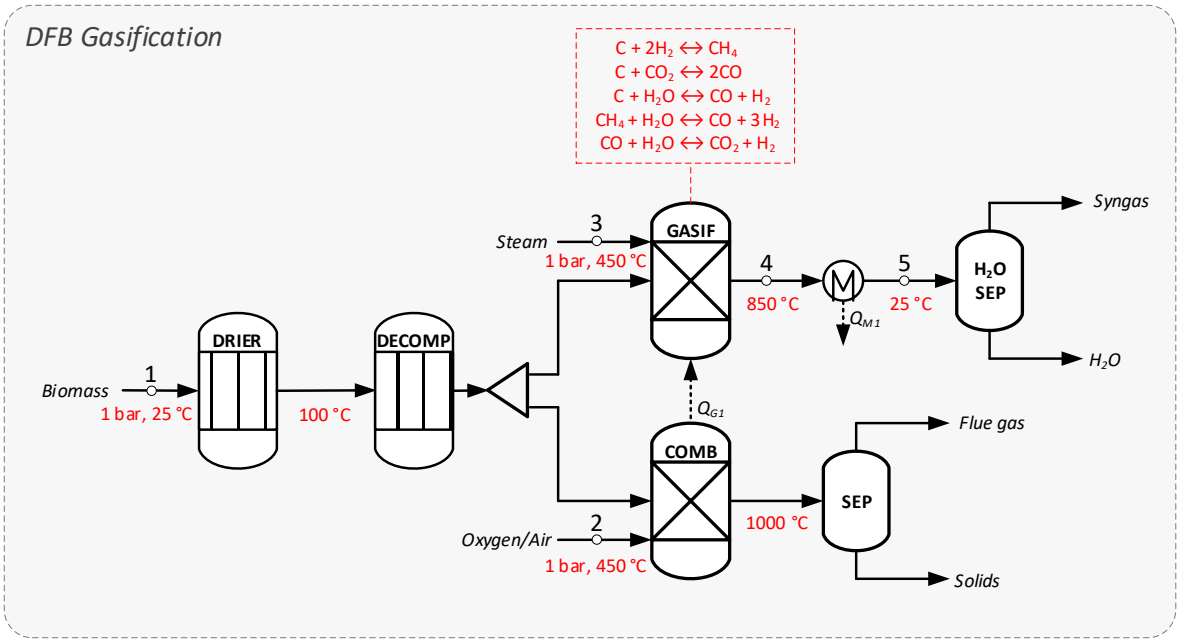

Figure 6.5 The main assumptions for the thermodynamic model of the DFB gasification process

After cleaning, the water content in syngas from the gasification simulation is removed and gas is used in the methanation process (METH). It is modelled with an equilibrium reactor (*REquil*) with specified reactions of carbon dioxide hydrogenation, carbon monoxide hydrogenation and water-gas shift reaction. Prior to the methanation process, there are compressors to increase the pressure of the reactant gases and a heat exchanger for setting the required temperature of inlet gases. The assumptions needed for the methanation process model are as follows:

– temperature of catalyst bed T_m = 350 °C,

– pressure drops neglected,

– isentropic efficiency of compressors $\eta_{i,c}$= 88%,

– mechanical efficiency of compressors $\eta_{m,c}$= 99%.

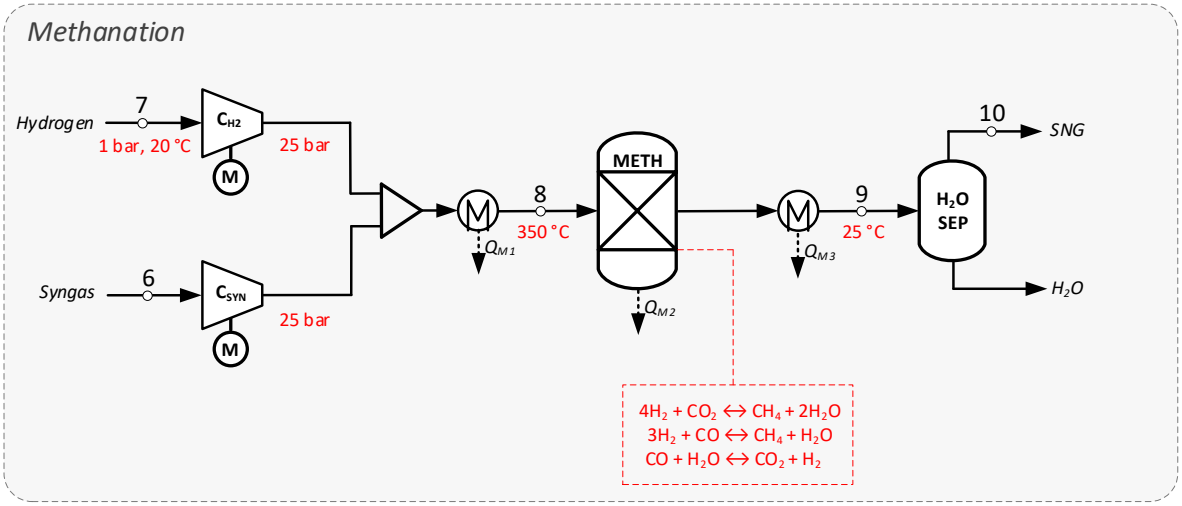

Figure 6.6 The main assumptions for the thermodynamic model of the methanation processes

A CO_2 capture model consists of an absorption and a desorption column, a solution lean-rich heat exchanger for heat recovery, a solution pump, a reboiler as well as a reflux-system for the desorber. The assumptions made for the carbon dioxide capture simulation model are as follows:

– carbon capture rate r_c = 95%,

– steam inlet pressure p_{H_2O} = 3 bar,

– steam inlet temperature T_{H_2O}= 180 °C.

6.5.2. Results and discussion

In the first stage of the calculations, the individual elements of the model were validated. The composition of the syngas from biomass gasification used in the simulation in comparison to the literature data is presented in Table 6.2. In both cases, a gasification temperature of 850 °C was assumed. The highest relative error between the values from the simulation and the literature [81,89] for the DFB gasification process is equal to 1.5%, and in the case of CFB gasification model error value is equal to 0.73% assuming dry gas composition.

Table 6.2 Composition of syngas from biomass gasification achieved from the simulation in comparison to literature data (for the gasification temperature of 850 °C)

	DFB		CFB	
	Literature [81]	Model	Literature [89]	Model
H_2	45.8	45.8	32.6	32.7
CO	21.6	21.7	30.2	30.8
CH_4	10.0	11.5	11.8	11.1
CO_2	21.2	19.8	25.4	25.5

Figure 5.7 presents the results of the simulation of the process models for (a) gasification and (b) methanation processes. The methanation process was validated with the work by Falbo et al. [90] and Bailera et al. [91]. In the simulation, the equilibrium reactor model was used and it was found that it reflects the experimental results for the catalyst temperature range of 350-450 °C (the value of 350 °C was adopted for further calculations).

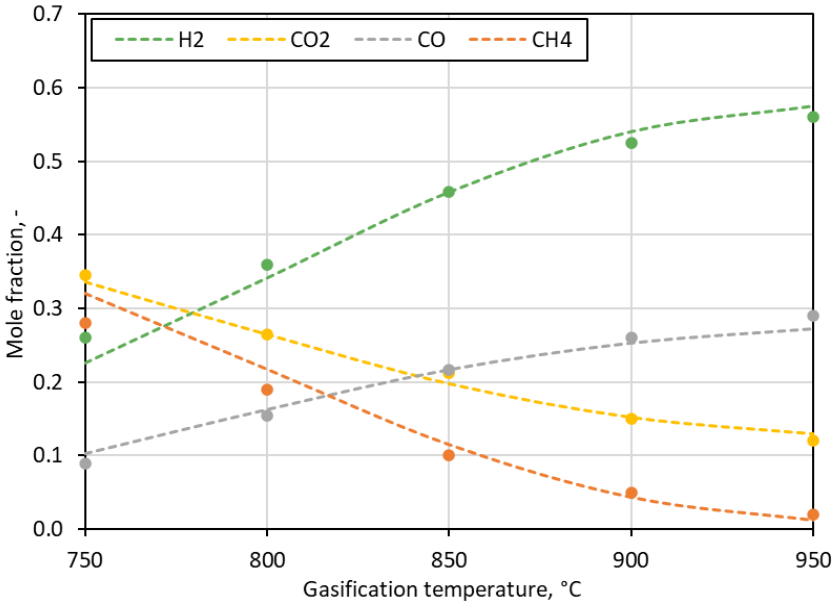

a)

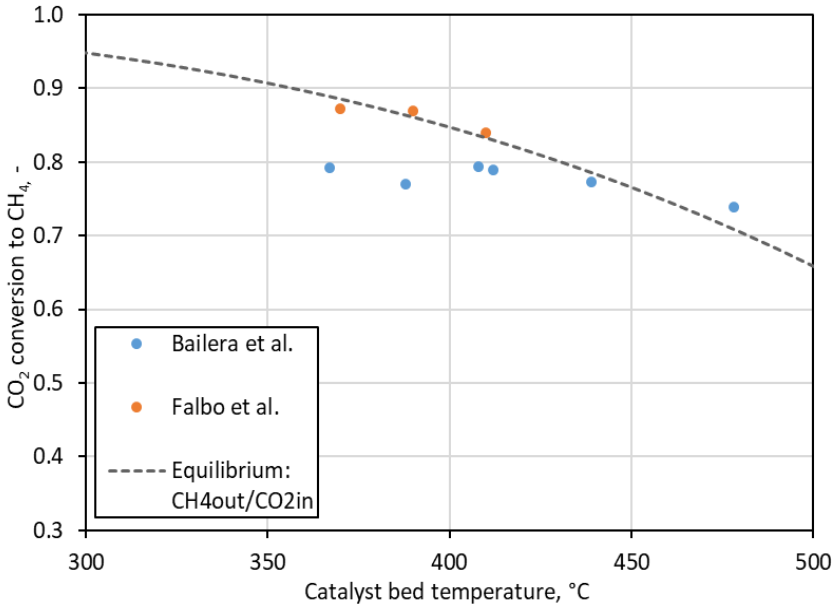

b)

Figure 6.7 Results of biomass DFB gasification (a) and methanation (b) processes simulation

The methanation process was verified in terms of various conditions set in the biomass gasification process (such as gasification temperature), which affect the composition of the resulting syngas. It also has an influence on the amount of additional hydrogen from the water electrolysis process needed for methanation. In order to obtain SNG composition with CH_4 content equal to or higher than 90% and H_2 content equal to 5% or less [92], it was necessary to perform a methanation

simulation in the nonstoichiometric ratio of H_2:CO_2:CO. A sensitivity analysis was carried out for various pressures of the methanation process, to obtain the desired SNG composition (at least 90% methane and 5% or less hydrogen in SNG).

Assuming 8000 h of annual operation of gasification and methanation units (consequently, the CO_2 sequestration unit also works for this number of hours per year) and 4000 h of operation of hydrogen generation unit, the annual energy streams of the considered SNG production system were calculated. The shorter operation time of hydrogen generators adopted for the analysis is due to the fact that they are powered by energy from RES dependent on weather conditions, in contrast to gasification and methanation units, which can work continuously. The results of the analysis for proposed SNG production cases are presented in Tables 6.3 – 6.5.

Table 6.3 Selected results from the first (CFB+EL+M) SNG production system considered model (points according to Fig.6.5 and 6.6)

Stream	Parameter	Unit	Value
1	Biomass stream	kg/h	100
	Biomass LHV	MJ/kg	19.09
2	Oxygen stream	kg/h	30.4
3	Steam stream	kg/h	20.0
6	Syngas stream	kg/h	130.71
	Syngas LHV	MJ/kg	11.97
7	Hydrogen stream	kg/h	18.06
	Hydrogen LHV	MJ/kg	119.83
	Hydrogen generator power	MW	1.98
	Hydrogen generator efficiency [80]	%	71
10	SNG stream	kg/h	71.95
	SNG LHV	MJ/kg	43.66
	SNG chemical energy	MW	0.87

Table 6.4 Selected results from the second (DFB+EL+M) SNG production system considered model (points according to Fig.6.4 and 6.6)

Stream	Parameter	Unit	Value
1	Biomass stream	kg/h	100
	Biomass LHV	MJ/kg	19.09
2	Oxygen stream	kg/h	48.3
3	Steam stream	kg/h	42.0
6	Syngas stream	kg/h	92.89
	Syngas LHV	MJ/kg	15.06
7	Hydrogen stream	kg/h	9.70
	Hydrogen LHV	MJ/kg	119.83
	Hydrogen generator power	MW	1.06
	Hydrogen generator efficiency [80]	%	70
10	SNG stream	kg/h	49.10
	SNG LHV	MJ/kg	44.36
	SNG chemical energy	MW	0.60

Table 6.5 Selected results from the third (DFB+M+CCS) SNG production system considered model (points according to Fig.6.4 and 6.6)

Stream	Parameter	Unit	Value
1	Biomass stream	kg/h	100
	Biomass LHV	MJ/kg	19.09
2	Air stream	kg/h	210
3	Steam stream	kg/h	42
6	Syngas stream	kg/h	92.89
	Syngas LHV	MJ/kg	15.06
10	SNG stream (before CO_2 separation)	kg/h	81.62
	SNG LHV	MJ/kg	14.80
	Stream of CO_2 captured	kg/h	54.62
	Heat flow stream to the reboiler	MJ/h	96.95
	SNG stream (after CO_2 separation)	kg/h	27.00
	SNG LHV	MJ/kg	44.74
	SNG chemical energy	MW	0.34

Table 6.6 presents the composition of syngas and SNG produced within considered installations.

Table 6.6 Composition of syngas and SNG for considered cases of SNG production systems

	CFB+EL+M		DFB+EL+M		DFB+M+CCS	
	syngas	SNG	syngas	SNG	syngas	SNG
H_2	0.2979	0.0481	0.4629	0.0499	0.4629	0.0162
CO_2	0.2374	0.0518	0.2009	0.0461	0.2009	0.0411
CO	0.3369	0.0001	0.2189	0.0001	0.2189	0.0016
CH_4	0.1277	0.9000	0.1173	0.9040	0.1173	0.9411

The reference level for the analyzed systems in the performed calculations is the same biomass stream used in each case (100 kg/h). From the same amount of biomass, it is possible to produce the largest amount of synthetic natural gas (6979.65 MWh of SNG annually) in the case of a first system based on direct steam-oxy biomass gasification and syngas methanation with an additional source of hydrogen (CFB +EL+M). On an annual basis, this is about 1.4 times more than the amount of SNG generated for the second case based on indirect direct steam-oxy biomass gasification and syngas methanation with an additional source of hydrogen (DFB+EL+M), which equals to 4839.79 MWh_{SNG} and about 2.6 times more than for the third case (DFB+M+CCS), which is 2683.90 MWh_{SNG}. This is due to the fact that the largest amount of syngas is obtained in the case of direct (CFB) gasification (in the case of indirect (DFB) gasification, part of the feedstock is separated for the combustion process).

Using the data in Table 6.7 and the definitions of key performance indicators formulated in (6.1-6.3), it is possible to calculate the energy efficiency for the considered cases of SNG production. For the first case (CFB+EL+M) the cold gas efficiency of the power to SNG plant is equal to 77.10%. For the second case (DFB+EL+M), which assumes the use of hydrogen produced in the electrolysis process and complete utilization of carbon oxides in the methanation process, the cold gas efficiency is 70.92%. And for the third case (DFB+M+CCS), assuming the production of biomethane by biomass gasification and methanation with CO_2 capture, the cold gas efficiency value is 63.27%. The negative CO_2 emission for the third case is equal to 437 tonnes of CO_2 annually by producing 9663.8 GJ of biomethane.

Table 6.7 Results of the calculated key performance parameters of the considered SNG production systems

	Case 1 CFB +EL+M	Case 2 DFB+EL+M	Case 3 DFB+M+CCS
Biomass annual use	4242.22 MWh	4242.22 MWh	4242.22 MWh
Hydrogen annual use	4810.24 MWh	2582.20 MWh	-
SNG annual production	6979.65 MWh	4839.79 MWh	2683.90 MWh
Cold gas efficiency (η_{En})	77.10%	70.92%	63.27%
System efficiency ($\eta_{\mathrm{En,Q}}$)	75.58%	72.40%	69.10%
Carbon recovery (*CR*)	98.16%	67.61%	37.69%

Considering the definition of system efficiency (6.2) the calculated values are equal to 75.58%, 72.40% and 69.10% respectively for the successive cases of the considered SNG production systems. The main factors that are influencing methanation system losses are syngas and hydrogen compressors and also certain heat losses on the reactor that cannot be recovered.

Looking at carbon recovery values of the particular systems it can be seen that the *CR* value calculated for the third system (DFB+M+CCS) is significantly lower than in the cases of the systems with complete CO_2 utilization with renewable hydrogen. The differences in *CR* values between cases involving the use of additional hydrogen from the electrolysis process are primarily determined by the type of gasification reactor used. In the case of the DFB reactor, a portion of the char from biomass is separated for combustion and heat generation for the gasification reaction. The carbon dioxide produced during the oxy-combustion process is mostly recirculated back into the combustion chamber to maintain stable reaction conditions, dilute oxygen, and keep the combustion temperature stable. Therefore, the highest value of carbon recowery was found for the first system (CFB+EL+M).

6.6.Economic analysis of the selected SNG production processes

6.6.1. Assumptions

Economic analysis was performed regarding the specific assumptions for the considered power to gas system presented in Table 6.8. The depreciation of investment costs during the first 10 years of the investment was assumed. It was also

assumed that the investment will be recovered by selling the products from the process without adding any commercial credits. Additional income from selling electrolysis co-product, oxygen, can decrease the annual costs of the plant.

Table 6.8 Main assumptions for economic analysis

Parameter	Unit	Value
Lifetime	year	20
Annual operation time (G+M)	h	8000
Annual operation time (EL)	h	4000
Construction time	year	1
Own means in the investment costs	%	100
Discount rate (*r*)	%	5.0
Income tax rate (*p*)	%	25.0
Personnel annual salary	€/person	36000
Number of personnel	persons	6

Table 6.9 describes capital investment costs for the most important installation of the considered systems.

Table 6.9 Assumed unit capital investment costs of analysed installations

Installation	Unit	Cost (2020)
Hydrogen generator [93]	€/kW_{el}	630
Hydrogen storage [94]	€/Nm^3	33
Oxygen storage [94]	€/Nm^3	16.5
DFB biomass gasification [95]	k€	304
CFB biomass gasification [95]	k€	391
Syngas cleaning and cooling [96]	€/Nm^3/h	320
Methanation [24]	€/kW_{SNG}	425
Carbon capture [97]	k€	97.4
Grid injection [98]	k€	75

Other values assumed for estimation of operational costs of proposed SNG production plants are presented in the Table 6.10.

Table 6.10 Assumptions for operational costs estimation

Parameter	Unit	Cost
Water price [98]	€/kg	0.00069
Oxygen sale price [99]	€/kg	0.049
Gas cleaning [64]	€/tonne	2.4
Water demineralization [64]	%(variable costs)	2.43
Hydrogen storage [98]	%(H_2 storage CAPEX)	1.5
Oxygen storage [98]	%(O_2 storage CAPEX)	1.5
Ash disposal [64]	%(variable costs)	0.36
Pre-reformer and catalyst [64]	%(variable costs)	4.5
Carbon capture [64]	%(CO_2 separation CAPEX)	2
Grid injection [98]	%(grid injection CAPEX)	2

6.6.2. Results and discussion

Economic analysis was performed in order to verify which of the proposed systems is the most competitive. Currently, power to methane technology is not very competitive on the market because of the high expenditures on electrolyzers. Among technologies that assumed investment in hydrogen generators, the CAPEX of the first case (CFB+EL+M) is visibly higher (Figure 6.8). This is due to the difference in the syngas composition as both cases assume different types of gasifiers. In the second case (DFB+EL+M), syngas from gasification contains much more hydrogen than in the third system case. That is why for the first case a bigger electrolyzer is needed to cover all the system needs for hydrogen and, thus, investment in a hydrogen generator is much higher. The size of the gasification unit for all cases was the same, and the methanation unit sizes differ among the cases as the number of process gases introduced to the system varied. The total CAPEX calculated for the first and second cases of the SNG production system is equal to 3 023 085 € and 1 904 031 € (Fig. 6.8), respectively. The largest percentage share (55.7% for the first and 47.5% for the second case) constitutes the investment costs of hydrogen generators. However, it is predicted that the capital expenditures will decrease in the following decades [100], which could significantly influence the total CAPEX of the investment. The second largest investment is similar for the methanation units (17.5% and 21.6% for the Case

1 and Case 2 respectively) and gasification units (16.6% and 18.3% and for the Case 1 and Case 2 respectively).

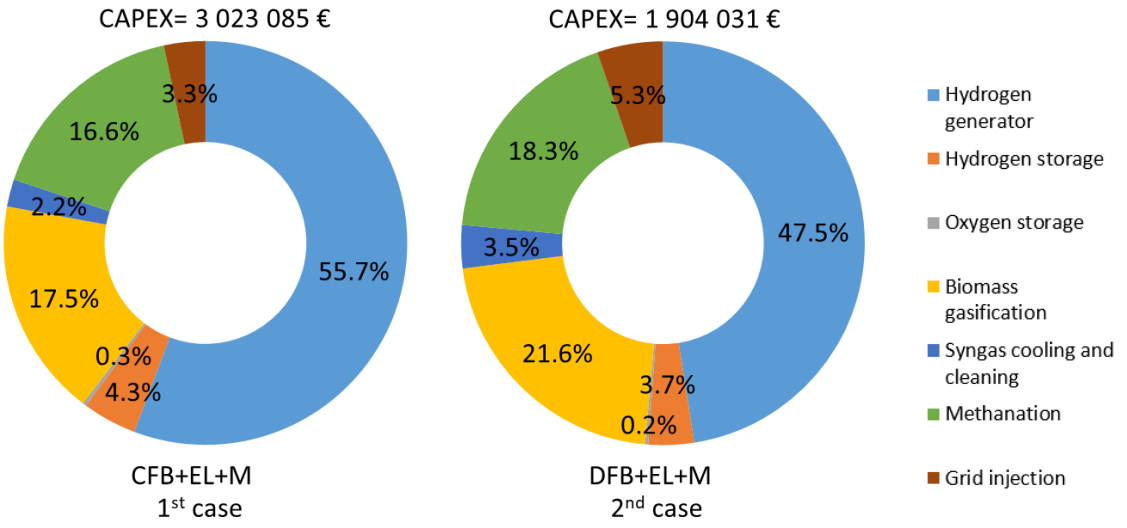

Figure 6.8 Shares of individual investment outlays on total CAPEX of system DFB+EL+M and CFB+EL+M

The calculated total capital cost (CAPEX) of the considered cases shows, that the lowest investment in capital expenditures is on the third case (DFB+M+CCS), so the one excluding electrolyzers work (Fig. 6.9). The CAPEX value for the third case scenario equals 901 966 € and the biggest share (45.6%) is covered by the gasification unit, followed by methanation (21.4%).

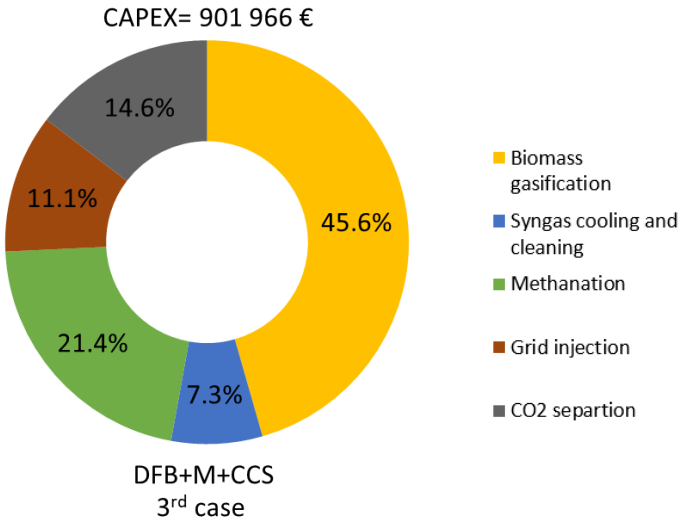

Figure 6.9 Shares of individual investment outlays on total CAPEX of system DFB+M+CCS

The total value of operational expenditures (OPEX) for a one-year operation is equal to 319 566 € (CFB+EL+M), 267 552 € (DFB+EL+M) and 183 740 € (DFB+M+CCS), excluding the costs of electricity from RES purchased to drive the hydrogen generators. As the size of the gasification unit is assumed the same for every considered case, the fuel costs are constant and equal to 40 000 €/year.

Variable operation and maintenance costs assumed consist mainly of electrical energy costs in biomass gasification and methanation processes, gas cleaning costs, renewable electricity and water for hydrogen generators costs. Fixed operation and maintenance costs included gasifier bed material, ash disposal, methanation catalyst, grid injection, personnel, CO_2 separation, water demineralization, and H_2 and O_2 storage. All the calculated results are presented in Table 6.11.

Table 6.11 Results of operational and maintenance costs calculated for all considered cases

	Case 1 CFB +EL+M	Case 2 DFB +EL+M	Case 3 DFB +M+CCS
	Variable O&M costs		
Hydrogen generator	885 €/y	468 €/y	-
Biomass gasification	18 581 €/y	18 581 €/y	18 581 €/y
Syngas cooling and cleaning	1 920 €/y	1 920 €/y	1 920 €/y
Methanation	30 616 €/y	20 751 €/y	10 566 €/y
Total	**92 002 €/y**	**41 720 €/y**	**31 067 €/y**
	Fixed O&M cost		
Hydrogen generator	2 236 €/y	1 986 €/y	-
Hydrogen storage	1 971 €/y	1 043 €/y	-
Oxygen storage	134 €/y	71 €/y	-
Biomass gasification	745 €/y	662 €/y	576 €/y
Syngas cooling and cleaning	331 €/y	294 €/y	256 €/y
Methanation	4 140 €/y	3 677 €/y	3 198 €/y
Grid injection	2 007 €/y	2 007 €/y	2 007 €/y
CO_2 separation	-	-	2 637 €/y
Other	144 000 €/y	144 000 €/y	144 000 €/y
Total	**227 564 €/y**	**225 832 €/y**	**152 673 €/y**

Figure 6.10 presents the levelised cost of SNG production, which was calculated as a ratio of the sum of annual investment costs fixed and variable operation and maintenance costs to the total amount of SNG produced. Calculated values of the levelised cost of SNG production are strictly dependent on the assumed cost of biomass and electricity from RES. For the purposes of comparing the three considered cases, the following prices were assumed: biomass = 9.43 €/MWh (50 €/t) and electricity = 50 €/MWh. The levelised cost of SNG production is equal to 104.54 €/MWh_{SNG} for CFB+EL+M, 112.12 €/MWh_{SNG} for DFB+EL+M and 100.17 €/MWh_{SNG} for DFB+M+CCS. The amount of produced SNG rigorously influences the distribution of the individual parts that make up the final cost of SNG production. In the case of the first system, variable operating and maintenance costs account for the largest share, while in the other two cases where SNG production was lower, fixed operating and maintenance costs account for the largest share.

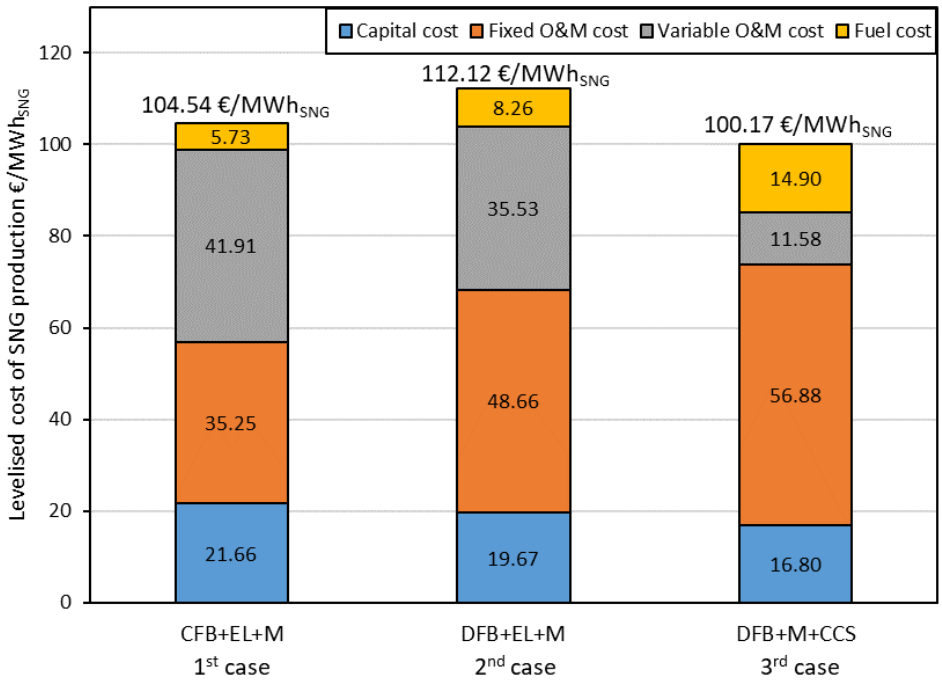

Figure 6.10 Results of the calculated levelised cost of SNG production for considered cases

Due to the changing prices of goods and services over the years the sensitivity analysis of +/- 20% of the investment costs to selected parameters (Figure 6.11). The difference in total OPEX costs calculated for all the cases do not differ a lot. The capital expenditure related to hydrogen generators has the greatest impact on the total CAPEX in cases considering using renewable hydrogen (CFB+EL+M and DFB+EL+M). The hypothetical 20% change in the investment costs for hydrogen generators would contribute to a reduction of the SNG break-even price by 6.68 €/MWh_{SNG} for the case CFB+EL+M and by 4.22 €/MWh_{SNG} for the case DFB+EL+M. With the case of no hydrogen generators in the system (DFB+M+CCS), the biggest impact on total CAPEX is the capital cost of the biomass gasification unit. For DFB+M+CCS system configuration, SNG break-even price would change by 6.19 €/MWh_{SNG} in the case of a 20% difference in investment costs with the reference to base case scenario.

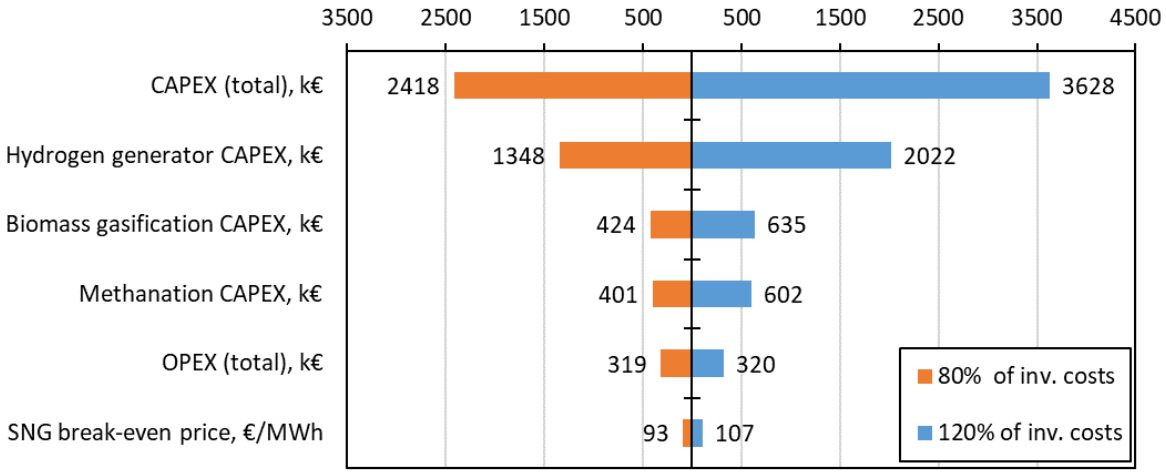

a)

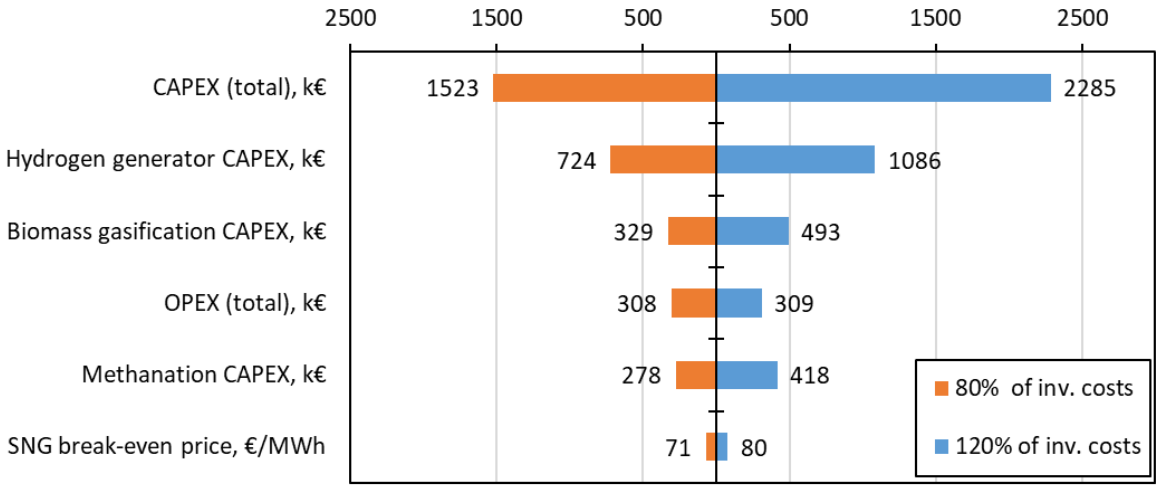

b)

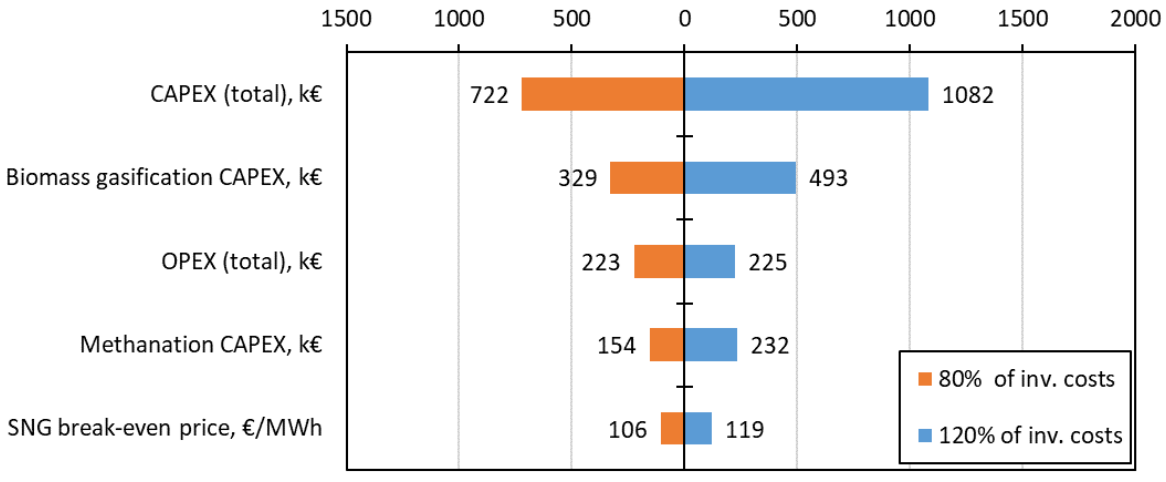

c)

Figure 6.11 Results of sensitivity analysis of selected CAPEX, OPEX and SNG break-even price values for +/- 20% change in capital expenditures (2022 base case) for cases: a) CFB+EL+M, b) DFB+EL+M, c) DFB+M+CCS

Given the uncertainty of feedstock prices, including, in particular, fluctuating energy prices from RES, Figure 6.12 presents the results of the sensitivity analysis of the SNG break-even price for the range of biomass prices of 50-100 €/tonne (9.43-18.86 €/MWh) and electricity from RES for the assumed range of 0-100 €/MWh. Two scenarios were considered for each case: the 2020 (Fig. 6.12a) and 2022 (Fig. 6.12b) year scenario. This sensitivity analysis was performed for the years 2020 and 2022 mostly in order to compare calculated SNG break-even prices of the proposed systems with the NG market price in the EU as the fuel market situation over those years has changed drastically due to the economic crisis and the cessation of import of natural gas from Russia by most European Union countries. For the assumed ranges of feedstock prices, the break-even price of SNG for the Case 1 (CFB+EL+M) of the considered systems prices differ from 58.88 €/MWh_{SNG} to 129.28 €/MWh_{SNG} for the year 2020 and from 67.25 €/MWh_{SNG} to 137.65 €/MWh_{SNG} in the year 2022. The break-even price of SNG for Case 3 (DFB+M+CCS) ranged from 105.52 €/MWh_{SNG} to 121.27 €/MWh_{SNG} in the 2020 year scenario and from 112.60 €/MWh_{SNG} to 128.35 €/MWh_{SNG} in the 2022 year scenario. As this case is not dependent on the varied prices of electricity from RES, the SNG break-even price remained constant. The similarity of SNG break-even prices of Case 1 considered with Case 3 is directly connected to the assumed price of electricity from RES, as up to 60 €/MWh, the break-even price of SNG produced in Case 1 of the system is lower than the calculated price of SNG for Case 3. For the higher electricity prices, it is competitive or even higher than the DFB+M+CCS case. The lowest SNG break-even price is represented by Case 2 of the considered systems (DFB+EL+M) and prices differ from 52.67 €/MWh_{SNG} to 92.97 €/MWh_{SNG} for the year 2020 and from 57.87 €/MWh_{SNG} to 98.17 €/MWh_{SNG} in the year 2022.

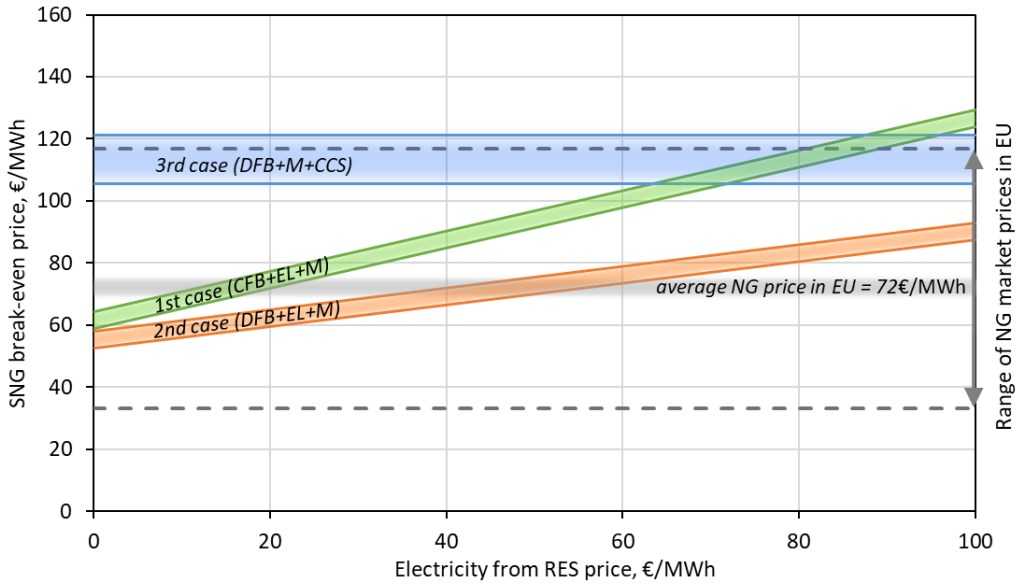

a)

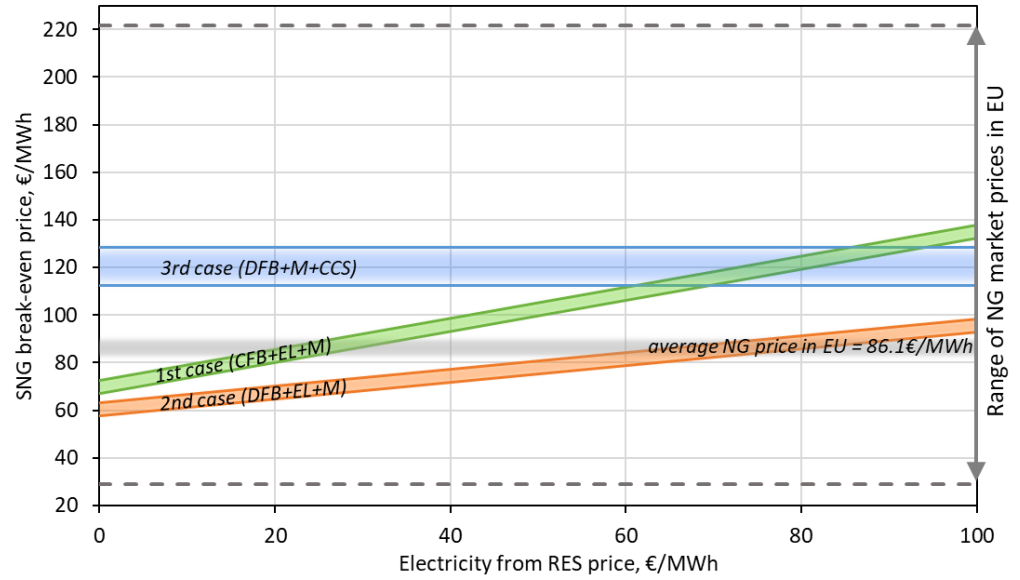

b)

Figure 6.12 Results of the sensitivity analysis of SNG break-even price for variable prices of biomass feedstock and electricity from RES a) 2020 scenario, b)2022 scenario

According to data available in [101], natural gas market price across the EU for the first half of 2020 was in the range of 33.2 €/MWh (Hungary) – 116.7 €/MWh (Sweden) with an average price of 72.0 €/MWh, and for the first half of 2022 was in the range of 29.1 €/MWh (Hungary) – 221.6 €/MWh (Sweden) with an average price of 86.1 €/MWh. Natural gas price varies greatly depending on a specific country and

that is the main reason why the competitiveness of the proposed systems is not so easy to assess. Looking at the average NG price in the EU for the given years it can be stated that for the assumed feedstock prices CFB+EL+M system (Case 1) can be competitive when the price of electricity from RES is not higher than 57.9 €/MWh for 2020 and 70.5 €/MWh in the 2022 scenario, while DFB+EL+M (Case 2) can be competitive when the price of RES electricity does not exceed 63.9 €/MWh for 2020 and 57.9 €/MWh in 2022. Still, the competitiveness of the proposed systems with the natural gas market has to be considered on a country-by-country basis due to the high divergence in NG market prices and different energy policies.

Figure 6.13 presents the results of the analysis of the break-even price of SNG calculated for each of the proposed system cases for the years: 2018 (before the economic crisis), 2020 (COVID-19 breakthrough) and 2022 (during the economic crisis). The assumed average monthly prices of electricity from RES and natural gas were assumed according to [102] while the assumed price of biomass for 2018 was set at 50 €/tonne and increased by inflation in the following years. As it is presented in the graph, prices of natural gas in the exemplary (Polish) market were quite stable and low in the years 2018 and 2020 in comparison to the year 2022. Referring to years 2018 and 2020, the calculated SNG break-even prices of the considered systems were not competitive with the market natural gas price. Taking into account the very high prices of natural gas in 2022, it can be concluded that the calculated SNG break-even price for the second system (DFB+EL+M) were in each case lower than the price of NG, while for the first case (CFB+EL+M) the prices of SNG were lower than the NG price for 75% of the year, and in the third case proposed (DFB+M+CCS) for 42% of the year.

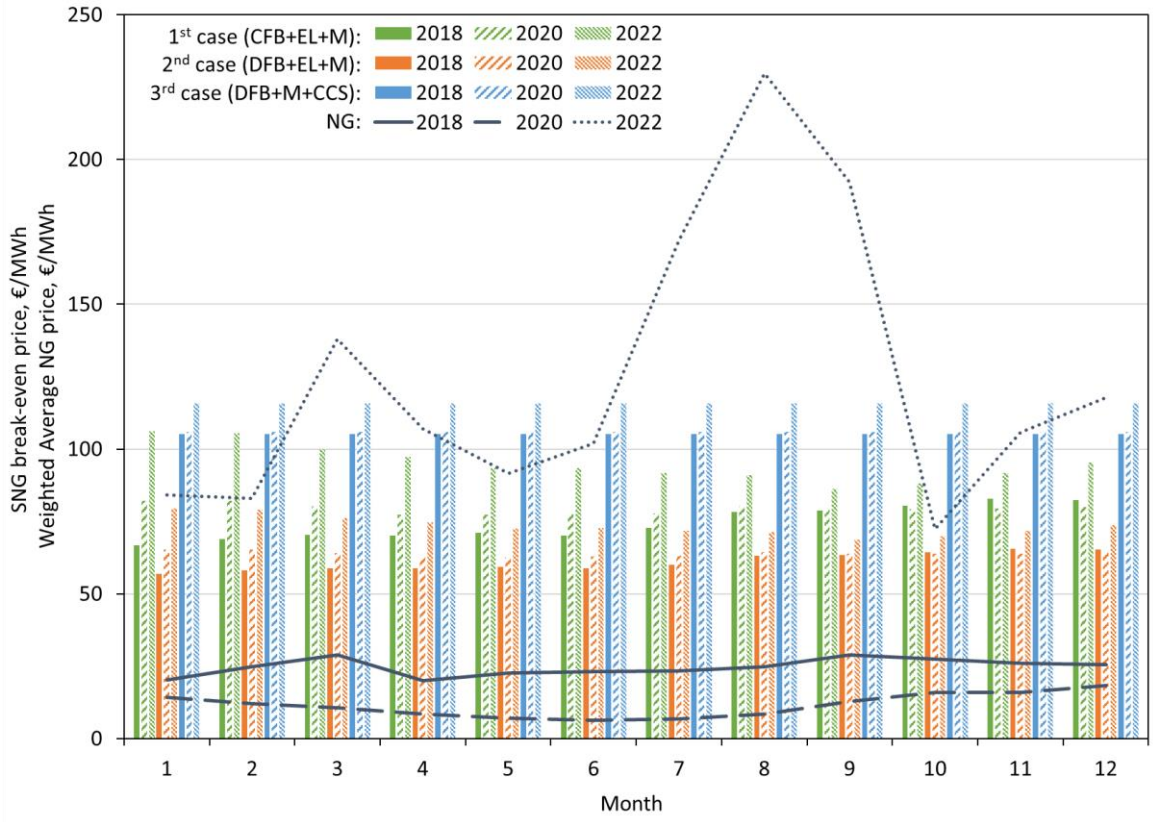

Figure 6.13 Results of the SNG break-even price for variable prices of electricity from RES (data from [102]) calculated for years 2018, 2020 and 2022

Based on the conducted analysis, it can be stated that the analyzed cases of SNG production can achieve high efficiencies and can be competitive with the natural gas market. In addition, the production of SNG from renewable sources can help to reduce dependence on fossil fuels and increase energy security. However, there are also some challenges associated with the use of SNG in power and heat generation. One of the main challenges is the cost of production and distribution, which can be higher than for conventional fuels. In addition, the availability of renewable energy sources for SNG production can be variable, which can impact the reliability and cost of the fuel. Despite these challenges, the potential for SNG production as an energy storage option is significant, provided that SNG production costs are lower in the future.

7. Synthetic natural gas potential market

With reference to the power to SNG systems analyzed in Chapter 6, and mainly based on the thermodynamic outputs and economic data, a rough idea of the potential market opportunities for SNG production is briefly described in the present chapter. The proposed SNG production systems show high potential as energy storage systems (in terms of size, performance and environmental aspects), but production costs must be reduced to make the technology more viable.

In the whole value chain of the proposed solutions, hydrogen generators account for the largest share of the capital costs of power to SNG systems, however, the investment in hydrogen generators is projected to decrease in the future [100]. For the year 2050, as presented in Table 7.1, it is estimated that the capital costs for hydrogen generators will drop significantly. This will contribute primarily to lowering the cost of hydrogen generation, and therefore to lowering the cost of SNG production. It can also be assumed that by 2050, with lower hydrogen production costs, further conversion to SNG will not be economically justified. However, this is dependent on the level of development of the hydrogen economy in the respective countries.

Table 7.1 Key performance parameters for different electrolyser technologies in 2020 and in 2050 [100]

	2020				2050			
	AEL	PEM	AEM	SOEC	AEL	PEM	AEM	SOEC
Cell pressure, bar	<30	<70	<35	<10	>70	>70	>70	>20
System efficiency, kWh/kgH_2	50-78	50-83	57-69	45-55	<45	<45	<45	<40
Lifetime, 10^3 hours	60	50-80	>5	<20	100	100-120	100	80
Capital costs for stacks only (> 1 MW), USD/kW_{el}	270	400	-	>2000	<100	<100	<100	<200
Capital costs for the entire system (> 10 MW), USD/kW_{el}	500-1000	700-1400	-	-	<200	<200	<200	<300

Possible variants of SNG utilization are shown in Figure 7.1. The most useful pathways for using SNG are as a fuel in power and heat generation or in mobility. The diagram shows end-users of SNG or biomethane, however, SNG injection into the natural gas grid represents a huge potential market. The goal of power to methane plants is to produce SNG with a similar composition to natural gas. As a result, unlike hydrogen, no special constraints should be expected for SNG injection into the grid. Pipelines of natural gas grids were not designed to withstand hydrogen's properties, such as higher than in case of natural gas permeability and corrosive properties. The hydrogen concentration in gas grids must be controlled for safety reasons. In Europe, depending on the country, the maximum hydrogen concentration permitted by quality regulations for gas injection into grids ranges from 0.1 to 10% in volume [103].

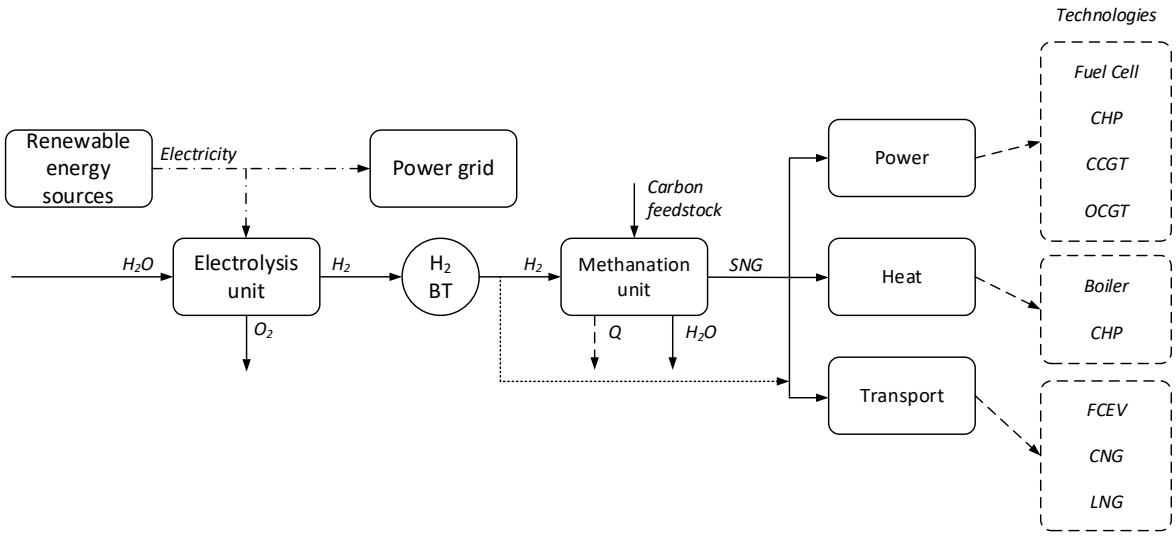

Figure 7.1 Potential power to SNG market pathways [104]; where: CHP – Combined Heat and Power, CCGT – Combined Cycle Gas Turbine, OCGT – Open Cycle Gas Turbine, FCEV – Fuel Cell Electric Vehicle, CNG – Compressed Natural Gas; LNG – Liquified Natural Gas

The great advantage of SNG in terms of heat and power generation technologies is the fact that it can be basically used as conventional natural gas within existing infrastructure. For power generation such videly known technologies as combined heat and power (CHP), combined cycle gas turbine (CCGT) and open cycle gas turbine (OCGT) can be distinguished. For heat generation SNG can be used in natural gas boiler or in a combined heat and power unit [105].

BioCNG or e-CNG cars are currently leading the way in replacing gasoline and diesel with lower well-to-wheel footprints. In the future, electric cars are expected

to grow rapidly, reaching 100-140 million vehicles by 2030, while FCEVs are expected to grow more slowly, not becoming significant in the market until 2025 [104]. Another potential SNG market in terms of transport are bioLNG/e-LNG end-users, such as ships [106]. It is expected that switching to renewable LNG in marine sector can result in significant reduction of greenhouse gas emissions on a LCA (life-cycle analysis) basis.

Based on Eurostat data [107], presenting that 153 457 396 tons of biomass were produced in Poland in 2020, an own assumption of using 5% of this biomass capacity for SNG production was made. The amount of produced SNG and its potential use was determined based on the results of the analysis of the proposed systems described in Chapter 6 and is presented in Table 7.2.

Table 7.2 Annual production of SNG with its potential use, assuming utilization of 5% of annual biomass production in the Polish market (for the systems described in Chapter 6)

	Case 1 CFB+EL+M	Case 2 DFB+EL+M	Case 3 DFB+M+CCS
annual SNG production, MWh_{SNG}	66 942 420	46 418 807	25 746 229
amount of heated houses	4 169 828	2 891 417	1 603 727
amount of cars driven	6 694 242	4 641 881	2 574 623
amount of electricity produced, MWh_{el}	23 429 847	16 246 582	9 011 180

Based on available statistical data , the market potential of the SNG produced can be estimated. Assuming that the mean gas consumption by detached houses in 2020 was equal to 16 054 kWh [108], it was estimated that about 4.2 million homes could be heated with the solution represented by Case 1 (CFB+EL+M), 2.9 million homes in Case 2 (DFB+EL+M) and 1.6 million homes in Case 3 (DFB+M+CCS). On the other hand, assuming an average annual gas consumption per car of 10 MWh, it was estimated that about 6.7 million cars would be fueled in Case 1 (CFB+EL+M), 4.6 million cars in Case 2 (DFB+EL+M), and 2.6 million cars in Case 3 (DFB+M+CCS) of considered SNG production systems. In the case of electricity production using a gas turbine with 35% [109] efficiency, it was estimated that about $23.4 \cdot 10^6$ MWh_{el} would be produced in Case 1, $16.2 \cdot 10^6$ MWh_{el} in Case 2 and $9.0 \cdot 10^6$ MWh_{el} in Case 3.

Based on the results obtained, it can be concluded that the potential to develop SNG production technology alongside other energy storage and production systems is high. Also, using renewable sources to produce feedstocks for SNG generation can help the diversification of the market with more sustainable fuel.

8. Summary and conclusions

Based on the conducted analysis, it can be stated that SNG production systems can achieve high efficiency and this technology can be competitive with the natural gas market. The dissertation involved research on methanation process based on two main parts - experimental and techno-economic analysis.

Experimental part:

For the proper design of power to SNG or biomethane production facilities, it is essential to understand the working principles of methanation reactors. Experimental studies were carried out in order to broaden the knowledge on the methanation process under various process conditions. The experimental tests were conducted on the laboratory stand of the methanation reactor at the Silesian University of Technology.

In the performed tests, the effect of different volumetric flows of CO_2 and H_2, as well as the effect of pressure on the produced gas composition, was examined. The methanation process was carried out for about 45 minutes after the cold start (30 minutes of heating and 15 minutes of hydrogen activation).

Theoretically, for the highest conversion rates achieved, the obtained composition of the analyzed synthetic natural gas would be suitable for injection directly into the gas network. However, it should be noted that in this case the methanation process was carried out on pure carbon dioxide and hydrogen. In practice, with the use of process gases, the proportion of methane in SNG could be lower and further steps requiring its purification or separation of unreacted carbon dioxide or hydrogen could be required.

Most important conclusions for the experimental part:

- The methanation reactor filled up with ruthenium on alumina catalyst was tested with carbon dioxide and hydrogen fluxes (in stoichiometric ratio, H_2:CO_2 = 4:1) ranging from 4.5 Ndm^3/min to 10 Ndm^3/min, resulting in chemical energy of SNG produced ranging from 0.81 kW to 1.44 kW.
- It was discovered that the upper limit of the reaction gas inlet flux for a given volume of catalytic bed is 7.5 Ndm^3/min (for larger inlet streams, the conversion rate decreases significantly).

– The values of the carbon dioxide conversion (x_{CO_2}) coefficient for the methanation reactor operation in atmospheric conditions are from 84.37% to 88.47%. Carbon dioxide conversion to methane is kinetically boosted by raising the pressure. For the case of gauge pressure in the methanation reactor of 6 bar, CO_2 conversion parameter is equal to 94.36 – 95.83%.

Techno-economic analysis:

Techno-economic analyses of various cases of power to SNG plants and biomethane production plants based on water electrolysis and biomass gasification processes were performed.

Firstly, the effect of different carbon feedstocks on the methanation process was analyzed. Calculations were made for various compositions of carbon feedstock, assuming three different biomass processing technologies (biomass gasification process, carbon dioxide capture after the process of oxy-combustion of biomass and biomass combustion in an atmosphere of oxygen and carbon dioxide).

Simulations were carried out using minimization of the Gibbs free energy method for different initial temperature, pressure and recycle ratio of the process in terms of investigating its influence on the final product molar composition and other response indicators (such as demand for electricity or heat received in the heat exchangers after the adiabatic beds). The results indicate that a high conversion rate (~99%) and a high CH_4 content (>94%) can be obtained from hydrogenation of biomass gasification process gas for low process temperature (200 °C) at a pressure of 10 bar.

The performed analyzes showed that the selection of the type of biomass and its processing technology also has a significant impact on the operation of the methanation system. The most favourable cases are where the process gases resulting from gasification of biomass are rich in carbon oxides, then the methanation system requires less carbon feedstock. However, hydrogen-rich process gases also appear appealing, since in this case the hydrogen demand generated by the electrolysis process drops. Therefore, it can be concluded that a specific type of biomass should be selected appropriately to the considered case, depending on what are the requirements and expectations of the system.

Then, the first exemplary case of the power to SNG system as an integrated plant based on electrolysis, methanation and biomass gasification processes was analyzed (with extended possibility of using process gas in the CHP unit), considering the most effective options for the plant operation. Different levels of availability of hydrogen were considered and two stages of the operation of the SNG production plant were proposed.

The simulations were performed with the use of the Aspen Plus software and the influence of different biomass gasification parameters was studied in terms of the composition of syngas as a carbon feedstock for the methanation process.

A techno-economic analysis of three selected cases of SNG production system was performed: Case 1 of the SNG production plant consisted of dual fluidised bed biomass gasifier, syngas methanation and CO_2 capture and sequestration (DFB+M+CCS); Case 2 assumed the same type of gasification and syngas methanation with an additional source of hydrogen feed produced from renewable energy (DFB+EL+M); and Case 3 assumed a direct biomass gasifier and syngas methanation with renewable hydrogen (CFB+EL+M).

Most important conclusions for the techno-economic analysis of selected power to SNG systems:

- In order to obtain SNG composition with CH_4 content equal to or higher than 90% and H_2 content equal to 5% or less (to fulfil the requirements of the conventional natural gas grid), it was necessary to perform a methanation simulation in the nonstoichiometric ratio of H_2:CO_2:CO. Considering the same size of gasification unit, and the same amount of biomass feed, the calculated cold gas efficiency of proposed SNG production systems is equal to 77.10% (CFB+EL+M), 70.92% (DFB+EL+M) and 63.27% (DFB+M+CCS).
- The sensitivity analysis on the break-even price of SNG (for the condition of $NPV = 0$) was performed for different prices of biomass and electricity from RES. Considering the scenario for the year 2022, the break-even price of SNG of Case 1 (CFB+EL+M) differ from 67.3 €/MWh_{SNG} to 137.7 €/$MWh_{SNG.}$ The lowest SNG break-even price is represented by the Case 2 of the considered systems (DFB+EL+M) and prices differ from 57.9

€/MWh_{SNG} to 98.2 €/MWh_{SNG}. For Case 3 (DFB+M+CCS) of the considered systems prices ranged from 112.6 €/MWh_{SNG} to 128.4 €/MWh_{SNG}. Achieved ranges of SNG production costs are in line with the data found in the literature.

- For the first half of 2022 natural gas prices in the EU were in the range of 29.1 €/MWh (Hungary) – 221.6 €/MWh (Sweden) with an average price of 86.1 €/MWh. Looking at the average NG price in the EU for the given years it can be stated that for the assumed feedstock prices DFB+EL+M (Case 2) is competitive when the price of RES electricity does not exceed 57.9 €/MWh, while CFB+EL+M system (Case 1) is competitive when the price of electricity from RES is not higher than 70.5 €/MWh. However, the competitiveness of the proposed systems with the natural gas market has to be considered individually for each country due to the high divergence in NG market prices and different energy policies. In addition, targeted policies and incentives can make the proposed systems for SNG production competitive.
- The comparison with natural gas prices on the exemplary Polish market was performed for the years 2018, 2020 and 2022. Considering the very high prices of natural gas in 2022, it can be concluded that the calculated SNG break-even price for the second system (DFB+EL+M) in each case was lower than the price of NG, while for the first case (CFB+EL+M) the price of SNG is lower than the NG price for 75% of the year, and in the third case proposed (DFB+M+CCS) for 42% of the year.
- It can be concluded that the analyzed power to SNG systems are characterized by high efficiency and have the potential to produce SNG, which may become competitive with conventional natural gas in the future. Basing the proposed systems on the electrolysis process also contributes to the possibility of balancing energy systems by storing surplus energy accumulated by the RES.

References

[1] European Commission. Renewable energy targets, https://energy.ec.europa.eu 2022:1–3.

[2] European Commission. COM(2014) 15 final: A policy framework for climate and energy in the period from 2020 to 2030 2012:1–18.

[3] EU. Directive (EU) 2018/2001 of the European Parliament and of the Council of 11 December 2018 on the promotion of the use of energy from renewable sources (recast). Off J Eur Union 2018;2018:82–209.

[4] European Commission. The European Green Deal. Eur Comm 2019;53:24. https://doi.org/10.1017/CBO9781107415324.004.

[5] European Commission. EU economy and society to meet climate ambitions. Eur Green Deal Comm Propos Transform EU Econ Soc to Meet Clim Ambitions 2021:1–5.

[6] European Commission. REPowerEU Plan 2022:21.

[7] IPCC. Climate Change 2022 - Mitigation of Climate Change - Full Report. 2022.

[8] Tong D, Zhang Q, Zheng Y, Caldeira K, Shearer C, Hong C, et al. Committed emissions from existing energy infrastructure jeopardize 1.5 °C climate target. Nature 2019;572:373–7. https://doi.org/10.1038/s41586-019-1364-3.

[9] Ilo ZD, Dotycz C, Kse CF, Zainstalowana MOC, Krajowych E, Dyspozycyjna MOC, et al. Raport 2022 KSE 2022.

[10] Chen S, Li Z, Li W. Integrating high share of renewable energy into power system using customer-sited energy storage. Renew Sustain Energy Rev 2021;143:110893. https://doi.org/10.1016/j.rser.2021.110893.

[11] Lund PD, Lindgren J, Mikkola J, Salpakari J. Review of energy system flexibility measures to enable high levels of variable renewable electricity. Renew Sustain Energy Rev 2015;45:785–807. https://doi.org/10.1016/j.rser.2015.01.057.

[12] Katla D, Jurczyk M, Skorek-Osikowska A, Uchman W. Analysis of the integrated system of electrolysis and methanation units for the production of synthetic natural gas (SNG). Energy 2021;237. https://doi.org/10.1016/j.energy.2021.121479.

[13] European Commission. Energy storage – the role of electricity. Comm Staff Work Doc 2017:25.

[14] Bartela Ł, Katla D, Skorek-Osikowska A. Evaluation of conceptual electrolysis-based energy storage systems using gas expanders. Int J Hydrogen Energy 2021;46:20171–82. https://doi.org/10.1016/j.ijhydene.2020.01.233.

[15] Katla D, Bartela Ł, Skorek-Osikowska A. Evaluation of electricity generation subsystem of power-to-gas-to-power unit using gas expander and heat recovery steam generator. Energy 2020;212.

https://doi.org/10.1016/j.energy.2020.118600.

[16] Skorek-Osikowska A, Bartela Ł, Katla D, Waniczek S. Thermodynamic assessment of the novel concept of the energy storage system using compressed carbon dioxide, methanation and hydrogen generator. Fuel 2021;304. https://doi.org/10.1016/j.fuel.2021.120764.

[17] Thema M, Weidlich T, Hörl M, Bellack A, Mörs F, Hackl F, et al. Biological CO 2 -Methanation : An Approach. Energies 2019;12:1–32.

[18] Pickering D. Bio-synthetic natural gas for heating and transport applications: The UK case. Elsevier Inc.; 2019. https://doi.org/10.1016/B978-0-12-815554-7.00012-X.

[19] European commission. Implementing REPowerEU Plan. RePowerEU Plan 2022.

[20] Katla D, Węcel D, Jurczyk M, Skorek-Osikowska A. Preliminary experimental study of a methanation reactor for conversion of H2 and CO2 into synthetic natural gas (SNG). Energy 2023;263. https://doi.org/10.1016/j.energy.2022.125881.

[21] Katla D, Skorek-Osikowska A. Assessment of the Impact of Selected Parameters and Optimisation of the Methanation System Operation in a Hybrid Power-to-Gas Installation. 15th Conf Sustain Dev Energy, Water Environ Syst (SDEWES 2020), Col Ger 1-5 Sept 2020, ISSN 2706-3690 2020:214.

[22] Smolinka T, Ojong ET, Garche J. Hydrogen Production from Renewable Energies-Electrolyzer Technologies. Electrochem Energy Storage Renew Sources Grid Balanc 2015:103–28. https://doi.org/10.1016/B978-0-444-62616-5.00008-5.

[23] Shiva Kumar S, Lim H. An overview of water electrolysis technologies for green hydrogen production. Energy Reports 2022;8:13793–813. https://doi.org/10.1016/j.egyr.2022.10.127.

[24] Götz M, Lefebvre J, Mörs F, McDaniel Koch A, Graf F, Bajohr S, et al. Renewable Power-to-Gas: A technological and economic review. Renew Energy 2016;85:1371–90. https://doi.org/10.1016/j.renene.2015.07.066.

[25] Bhandari R, Trudewind CA, Zapp P. Life cycle assessment of hydrogen production via electrolysis - A review. J Clean Prod 2014;85:151–63. https://doi.org/10.1016/j.jclepro.2013.07.048.

[26] Xu Z, Ren N, Tang M, Zhang X, Wang F, Li G. Numerical investigations for a solid oxide electrolyte cell stack. Int J Hydrogen Energy 2019;44:20997–1009. https://doi.org/10.1016/j.ijhydene.2019.04.141.

[27] Abdalla AM, Hossain S, Nisfindy OB, Azad AT, Dawood M, Azad AK. Hydrogen production, storage, transportation and key challenges with applications: A review. Energy Convers Manag 2018;165:602–27. https://doi.org/10.1016/j.enconman.2018.03.088.

[28] Tang D, Tan GL, Li GW, Liang JG, Ahmad SM, Bahadur A, et al. State-of-

the-art hydrogen generation techniques and storage methods: A critical review. J Energy Storage 2023;64:107196. https://doi.org/10.1016/j.est.2023.107196.

[29] Durmus GNB, Colpan CO, Devrim Y. A review on the development of the electrochemical hydrogen compressors. J Power Sources 2021;494:229743. https://doi.org/10.1016/j.jpowsour.2021.229743.

[30] Nagar R, Srivastava S, Hudson SL, Amaya SL, Tanna A, Sharma M, et al. Recent developments in state-of-the-art hydrogen energy technologies – Review of hydrogen storage materials. Sol Compass 2023;5:100033. https://doi.org/10.1016/j.solcom.2023.100033.

[31] ENTEC European Commission. ENTEC Energy Transition Expertise Centre The role of renewable H_2 import & storage to scale up the EU deployment of renewable H_2. 2022. https://doi.org/10.2833/727785.

[32] Ghaib K, Ben-Fares FZ. Power-to-Methane: A state-of-the-art review. Renew Sustain Energy Rev 2018;81:433–46. https://doi.org/10.1016/j.rser.2017.08.004.

[33] Frontera P, Macario A, Ferraro M, Antonucci P. Supported Catalysts for CO 2 Methanation : A Review 2017:1–28. https://doi.org/10.3390/catal7020059.

[34] Bargiacchi E, Candelaresi D, Spazzafumo G. Power to methane. INC; 2021. https://doi.org/10.1016/B978-0-12-822813-5.00001-1.

[35] Boggula RR, Fischer D, Born J. Biomass and Bioenergy Methanation potential : Suitable catalyst and optimized process conditions for upgrading biogas to reach gas grid requirements 2020;133. https://doi.org/10.1016/j.biombioe.2019.105447.

[36] Hussain I, Jalil AA, Hassan NS, Hamid MYS. Recent advances in catalytic systems for CO2 conversion to substitute natural gas (SNG): Perspective and challenges. J Energy Chem 2021;62:377–407. https://doi.org/10.1016/j.jechem.2021.03.040.

[37] Lee WJ, Li C, Prajitno H, Yoo J, Patel J, Yang Y, et al. Recent trend in thermal catalytic low temperature CO2 methanation: A critical review. Catal Today 2021;368:2–19. https://doi.org/10.1016/j.cattod.2020.02.017.

[38] Bailera, M., Lisbona Martín, M.P., Peña, B., Romeo L. Energy Storage. Hybridization of Power-to-Gas Technology and Carbon Capture. 2020.

[39] Rönsch S, Schneider J, Matthischke S, Schlüter M, Götz M, Lefebvre J, et al. Review on methanation - From fundamentals to current projects. Fuel 2016;166:276–96. https://doi.org/10.1016/j.fuel.2015.10.111.

[40] Kopyscinski J, Schildhauer TJ, Biollaz SMA. Production of synthetic natural gas (SNG) from coal and dry biomass - A technology review from 1950 to 2009. Fuel 2010;89:1763–83. https://doi.org/10.1016/j.fuel.2010.01.027.

[41] Bassano C, Deiana P, Lietti L, Giorgio C. P2G movable modular plant operation on synthetic methane production from CO 2 and hydrogen from renewables sources. Fuel 2019;253:1071–9.

https://doi.org/10.1016/j.fuel.2019.05.074.

[42] Halder Topsøe. From solid fuels to substitute natural gas (SNG) using TREMP. Tech Report, Halder Topsøe 2009:8.

[43] Pala LPR, Wang Q, Kolb G, Hessel V. Steam gasification of biomass with subsequent syngas adjustment using shift reaction for syngas production: An Aspen Plus model. Renew Energy 2017;101:484–92. https://doi.org/10.1016/j.renene.2016.08.069.

[44] Skorek-Osikowska A. Thermodynamic and environmental study on synthetic natural gas production in power to gas approaches involving biomass gasification and anaerobic digestion. Int J Hydrogen Energy 2022;47:3284–93. https://doi.org/10.1016/j.ijhydene.2021.01.002.

[45] Gutiérrez-Martín F, Rodríguez-Antón LM. Power-to-SNG technologies by hydrogenation of CO 2 and biomass resources : A comparative chemical engineering process analysis n 2019:12544–53. https://doi.org/10.1016/j.ijhydene.2018.09.168.

[46] Miguel C V., Soria MA, Mendes A, Madeira LM. Direct CO2 hydrogenation to methane or methanol from post-combustion exhaust streams - A thermodynamic study. J Nat Gas Sci Eng 2015;22:1–8. https://doi.org/10.1016/j.jngse.2014.11.010.

[47] Speight JG. Gasifier Types and Gasification Chemistry. Synth Gas 2020:95–124. https://doi.org/10.1002/9781119707875.ch3.

[48] Couto N, Rouboa A, Silva V, Monteiro E, Bouziane K. Influence of the biomass gasification processes on the final composition of syngas. Energy Procedia 2013;36:596–606. https://doi.org/10.1016/j.egypro.2013.07.068.

[49] Hannula I. Co-production of synthetic fuels and district heat from biomass residues, carbon dioxide and electricity: Performance and cost analysis. Biomass and Bioenergy 2015;74:26–46. https://doi.org/10.1016/j.biombioe.2015.01.006.

[50] Martínez I, Romano MC. Flexible sorption enhanced gasification (SEG) of biomass for the production of synthetic natural gas (SNG) and liquid biofuels: Process assessment of stand-alone and power-to-gas plant schemes for SNG production. Energy 2016;113:615–30. https://doi.org/10.1016/j.energy.2016.07.026.

[51] Dahiru AR, Vuokila A, Huuhtanen M. Recent development in Power-to-X: Part I - A review on techno-economic analysis. J Energy Storage 2022;56:105861. https://doi.org/10.1016/j.est.2022.105861.

[52] Sarić M, Dijkstra JW, Haije WG. Economic perspectives of Power-to-Gas technologies in bio-methane production. J CO2 Util 2017;20:81–90. https://doi.org/10.1016/j.jcou.2017.05.007.

[53] Koytsoumpa EI, Karellas S, Kakaras E. Modelling of Substitute Natural Gas production via combined gasification and power to fuel. Renew Energy 2019;135:1354–70. https://doi.org/10.1016/j.renene.2018.09.064.

[54] Menin L, Asimakopoulos K, Sukumara S, Rasmussen NBK, Patuzzi F, Baratieri M, et al. Competitiveness of syngas biomethanation integrated with carbon capture and storage, power-to-gas and biomethane liquefaction services: Techno-economic modeling of process scenarios and evaluation of subsidization requirements. Biomass and Bioenergy 2022;161:106475. https://doi.org/10.1016/j.biombioe.2022.106475.

[55] Peters R, Baltruweit M, Grube T, Samsun RC, Stolten D. A techno economic analysis of the power to gas route. J CO2 Util 2019;34:616–34. https://doi.org/10.1016/j.jcou.2019.07.009.

[56] McDonagh S, O'Shea R, Wall DM, Deane JP, Murphy JD. Modelling of a power-to-gas system to predict the levelised cost of energy of an advanced renewable gaseous transport fuel. Appl Energy 2018;215:444–56. https://doi.org/10.1016/j.apenergy.2018.02.019.

[57] Devaraj D, Syron E, Donnellan P. Determining the optimal process configurations for Synthetic Natural Gas production by analysing the cost factors. Energy Reports 2021;7:6515–29. https://doi.org/10.1016/j.egyr.2021.09.078.

[58] Guilera J, Ramon Morante J, Andreu T. Economic viability of SNG production from power and CO2. Energy Convers Manag 2018;162:218–24. https://doi.org/10.1016/j.enconman.2018.02.037.

[59] Chauvy R, Dubois L, Lybaert P, Thomas D, De Weireld G. Production of synthetic natural gas from industrial carbon dioxide. Appl Energy 2020;260:114249. https://doi.org/10.1016/j.apenergy.2019.114249.

[60] Gorre J, Ortloff F, van Leeuwen C. Production costs for synthetic methane in 2030 and 2050 of an optimized Power-to-Gas plant with intermediate hydrogen storage. Appl Energy 2019;253:113594. https://doi.org/10.1016/j.apenergy.2019.113594.

[61] van der Meijden CM, Veringa HJ, Rabou LPLM. The production of synthetic natural gas (SNG): A comparison of three wood gasification systems for energy balance and overall efficiency. Biomass and Bioenergy 2010;34:302–11. https://doi.org/10.1016/j.biombioe.2009.11.001.

[62] Vitasari CR, Jurascik M, Ptasinski KJ. Exergy analysis of biomass-to-synthetic natural gas (SNG) process via indirect gasification of various biomass feedstock. Energy 2011;36:3825–37. https://doi.org/10.1016/j.energy.2010.09.026.

[63] Gröbl T, Walter H, Haider M. Biomass steam gasification for production of SNG - Process design and sensitivity analysis. Appl Energy 2012;97:451–61. https://doi.org/10.1016/j.apenergy.2012.01.038.

[64] Haro P, Johnsson F, Thunman H. Improved syngas processing for enhanced Bio-SNG production: A techno-economic assessment. Energy 2016;101:380–9. https://doi.org/10.1016/j.energy.2016.02.037.

[65] Ren J, Liu YL, Zhao XY, Cao JP. Methanation of syngas from biomass

gasification: An overview. Int J Hydrogen Energy 2020;45:4223–43. https://doi.org/10.1016/j.ijhydene.2019.12.023.

[66] Iskov H, Rasmussen NB. Global screening of projects and technologies for Power-to-Gas and Bio-SNG A reference report. n.d.

[67] Bailera M, Lisbona P, Romeo LM, Espatolero S. Power to Gas projects review: Lab, pilot and demo plants for storing renewable energy and CO2. Renew Sustain Energy Rev 2017;69:292–312. https://doi.org/10.1016/j.rser.2016.11.130.

[68] MRU. User Manual VARIOluxx SYNGAS. n.d.

[69] Loha C, Chatterjee PK, Chattopadhyay H. Performance of fluidized bed steam gasification of biomass - Modeling and experiment. Energy Convers Manag 2011;52:1583–8. https://doi.org/10.1016/j.enconman.2010.11.003.

[70] Skorek-Osikowska A, Bartela Ł, Kotowicz J, Dubiel K. Journal of Power Technologies 96 (2) (2016) 73-80 Use of a gas turbine in a hybrid power plant integrated with an electrolyser, biomass gasification generator and methanation reactor. n.d.

[71] Prasad L, Pala R, Wang Q, Kolb G, Hessel V. Steam gasi fi cation of biomass with subsequent syngas adjustment using shift reaction for syngas production : An Aspen Plus modelPrasad, L., Pala, R., Wang, Q., Kolb, G., & Hessel, V. (2017). Steam gasi fi cation of biomass with subsequent syngas adjustm. Renew Energy 2017;101:484–92. https://doi.org/10.1016/j.renene.2016.08.069.

[72] Dellavedova M, Derudi M, Biesuz R, Lunghi A, Rota R. On the gasification of biomass: Data analysis and regressions. Process Saf Environ Prot 2012;90:246–54. https://doi.org/10.1016/j.psep.2011.08.001.

[73] Machner K. Die Mikrobestimmung von Hippursäure im Urin. Fresenius' Zeitschrift Für Anal Chemie 1958;163:69. https://doi.org/10.1007/BF00447266.

[74] Er-rbib H, Bouallou C. Modeling and simulation of CO methanation process for renewable electricity storage. Energy 2014;75:81–8. https://doi.org/10.1016/j.energy.2014.05.115.

[75] Kakoee A, Gharehghani A. Carbon oxides methanation in equilibrium; a thermodynamic approach. Int J Hydrogen Energy 2020;45:29993–30008. https://doi.org/10.1016/j.ijhydene.2020.08.073.

[76] Nikoo MK, Amin NAS. Thermodynamic analysis of carbon dioxide reforming of methane in view of solid carbon formation. Fuel Process Technol 2011;92:678–91. https://doi.org/10.1016/j.fuproc.2010.11.027.

[77] Puig-Arnavat M, Bruno JC, Coronas A. Review and analysis of biomass gasification models. Renew Sustain Energy Rev 2010;14:2841–51. https://doi.org/10.1016/j.rser.2010.07.030.

[78] Fremaux S, Beheshti SM, Ghassemi H, Shahsavan-Markadeh R. An

experimental study on hydrogen-rich gas production via steam gasification of biomass in a research-scale fluidized bed. Energy Convers Manag 2015;91:427–32. https://doi.org/10.1016/j.enconman.2014.12.048.

[79] Uchman W, Skorek-Osikowska A, Jurczyk M, Węcel D. The analysis of dynamic operation of power-to-SNG system with hydrogen generator powered with renewable energy, hydrogen storage and methanation unit. Energy 2020;213. https://doi.org/10.1016/j.energy.2020.118802.

[80] Kotowicz J, Jurczyk M, Węcel D. The possibilities of cooperation between a hydrogen generator and a wind farm. Int J Hydrogen Energy 2021;46:7047–59. https://doi.org/10.1016/j.ijhydene.2020.11.246.

[81] Doherty W, Reynolds A, Kennedy D. Aspen plus simulation of biomass gasification in a steam blown dual fluidised bed. Mater Process Energy 2013:212–20.

[82] Kok MV, Özgür E. Thermal analysis and kinetics of biomass samples. Fuel Process Technol 2013;106:739–43. https://doi.org/10.1016/j.fuproc.2012.10.010.

[83] Begum S, Rasul MG, Akbar D, Ramzan N. Performance analysis of an integrated fixed bed gasifier model for different biomass feedstocks. Energies 2013;6:6508–24. https://doi.org/10.3390/en6126508.

[84] Sigma-Aldrich. Ruthenium on alumina. n.d.

[85] Hofbauer H, Veronik G, Fleck T, Rauch R, Mackinger H FE. The FICFB — Gasification Process. In: Bridgw. 1997.

[86] Antonini C, Pérez-Calvo JF, van der Spek M, Mazzotti M. Optimal design of an MDEA CO2 capture plant for low-carbon hydrogen production — A rigorous process optimization approach. Sep Purif Technol 2021;279:119715. https://doi.org/10.1016/j.seppur.2021.119715.

[87] Hansen JR. A Guide to the Guidelines: The UNIDO Method: of the Economic Project Evaluation 1973;166:1–110.

[88] Gerloff N. Levelized and environmental costs of power-to-gas generation in Germany. Int J Hydrogen Energy 2023:1–16. https://doi.org/10.1016/j.ijhydene.2023.01.347.

[89] Khallaghi N, Jeswani H, Hanak DP, Manovic V. Techno-economic-environmental assessment of biomass oxy-gasification staged oxy-combustion for negative emission combined heat and power. Appl Therm Eng 2021;196:117254. https://doi.org/10.1016/j.applthermaleng.2021.117254.

[90] Falbo L, Martinelli M, Visconti CG, Lietti L, Bassano C, Deiana P. Kinetics of CO2 methanation on a Ru-based catalyst at process conditions relevant for Power-to-Gas applications. Appl Catal B Environ 2018;225:354–63. https://doi.org/10.1016/j.apcatb.2017.11.066.

[91] Bailera M, Peña B, Lisbona P, Marín J, Romeo LM. Lab-scale experimental tests of power to gas-oxycombustion hybridization: System design and

preliminary results. Energy 2021;226. https://doi.org/10.1016/j.energy.2021.120375.

[92] Romeo LM, Cavana M, Bailera M, Leone P, Peña B, Lisbona P. Non-stoichiometric methanation as strategy to overcome the limitations of green hydrogen injection into the natural gas grid. Appl Energy 2022;309. https://doi.org/10.1016/j.apenergy.2021.118462.

[93] Bertuccioli L, Chan A, Hart D, Lehner F, Madden B, Standen E. Study on development of water electrolysis in the EU. Final Rep Fuel Cells Hydrog Jt Undert 2014;1:1–160.

[94] Gorre J, Ruoss F, Karjunen H, Schaffert J, Tynjälä T. Cost benefits of optimizing hydrogen storage and methanation capacities for Power-to-Gas plants in dynamic operation. Appl Energy 2020;257. https://doi.org/10.1016/j.apenergy.2019.113967.

[95] Silva Ortiz P, Maier S, Dietrich R-U, Pinto Mariano A, Maciel Filho R, Posada J. Comparative Techno-Economic and Exergetic Analysis of Circulating and Dual Bed Biomass Gasification Systems. Front Chem Eng 2021;3:1–12. https://doi.org/10.3389/fceng.2021.727068.

[96] Witte J, Kunz A, Biollaz SMA, Schildhauer TJ. Direct catalytic methanation of biogas – Part II: Techno-economic process assessment and feasibility reflections. Energy Convers Manag 2018;178:26–43. https://doi.org/10.1016/j.enconman.2018.09.079.

[97] Zhang L, Geng S, Yang L, Hao Y, Yang H, Dong Z, et al. Technical and economic evaluation of co2 capture and reinjection process in the co2 eor and storage project of xinjiang oilfield. Energies 2021;14. https://doi.org/10.3390/en14165076.

[98] Leeuwen C van, Zauner A. Deliverable 8.3 - Report on the costs involved with PtG technologies and their potentials across the EU. Store GO Proj 2018;April:51.

[99] Ottosson A. Integration of Hydrogen Production via Water Electrolysis at a CHP Plant A feasibility study. Sustain Energy Eng 2021:39.

[100] IRENA. Green Hydrogen Cost Reduction. 2020.

[101] Eurostat. Natural gas price statistics. Eur Comm 2022:1–12.

[102] Towarowa Giełda Energii. Raport roczny 2020 2020. https://tge.pl/.

[103] Consulting E. The potential of Power-to-Gas. Technology review and economic potential assessment. n.d.

[104] Blanco H, Faaij A. A review at the role of storage in energy systems with a focus on Power to Gas and long-term storage. Renew Sustain Energy Rev 2018;81:1049–86. https://doi.org/10.1016/j.rser.2017.07.062.

[105] Steubing B, Zah R, Ludwig C. Life cycle assessment of SNG from wood for heating, electricity, and transportation. Biomass and Bioenergy 2011;35:2950–60. https://doi.org/10.1016/j.biombioe.2011.03.036.

[106] Comer B, O'malley J, Osipova L, Pavlenko N, 2022 S. Comparing the future demand for, supply of, and life-cycle emissions from bio, synthetic, and fossil LNG marine fuels in the European Union AND LIFE-CYCLE EMISSIONS FROM BIO, SYNTHETIC, AND FOSSIL LNG MARINE FUELS IN THE EUROPEAN UNION. Int Counc Clean Transp 2022.

[107] Eurostat. Material flow accounts in raw material equivalents - modelling estimates 2022. https://ec.europa.eu/eurostat/.

[108] Central Statistics Office. Household Gas Consumption by Building Energy Ratings 2020 2022. https://www.cso.ie/.

[109] Storm K. Combined cycle power plant (1×1) labor estimate. Ind. Constr. Estim. Man., 2020, p. 95–159. https://doi.org/10.1016/b978-0-12-823362-7.00006-5.

Abstract

The doctoral disseration presents the results of research on the power to synthetic natural gas (PtSNG) systems based on water electrolysis and oxy-gasification of biomass. The main benefit of such a method is the production of a fuel that, in contrast to pure hydrogen, has a greater potential for use in current energy systems, can be easily transported through current transmission networks, and is significantly simpler to store. The various configurations of proposed power to SNG systems studied within the scope of this dissertation are in line with the direction of research into new energy storage systems.

The dissertation involved research on methanation process based on two main parts - experimental and techno-economic analysis. Experiments were conducted to broaden understanding of the methanation process under various operating conditions and to collect data relevant to research on PtSNG applications. The goal was to develop a methanation reactor with main aim of being effective, simple, and inexpensive (in terms of capital and operation costs) at the same time, as well as to evaluate the influence of the main process conditions on the effectiveness of methane production. The experimental work additionally allowed to determine the influence of selected parameters on the course and indicators of thermodynamic evaluation of the methanation process, as well as to optimize the operational parameters of the process.

In case of experimental analysis on methanation installation, the reactor filled up with ruthenium on alumina catalyst was tested with carbon dioxide and hydrogen volumetric flows (in stoichiometric ratio, H_2:CO_2 = 4:1) ranging from 4.5 Ndm^3/min to 10 Ndm^3/min, resulting in chemical energy of SNG produced ranging from 0.81 kW to 1.44 kW. The values of the carbon dioxide conversion coefficient for the methanation reactor operation in atmospheric conditions are from 84.37% to 88.47%. Carbon dioxide conversion to methane is kinetically boosted by raising the pressure. For the case of gauge pressure in the methanation reactor of 6 bar, CO_2 conversion parameter is equal to 94.36 – 95.83%.

A techno-economic analysis of various configurations of SNG production system was performed depending on type of gasifier used for simulations and also on the availability of renewable hydrogen. In order to obtain SNG composition with CH_4

content equal to or higher than 90% and H_2 content equal to 5% or less (to fulfil the requirements of the conventional natural gas grid), it was necessary to perform a methanation simulation in the nonstoichiometric ratio of H_2:CO_2:CO. The calculated cold gas efficiency of the proposed SNG production systems ranges from 63.27% to 77.10%.

The sensitivity analysis on the break-even price of SNG was performed for different prices of biomass and electricity from RES. Depending on the considered case and assumed feestocks prices, calculated SNG break-even prices ranged from 57.9 €/MWh_{SNG} to 137.7 €/MWh_{SNG}. Achieved ranges of SNG production costs are in line with the data found in the literature.

It can be concluded that the analyzed power to SNG systems are characterized by high efficiency and have the potential to produce SNG, which may become competitive with conventional natural gas in the future. Basing the proposed systems on the electrolysis process also contributes to the possibility of balancing energy systems by storing surplus energy accumulated by the renewable energy sources (RES).

Streszczenie

W rozprawie doktorskiej przedstawiono wyniki badań nad systemami power to synthetic natural gas (PtSNG) opartych na technologiach elektrolizy wody i tlenowego zgazowania biomasy. Główną zaletą systemów produkcji SNG jest produkcja paliwa, które w przeciwieństwie do czystego wodoru ma szeroki potencjał wykorzystania w obecnych systemach energetycznych, może być łatwo transportowane przez obecne sieci przesyłowe oraz jest znacznie prostsze w przechowywaniu. Badane w ramach niniejszej rozprawy różne konfiguracje proponowanych układów power to SNG wpisują się w kierunek badań nad nowymi systemami magazynowania energii.

Rozprawa doktorska obejmowała badania nad procesem metanizacji w oparciu o dwie główne części - eksperymentalną i analizę techniczno-ekonomiczną. Prace eksperymentalne zostały przeprowadzone w celu poszerzenia wiedzy na temat procesu metanizacji w różnych warunkach pracy oraz zebrania danych istotnych dla badań nad zastosowaniem PtSNG. Celem było opracowanie reaktora metanizacji, którego głównym założeniem będzie wysoka efektywność, prostota i jednocześnie niska cena (w aspekcie kosztów kapitałowych I eksploatacyjnych) oraz ocena wpływu wybranych warunków procesu na efektywność produkcji metanu. Prace eksperymentalne pozwoliły dodatkowo na określenie wpływu wybranych parametrów na przebieg i wskaźniki oceny termodynamicznej procesu metanizacji, a także na optymalizację parametrów operacyjnych procesu.

W przypadku analizy eksperymentalnej na instalacji metanizacji reaktor wypełniony katalizatorem rutenowym badano przy przepływach objętościowych dwutlenku węgla i wodoru (w stosunku stechiometrycznym, H_2:CO_2 = 4:1) w zakresie od 4.5 Ndm^3/min do 10 Ndm^3/min, uzyskując energię chemiczną wytworzonego SNG w zakresie od 0.81 kW do 1.44 kW. Wartości współczynnika konwersji dwutlenku węgla dla pracy reaktora metanizacji w warunkach atmosferycznych wynoszą od 84.37% do 88.47%. Konwersja dwutlenku węgla do metanu wzrasta przy podwyższonym ciśnieniu reakcji. Dla przypadku ciśnienia manometrycznego w reaktorze metanizacji wynoszącego 6 barów, parametr konwersji CO_2 jest równy 94.36 – 95.83%.

W pracy przeprowadzono również analizę techniczno-ekonomiczną różnych konfiguracji układu produkcji SNG w zależności od rodzaju technologii zgazowania biomasy założonej do symulacji, a także od dostępności produkcji wodoru ze źródeł odnawialnych. W celu uzyskania składu SNG o zawartości CH_4 równej lub wyższej niż 90% i zawartości H_2 równej lub niższej niż 5% (aby spełnić wymagania konwencjonalnej sieci gazu ziemnego), konieczne było przeprowadzenie symulacji metanizacji w niestechiometrycznym stosunku H_2:CO_2:CO. Obliczona sprawność proponowanych układów produkcji SNG wynosi od 63.27% do 77.10%.

Analiza wrażliwości granicznej ceny sprzedaży SNG została przeprowadzona dla różnych cen biomasy i energii elektrycznej z OZE. W zależności od rozpatrywanego przypadku i przyjętych cen surowców, obliczone ceny progu rentowności SNG wahały się od 57.9 €/MWh_{SNG} do 137.7 €/MWh_{SNG}. Uzyskane zakresy kosztów produkcji SNG są zgodne z danymi znalezionymi w literaturze.

Można stwierdzić, że analizowane układy power to SNG charakteryzują się wysoką sprawnością i mają potencjał do produkcji SNG, który w przyszłości może stać się konkurencyjny dla konwencjonalnego gazu ziemnego. Oparcie proponowanych układów na procesie elektrolizy przyczynia się również do możliwości bilansowania systemów energetycznych poprzez magazynowanie nadwyżek energii zgromadzonej przez odnawialne źródła energii (OZE).

Appendices

Appendix A – Suplementary materials for Figure 4.5 Results of methanation reaction operation conditions and SNG composition performed on the first reactor type

Appendix B - Suplementary materials for Figure 4.6 Results of SNG composition and catalytic bed temperature while increasing the operation pressure (p) for GHSV equal to a) 663 h-1, b) 737 h-1, c) 811 h-1, d) 885 h-1, e) 958 h-1, f) 1032 h-1 and g) 1106 h-1

Appendix C - Suplementary materials for Figure 5.10 Results of the quantitative analysis of the methanation process as a function of steam to biomass ratio for different amounts of oxygen supplied to the gasification process (a) 0.1, b) 0.3, c) 0.5)

Appendix A

time, min	T_1, °C	T_2, °C	T_3, °C	p, bar	v_{H_2in}, Ndm^3/min	v_{CO_2in}, Ndm^3/min	CO_2 %	CH_4 %	H_2 %	N_2 %	LHV, MJ/kg	HHV, MJ/kg
0.0	225	130	63	4.3	3.7	0.0	0.0	0.0	98.8	1.1	103.4	122.3
0.5	225	130	64	4.3	3.7	0.0	0.0	0.0	98.8	1.1	103.7	122.6
1.0	226	131	64	4.5	3.0	1.0	0.0	0.0	98.8	1.1	103.6	122.5
1.5	226	131	65	4.8	2.8	0.9	0.0	0.0	98.8	1.1	103.7	122.6
2.0	227	132	67	4.9	3.2	0.3	0.5	0.6	82.6	16.3	31.5	37.2
2.5	227	132	69	4.9	3.1	0.6	11.9	10.2	64.9	12.8	20.2	23.4
3.0	228	132	71	4.9	3.1	0.7	11.6	14.3	78.6	0.0	33.9	39.2
3.5	228	132	72	4.9	3.0	0.7	7.8	13.1	72.3	6.8	31.5	36.3
4.0	229	133	72	4.9	3.1	0.8	10.3	16.1	67.7	5.7	29.0	33.3
4.5	230	133	73	4.8	3.1	0.8	11.9	18.8	63.6	5.6	27.4	31.4
5.0	230	134	74	4.8	3.2	0.9	13.2	21.7	59.3	5.6	26.3	30.0
5.5	231	134	75	4.8	3.3	0.9	14.3	25.2	54.6	5.8	25.6	29.1
6.0	232	134	76	4.8	3.4	0.9	15.1	29.5	49.1	6.2	25.3	28.6
6.5	232	135	77	4.8	3.6	1.0	15.5	34.9	43.1	6.4	25.5	28.8
7.0	233	135	77	4.8	3.7	1.0	15.5	41.1	36.9	6.2	26.3	29.6
7.5	234	136	79	4.8	3.7	1.0	15.3	47.7	30.9	5.9	27.5	30.8
8.0	235	136	80	4.8	3.7	1.0	14.9	53.2	27.5	4.1	29.4	32.9
8.5	235	137	81	4.8	3.7	1.0	14.1	56.4	26.1	3.3	30.9	34.6
9.0	236	137	82	4.8	3.6	1.0	13.5	58.1	24.8	3.4	31.5	35.2
9.5	237	137	84	4.8	3.6	1.0	13.4	59.5	23.5	3.4	31.7	35.4
10.0	238	138	86	4.8	3.6	1.0	13.4	60.5	22.5	3.4	31.7	35.4
10.5	239	138	87	4.8	3.5	1.0	13.7	61.4	21.8	3.0	31.8	35.5
11.0	240	139	89	4.8	3.4	1.0	13.6	62.0	20.6	3.6	31.6	35.2
11.5	240	139	90	4.8	3.4	1.0	14.4	62.6	19.2	3.6	30.9	34.5
12.0	241	139	91	4.8	3.4	1.0	15.5	63.2	17.5	3.6	30.0	33.4
12.5	242	140	92	4.8	3.4	1.0	16.4	63.6	16.9	2.9	29.7	33.1
13.0	243	140	93	4.8	3.3	1.0	16.3	64.1	16.7	2.7	29.9	33.4

13.5	244	141	94	4.8	3.3	1.0	16.0	64.7	16.5	2.7	30.2	33.7
14.0	245	141	95	4.8	3.3	1.0	15.8	65.1	16.2	2.7	30.4	33.9
14.5	246	141	96	4.8	3.3	0.9	15.5	65.5	16.2	2.6	30.7	34.3
15.0	247	142	96	4.8	3.2	0.9	15.3	65.9	15.7	2.9	30.8	34.3
15.5	247	142	97	4.8	3.2	0.9	15.5	66.3	15.1	2.9	30.6	34.1
16.0	248	142	97	4.8	3.2	0.9	15.9	66.5	14.6	2.9	30.4	33.9
16.5	249	142	98	4.8	3.2	0.9	16.1	66.8	14.1	2.8	30.2	33.7
17.0	250	143	99	4.8	3.1	0.9	16.5	67.0	13.6	2.8	30.0	33.4
17.5	251	143	99	4.8	3.1	0.9	16.8	67.2	13.1	2.8	29.7	33.1
18.0	251	144	99	4.8	3.1	0.9	17.1	67.3	12.8	2.6	29.6	33.0
18.5	252	144	100	4.8	3.1	0.9	17.2	67.6	12.4	2.6	29.6	32.9
19.0	253	144	100	4.8	3.1	0.9	17.4	67.7	12.1	2.6	29.4	32.7
19.5	253	144	100	4.8	3.1	0.9	17.6	67.9	11.7	2.6	29.3	32.6
20.0	254	145	101	4.8	3.0	0.9	17.8	68.1	11.4	2.5	29.1	32.4
20.5	255	145	101	4.8	3.0	0.9	18.1	68.1	11.0	2.5	28.9	32.2
21.0	255	145	102	4.8	3.0	0.9	18.3	68.3	10.8	2.5	28.8	32.1
21.5	256	146	102	4.8	3.0	0.9	18.5	68.5	10.5	2.4	28.7	32.0
22.0	256	146	102	4.8	3.0	0.9	18.7	68.5	10.2	2.4	28.6	31.8
22.5	257	146	103	4.8	2.9	0.9	18.9	68.6	9.9	2.4	28.5	31.7
23.0	257	146	103	4.8	2.9	0.9	19.1	68.7	9.6	2.4	28.3	31.5
23.5	258	147	103	4.8	2.9	0.9	19.3	68.8	9.4	2.4	28.2	31.4
24.0	258	147	104	4.8	2.9	0.9	19.5	68.8	9.1	2.4	28.1	31.2
24.5	259	147	104	4.8	2.9	0.9	19.7	68.8	8.9	2.4	27.9	31.1
25.0	259	148	104	4.8	2.9	0.9	20.0	68.8	8.7	2.3	27.8	30.9
25.5	259	148	104	4.8	2.9	0.9	20.2	68.9	8.5	2.3	27.7	30.8
26.0	260	148	104	4.8	2.9	0.9	20.3	69.0	8.3	2.3	27.6	30.7
26.5	260	148	105	4.8	2.8	0.9	20.6	68.9	8.1	2.3	27.4	30.5
27.0	260	149	105	4.8	2.8	0.9	20.8	68.9	7.9	2.3	27.3	30.4
27.5	260	149	105	4.8	2.8	0.9	21.0	68.9	7.7	2.3	27.2	30.2
28.0	261	149	105	4.8	2.8	0.9	21.1	69.0	7.5	2.2	27.1	30.1

28.5	261	150	105	4.8	2.8	0.9	21.4	68.9	7.3	2.2	26.9	29.9
29.0	261	150	105	4.8	2.8	0.9	21.6	68.9	7.1	2.2	26.8	29.8
29.5	261	150	106	4.8	2.8	0.9	21.7	69.0	7.0	2.1	26.8	29.8
30.0	261	150	106	4.8	2.8	0.9	21.7	69.1	6.9	2.2	26.8	29.8
30.5	262	151	106	4.8	2.8	0.9	21.8	69.1	6.7	2.2	26.7	29.6
31.0	262	151	106	4.8	2.8	0.9	22.0	69.1	6.6	2.1	26.6	29.6
31.5	262	151	106	4.8	2.8	0.9	22.1	69.2	6.5	2.1	26.5	29.5
32.0	262	151	106	4.8	2.8	0.9	22.2	69.2	6.4	2.1	26.5	29.4
32.5	262	152	106	4.8	2.8	0.9	22.3	69.2	6.2	2.1	26.4	29.4
33.0	262	152	106	4.8	2.8	0.9	22.4	69.3	6.1	2.0	26.4	29.3
33.5	262	152	106	4.8	2.8	0.9	22.5	69.3	6.1	2.1	26.3	29.3
34.0	262	152	106	4.8	2.8	0.9	22.5	69.3	6.0	2.1	26.3	29.2
34.5	262	153	106	4.8	2.8	0.9	22.6	69.4	5.9	2.0	26.3	29.2
35.0	262	153	106	4.8	2.8	0.9	22.6	69.4	5.8	2.0	26.3	29.2
35.5	262	153	106	4.8	2.8	0.9	22.7	69.4	5.7	2.0	26.2	29.2
36.0	262	153	106	4.8	2.8	0.9	22.8	69.3	5.7	2.0	26.1	29.0
36.5	262	153	106	4.8	2.8	0.9	22.9	69.3	5.6	2.0	26.1	29.0
37.0	262	154	106	4.8	2.7	0.9	23.0	69.2	5.6	2.1	26.0	28.9
37.5	262	154	106	4.8	2.7	0.9	23.0	69.3	5.5	2.0	26.0	28.9
38.0	262	154	106	4.8	2.7	0.9	23.1	69.3	5.4	2.1	25.9	28.8
38.5	262	154	106	4.8	2.7	0.9	23.4	69.1	5.3	2.0	25.8	28.6
39.0	262	155	106	4.8	2.8	0.9	23.4	69.2	5.4	2.0	25.8	28.7
39.5	262	155	106	5.0	3.4	0.6	23.3	69.2	5.4	2.0	25.8	28.7
40.0	262	155	106	5.0	2.9	0.5	23.3	69.2	5.4	1.9	25.9	28.8
40.5	261	155	106	5.0	3.0	0.5	15.3	64.2	42.5	0.0	34.6	38.9
41.0	261	155	105	5.0	3.0	0.5	3.2	42.6	55.0	0.0	50.8	57.4
41.5	260	155	105	5.0	3.0	0.5	1.3	39.5	56.9	2.2	52.6	59.5
42.0	260	155	104	5.0	3.0	0.5	0.9	38.5	58.0	2.5	53.4	60.4
42.5	260	156	104	5.0	3.0	0.5	0.8	37.8	58.6	2.8	53.2	60.3
43.0	260	156	103	4.9	3.0	0.5	0.7	37.5	58.9	2.9	53.3	60.4

43.5	259	156	102	4.9	3.0	0.5	0.7	37.2	59.1	2.9	53.4	60.5
44.0	259	156	102	4.9	3.0	0.6	0.7	37.0	59.5	2.8	53.7	60.9
44.5	259	157	102	4.9	3.1	0.6	0.6	36.6	59.8	2.9	53.8	61.0
45.0	259	157	101	4.9	3.1	0.7	0.6	36.7	58.7	3.9	51.7	58.6
45.5	260	157	101	4.9	3.3	0.8	0.7	39.0	54.7	5.6	48.4	54.7
46.0	260	158	101	4.9	3.4	0.8	0.9	47.1	41.6	10.3	41.1	46.2
46.5	261	158	102	4.9	3.3	0.9	1.9	59.2	29.5	9.2	40.5	45.3
47.0	261	158	103	4.9	3.3	0.9	3.7	67.6	22.2	6.5	40.6	45.3
47.5	261	159	103	4.9	3.3	0.9	5.0	71.5	18.8	4.6	40.4	45.1
48.0	261	159	104	4.9	3.3	0.9	5.8	73.3	16.9	4.0	40.0	44.6
48.5	261	159	104	4.9	3.3	0.8	6.4	74.3	15.7	3.5	39.7	44.2
49.0	261	159	105	4.9	3.2	0.8	6.6	74.9	15.2	3.2	39.7	44.2
49.5	261	159	105	4.9	3.2	0.8	6.8	75.3	14.6	3.2	39.4	43.8
50.0	262	159	106	4.9	3.2	0.8	7.0	75.7	14.1	3.1	39.2	43.7
50.5	262	159	106	4.9	3.2	0.8	7.3	75.9	13.6	3.1	38.9	43.3
51.0	262	160	106	4.9	3.2	0.8	7.4	76.1	13.3	3.1	38.8	43.2
51.5	262	160	107	4.9	3.2	0.8	7.6	76.3	13.1	2.9	38.7	43.1
52.0	262	160	107	4.9	3.2	0.8	7.9	76.5	12.2	3.3	38.1	42.4
52.5	262	160	107	4.9	3.2	0.8	8.4	76.7	12.1	2.8	38.0	42.3
53.0	262	160	107	4.9	3.1	0.8	8.2	76.9	12.0	2.8	38.1	42.5
53.5	262	160	107	4.9	3.1	0.8	8.3	77.0	11.9	2.8	38.1	42.4
54.0	263	161	107	4.9	3.1	0.8	8.4	77.0	11.6	2.9	37.8	42.1
54.5	263	161	108	4.9	3.1	0.8	8.6	77.1	11.3	2.8	37.7	41.9
55.0	263	161	108	4.9	3.1	0.8	8.9	77.1	11.0	2.9	37.4	41.6
55.5	263	161	108	4.9	3.1	0.8	9.1	77.2	10.8	2.7	37.2	41.4
56.0	263	161	108	4.9	3.1	0.8	9.5	77.2	10.4	2.9	36.8	40.9
56.5	263	161	108	4.9	3.1	0.9	9.7	77.2	10.3	2.7	36.6	40.8
57.0	263	162	108	4.9	3.1	0.8	9.9	77.2	10.2	2.6	36.5	40.7
57.5	263	162	108	4.9	3.1	0.8	10.0	77.2	9.9	2.7	36.3	40.4
58.0	263	162	108	4.9	3.1	0.9	10.3	77.2	9.8	2.6	36.1	40.2

58.5	264	162	108	4.9	3.1	0.8	10.4	77.1	9.8	2.5	36.0	40.1
59.0	264	162	108	4.9	3.1	0.9	10.5	77.1	9.7	2.6	36.0	40.0
59.5	264	162	108	4.9	3.1	0.9	10.6	77.0	9.4	2.8	35.7	39.7
60.0	264	163	108	4.9	3.1	0.9	10.8	77.1	9.5	2.6	35.7	39.7
60.5	264	163	108	4.9	3.1	0.9	11.1	77.0	9.2	2.7	35.3	39.3
61.0	264	163	108	4.9	3.1	0.9	11.2	76.9	9.2	2.7	35.2	39.2
61.5	264	163	108	4.9	3.1	0.9	11.3	76.9	9.4	2.2	35.4	39.3
62.0	264	163	108	4.9	3.1	0.8	11.4	76.8	9.0	2.7	35.0	38.9
62.5	264	163	108	4.9	3.1	0.9	11.5	76.7	9.0	2.7	34.9	38.8
63.0	264	163	108	4.9	3.1	0.9	11.6	76.8	9.4	2.1	35.2	39.1
63.5	264	164	108	4.9	3.1	0.9	11.6	76.8	9.0	2.6	34.9	38.8
64.0	264	164	108	4.9	3.1	0.9	11.6	76.6	9.1	2.6	34.9	38.8
64.5	264	164	108	4.9	3.1	0.9	11.6	76.6	9.2	2.4	34.9	38.9
65.0	264	164	108	4.9	3.0	0.9	11.7	76.6	9.0	2.6	34.7	38.6
65.5	264	164	108	4.9	3.0	0.9	11.7	76.3	9.0	2.8	34.6	38.5
66.0	265	164	108	4.9	3.0	0.9	11.8	76.4	9.2	2.5	34.7	38.6
66.5	265	164	108	4.9	3.0	0.9	12.1	76.3	8.8	2.7	34.3	38.2
67.0	265	165	108	4.9	3.0	0.9	11.9	76.3	8.8	2.8	34.4	38.3
67.5	265	165	108	4.9	3.1	0.9	12.6	76.1	8.7	2.4	34.0	37.8
68.0	265	165	110	5.0	2.6	0.8	12.4	75.5	31.1	0.0	37.5	42.0
68.5	264	164	111	5.0	2.1	0.7	7.0	59.3	22.9	10.5	33.2	37.1
69.0	264	164	111	5.0	2.0	0.7	8.3	62.8	12.7	13.9	28.9	32.2
69.5	264	164	112	5.1	2.0	0.6	8.8	57.1	5.7	22.8	22.2	24.7
70.0	264	164	112	5.1	1.9	0.6	9.4	53.1	4.0	26.3	19.5	21.7
70.5	263	164	113	5.1	1.9	0.6	11.5	51.3	3.1	26.6	18.1	20.1
71.0	263	164	114	5.1	1.7	0.6	13.3	49.5	2.7	26.9	17.0	18.9
71.5	263	164	114	5.1	1.4	0.5	11.0	36.4	2.3	38.9	11.8	13.1
72.0	263	164	114	5.1	1.3	0.5	11.5	36.2	2.0	38.9	11.6	12.9
72.5	262	163	114	5.1	1.3	0.5	11.7	35.6	1.9	39.2	11.4	12.7
73.0	262	163	115	5.1	1.3	0.5	11.8	34.8	1.8	39.9	11.1	12.3

73.5	262	163	115	5.1	1.2	0.5	12.1	34.1	1.6	40.4	10.7	11.9
74.0	262	164	115	4.9	2.4	0.8	17.3	41.8	4.3	31.5	13.9	15.5
74.5	262	165	113	4.8	2.6	0.8	31.8	63.7	2.0	2.2	20.7	23.0
75.0	262	165	112	4.8	2.7	0.8	33.4	62.4	3.1	0.9	20.3	22.6
75.5	262	165	112	4.8	2.7	0.8	28.5	66.5	4.6	0.2	23.3	25.9
76.0	262	165	111	4.8	2.8	0.8	22.9	70.4	5.0	1.5	26.3	29.3
76.5	262	166	111	4.8	2.8	0.8	20.3	71.0	5.3	2.8	27.3	30.4
77.0	262	166	111	4.8	2.8	0.8	18.4	71.4	5.6	3.8	28.0	31.1
77.5	262	166	110	4.8	2.9	0.8	17.2	71.2	5.9	4.7	28.3	31.5
78.0	262	166	110	4.8	2.9	0.8	16.6	71.8	6.0	4.5	28.8	32.0
78.5	262	166	110	4.8	2.9	0.8	16.3	72.2	6.1	4.5	29.2	32.5
79.0	262	166	110	4.8	2.9	0.8	15.8	72.0	6.4	5.0	29.3	32.6
79.5	262	167	110	4.8	2.9	0.8	15.5	72.2	6.4	4.8	29.5	32.8
80.0	262	167	110	4.8	2.9	0.8	15.3	72.9	6.4	4.5	30.0	33.3
80.5	262	167	110	4.8	2.9	0.9	15.1	72.4	6.6	5.1	29.9	33.2
81.0	262	167	109	4.8	2.9	0.9	15.1	73.1	6.5	4.4	30.2	33.6
81.5	262	167	110	4.8	2.9	0.8	15.0	73.1	6.6	4.4	30.3	33.7
82.0	262	167	109	4.8	2.9	0.9	15.0	72.9	6.7	4.7	30.2	33.6
82.5	262	167	109	4.8	2.9	0.9	14.9	72.9	6.6	4.6	30.2	33.6
83.0	262	167	110	4.8	2.9	0.9	14.9	73.9	6.6	4.0	30.8	34.2
83.5	262	167	109	4.8	2.9	0.9	14.6	73.0	6.8	4.9	30.4	33.8
84.0	262	167	110	4.8	2.9	0.9	14.6	73.2	6.7	4.5	30.5	33.9
84.5	262	167	109	4.8	2.9	0.9	14.6	73.2	6.8	4.6	30.6	34.0
85.0	262	167	109	4.8	2.9	0.9	14.5	72.9	6.8	4.9	30.4	33.8
85.5	262	168	109	4.8	2.9	0.9	14.6	73.2	6.7	4.5	30.5	33.9
86.0	262	168	109	4.8	2.9	0.9	14.6	73.4	6.8	4.4	30.7	34.1
86.5	262	168	109	4.8	2.9	0.9	14.5	73.0	6.8	4.9	30.5	33.9
87.0	262	168	109	4.8	2.9	0.9	14.5	73.1	6.8	4.6	30.5	33.9
87.5	262	168	109	4.8	2.9	0.9	14.6	73.5	6.7	4.3	30.7	34.1
88.0	262	168	109	4.8	2.9	0.9	14.6	73.2	6.7	4.8	30.5	33.9

88.5	263	168	109	4.8	2.9	0.9	14.8	73.1	6.7	4.5	30.4	33.8
89.0	263	168	109	4.8	2.9	0.9	14.8	73.5	6.7	4.3	30.6	34.0
89.5	263	168	109	4.8	2.9	0.9	14.7	73.2	6.7	4.8	30.4	33.8
90.0	263	168	109	4.8	2.9	0.9	14.8	73.1	6.7	4.5	30.4	33.8
90.5	263	168	109	4.8	2.9	0.9	14.8	73.3	6.7	4.4	30.5	33.9
91.0	263	168	109	4.8	2.9	0.9	14.7	73.0	6.7	4.8	30.3	33.7
91.5	263	168	109	4.8	2.9	0.9	14.8	73.3	6.7	4.3	30.5	33.9
92.0	263	168	109	4.8	2.9	0.9	14.7	73.7	6.7	4.1	30.8	34.2
92.5	263	168	109	4.8	2.9	0.9	14.6	73.3	6.7	4.6	30.6	34.0
93.0	263	168	109	4.8	2.9	0.9	14.6	73.4	6.7	4.4	30.6	34.0
93.5	263	168	109	4.8	2.9	0.9	14.6	73.8	6.7	4.2	30.8	34.3
94.0	263	168	109	4.8	2.9	0.9	14.5	73.4	6.8	4.6	30.7	34.1
94.5	263	169	109	4.8	2.9	0.9	14.5	73.5	6.8	4.4	30.7	34.1
95.0	263	168	109	4.8	2.9	0.9	14.6	73.8	6.7	4.2	30.8	34.3
95.5	264	169	109	4.8	2.9	0.9	14.6	73.4	6.7	4.5	30.7	34.1
96.0	264	169	109	4.8	2.9	0.9	14.7	73.3	6.6	4.5	30.5	33.9
96.5	264	169	109	4.8	2.9	0.9	14.9	73.6	6.6	4.2	30.7	34.1
97.0	264	169	109	4.8	2.9	0.9	14.8	73.0	6.6	4.8	30.3	33.7
97.5	264	169	109	4.8	2.9	0.9	14.9	73.0	6.6	4.5	30.2	33.6
98.0	264	169	109	4.8	2.9	0.9	15.3	74.8	6.7	2.9	31.3	34.8
98.5	264	169	109	4.8	2.9	0.9	15.4	75.1	6.6	2.7	31.4	34.9
99.0	264	169	109	4.8	2.9	0.9	15.4	74.5	6.5	3.2	31.0	34.5
99.5	264	169	109	4.8	2.9	0.9	15.2	73.8	6.6	3.9	30.6	34.1
100.0	264	169	109	4.8	2.9	0.9	14.9	73.1	6.6	4.7	30.3	33.7
100.5	264	169	109	4.8	2.9	0.9	14.9	73.2	6.5	4.5	30.3	33.7
101.0	264	169	109	4.8	2.9	0.9	14.9	73.4	6.5	4.4	30.4	33.8
101.5	264	169	109	4.9	3.1	0.8	14.9	73.2	6.8	4.5	30.5	33.9
102.0	264	169	110	4.9	3.1	0.8	15.4	74.5	6.3	3.2	30.8	34.3
102.5	264	169	110	4.9	3.1	0.8	14.0	75.4	8.8	1.4	33.2	36.9
103.0	265	170	110	4.9	3.1	0.8	9.8	75.2	9.6	4.6	34.7	38.6

103.5	265	170	110	4.9	3.1	0.8	8.9	75.5	9.6	5.0	35.2	39.1
104.0	265	170	110	4.9	3.1	0.8	8.7	75.6	9.8	5.0	35.5	39.5
104.5	265	170	110	4.9	3.1	0.8	8.4	75.3	10.0	5.5	35.5	39.5
105.0	265	170	110	4.9	3.1	0.8	8.2	75.6	10.1	5.0	35.8	39.8
105.5	265	170	110	4.9	3.1	0.8	8.0	75.8	10.2	5.2	36.1	40.2
106.0	265	170	110	4.9	3.1	0.8	7.7	75.1	10.6	5.8	35.9	40.0
106.5	265	170	110	4.9	3.1	0.8	7.4	75.2	11.0	5.3	36.4	40.5
107.0	265	170	110	4.9	3.1	0.8	7.2	75.7	11.1	5.2	36.9	41.0
107.5	265	170	110	4.9	3.1	0.8	6.8	75.2	11.5	5.6	36.9	41.1
108.0	265	170	110	4.9	3.1	0.8	6.5	75.2	12.0	5.1	37.4	41.7
108.5	265	170	110	4.9	3.1	0.8	6.2	75.4	12.2	5.3	37.9	42.2
109.0	265	170	110	4.9	3.1	0.8	5.9	74.8	12.5	6.0	37.8	42.1
109.5	265	170	110	4.9	3.1	0.8	5.8	75.0	13.0	5.3	38.2	42.6
110.0	265	170	110	4.9	3.1	0.8	5.5	75.4	13.4	4.9	39.0	43.4
110.5	265	170	110	4.9	3.1	0.8	5.1	74.6	13.8	5.7	38.8	43.2
111.0	266	170	110	4.9	3.1	0.8	5.1	74.6	14.2	5.1	39.1	43.6
111.5	266	170	110	4.9	3.1	0.8	4.9	75.2	14.5	4.6	40.0	44.5
112.0	266	170	110	4.9	3.1	0.8	4.4	74.8	16.3	4.0	41.3	46.0
112.5	266	170	110	4.9	3.1	0.8	4.0	73.6	15.8	5.8	40.0	44.6
113.0	266	170	110	4.9	3.1	0.8	4.5	74.0	14.2	6.4	38.9	43.3
113.5	266	170	110	4.9	3.1	0.8	5.2	74.6	13.2	6.2	38.4	42.7
114.0	266	171	110	4.9	3.1	0.8	5.5	74.5	12.9	6.0	37.9	42.2
114.5	266	171	110	4.9	3.1	0.8	5.9	75.4	12.2	5.6	37.9	42.2
115.0	266	171	110	4.9	3.1	0.8	6.1	75.0	12.1	5.9	37.5	41.8
115.5	266	171	110	4.9	3.1	0.8	6.2	74.9	12.0	5.8	37.3	41.5
116.0	266	171	110	4.9	3.1	0.8	6.4	75.5	11.6	5.6	37.4	41.6
116.5	266	171	110	4.9	3.1	0.8	6.5	75.2	11.6	5.9	37.1	41.3
117.0	266	171	110	4.9	3.1	0.8	6.6	75.1	11.5	5.7	37.0	41.2
117.5	267	171	110	4.9	3.1	0.8	6.8	75.6	11.1	5.7	37.0	41.1
118.0	267	171	110	4.9	3.1	0.8	6.9	75.0	11.2	6.1	36.6	40.8

118.5	267	171	110	4.9	3.1	0.8	6.9	74.9	11.1	5.9	36.4	40.5
119.0	267	171	110	4.9	3.1	0.8	7.1	75.7	10.8	5.5	36.8	41.0
119.5	267	171	110	4.9	3.1	0.8	7.0	75.1	11.0	5.8	36.5	40.6
120.0	267	171	110	4.9	3.1	0.8	7.1	75.3	11.0	5.5	36.5	40.7
120.5	267	171	110	4.9	3.1	0.8	7.1	75.7	10.7	5.6	36.7	40.8
121.0	267	171	110	4.9	3.1	0.8	7.1	75.5	10.8	5.7	36.6	40.7
121.5	267	171	110	4.9	3.1	0.8	7.2	75.1	10.7	5.9	36.2	40.3
122.0	267	171	110	4.9	3.1	0.8	7.3	75.7	10.5	5.5	36.5	40.6
122.5	267	171	110	4.9	3.1	0.8	7.4	75.3	10.7	5.8	36.3	40.4
123.0	267	171	110	4.9	3.1	0.8	7.4	75.2	10.6	5.7	36.2	40.2
123.5	267	172	110	4.9	3.1	0.8	7.5	75.6	10.2	5.8	36.1	40.2
124.0	267	171	110	4.9	3.1	0.8	7.5	75.3	10.5	5.8	36.1	40.2
124.5	267	172	110	4.9	3.1	0.8	7.4	75.3	10.5	5.8	36.1	40.1
125.0	267	172	110	4.9	3.1	0.8	7.5	75.8	10.2	5.6	36.2	40.3
125.5	267	172	110	4.9	3.1	0.8	7.6	75.4	10.3	5.8	36.0	40.1
126.0	267	172	110	4.9	3.1	0.8	7.6	75.3	10.5	5.5	36.1	40.1
126.5	267	172	110	4.9	3.1	0.8	7.5	75.9	10.1	5.5	36.3	40.4
127.0	267	172	110	4.9	3.1	0.8	7.5	75.4	10.4	5.8	36.2	40.2
127.5	267	172	110	4.9	3.1	0.8	7.6	75.1	10.3	6.0	35.8	39.8
128.0	268	172	110	4.9	3.1	0.8	7.8	75.6	9.8	6.0	35.7	39.8
128.5	267	172	110	4.9	3.1	0.8	7.8	75.3	10.0	5.9	35.7	39.7
129.0	268	172	110	4.9	3.1	0.8	7.8	75.7	10.3	5.3	36.1	40.2
129.5	268	172	110	4.9	3.1	0.8	7.7	75.7	9.9	5.8	35.9	39.9
130.0	268	172	110	4.9	3.1	0.8	7.7	75.4	10.2	5.8	35.9	40.0
130.5	268	172	110	4.9	3.1	0.8	7.7	75.4	10.3	5.5	36.0	40.0
131.0	268	172	110	4.9	3.1	0.8	7.8	75.9	9.8	5.6	36.0	40.0
131.5	268	172	110	4.9	3.1	0.8	7.9	75.4	10.0	5.8	35.8	39.8
132.0	268	172	110	4.9	3.1	0.8	7.9	75.4	10.1	5.6	35.8	39.8
132.5	268	172	110	4.9	3.1	0.8	8.1	76.0	9.6	5.5	35.8	39.8
133.0	268	172	110	4.9	3.1	0.8	8.0	75.6	10.0	5.6	35.9	39.9

133.5	268	172	110	4.9	3.1	0.8	8.0	75.3	9.8	5.8	35.5	39.5
134.0	268	172	110	4.9	3.1	0.8	8.3	75.7	9.4	5.7	35.4	39.4
134.5	268	172	111	4.9	3.1	0.8	8.3	75.6	9.5	5.7	35.4	39.4
135.0	268	172	113	4.9	3.0	0.8	7.5	66.0	10.5	13.5	29.8	33.2
135.5	268	172	113	4.9	2.9	0.8	7.9	72.3	9.0	8.7	32.9	36.6
136.0	268	172	115	4.9	2.8	0.8	7.7	69.9	6.4	12.3	29.9	33.3
136.5	268	172	116	4.9	2.7	0.8	8.0	68.0	7.7	13.2	29.3	32.6
137.0	268	172	117	5.0	2.6	0.7	8.4	67.4	5.9	14.7	28.0	31.1
137.5	267	172	118	4.9	2.6	0.7	8.4	65.6	6.8	15.6	27.4	30.4
138.0	267	172	118	5.0	2.6	0.7	8.6	65.3	6.5	15.5	27.0	30.0
138.5	267	172	119	5.0	2.5	0.7	8.7	63.1	6.0	17.7	25.5	28.3
139.0	267	172	120	5.0	2.4	0.7	8.3	58.2	6.2	21.4	23.0	25.6
139.5	267	172	121	5.0	2.3	0.7	8.5	58.6	5.1	21.6	22.8	25.3
140.0	267	172	121	5.0	2.2	0.7	8.7	57.4	4.1	23.5	21.7	24.1
140.5	267	171	122	5.0	2.2	0.7	9.2	56.0	4.1	24.2	21.0	23.4
141.0	266	171	122	5.0	2.2	0.7	9.8	55.3	4.1	24.0	20.6	22.8
141.5	266	171	123	5.0	2.1	0.6	10.5	54.9	3.6	24.2	20.1	22.3
142.0	266	171	123	5.0	2.1	0.6	11.1	54.0	3.6	24.6	19.6	21.8
142.5	266	171	123	5.0	2.1	0.6	11.5	53.4	3.4	24.6	19.2	21.3
143.0	266	171	123	5.0	2.1	0.6	11.9	53.5	3.1	24.4	19.1	21.2
143.5	266	171	123	5.0	2.0	0.6	11.0	48.5	3.0	29.5	16.9	18.8
144.0	265	171	115	4.9	2.7	0.8	13.3	59.6	6.5	18.0	23.1	25.7
144.5	265	172	113	4.8	2.9	0.8	17.2	75.8	3.8	2.8	29.9	33.2
145.0	266	172	112	4.8	3.0	0.8	17.4	72.8	5.2	3.7	28.9	32.1
145.5	265	172	111	4.8	3.0	0.8	14.1	73.0	7.1	4.6	30.6	34.1
146.0	265	172	111	4.8	3.0	0.8	11.6	74.5	7.3	5.5	32.3	36.0
146.5	266	173	111	4.8	3.0	0.8	11.4	74.4	7.6	5.6	32.5	36.2
147.0	266	173	110	4.8	3.1	0.8	11.6	74.5	7.7	5.2	32.6	36.3
147.5	265	173	110	4.8	3.1	0.8	11.2	75.3	7.9	4.9	33.3	37.0
148.0	266	173	110	4.8	3.1	0.9	10.2	75.5	8.8	4.7	34.3	38.2

148.5	266	173	110	4.8	3.1	0.9	9.7	75.2	9.1	5.2	34.4	38.3
149.0	266	173	110	4.8	3.1	0.9	10.5	75.9	7.9	5.0	33.9	37.7
149.5	266	173	110	4.8	3.1	0.9	11.1	75.8	8.2	4.4	33.9	37.7
150.0	266	172	108	2.6	0.0	0.0	10.9	72.8	2.6	11.1	29.0	32.2
150.5	265	171	104	2.1	0.1	0.1	5.6	36.8	3.1	41.8	12.6	14.0

Appendix B

a) GHSV = 663 h^{-1}

time, min	T_1, °C	T_2, °C	T_3, °C	P, bar	v_{H_2in}, Ndm^3/min	v_{CO_2in}, Ndm^3/min	CO_2 %	CH_4 %	H_2 %	N_2 %	LHV, MJ/kg	HHV, MJ/kg
0.0	197	299	175	0.0	3.6	0.9	0.6	3.1	16.9	62.8	3.1	3.6
0.5	209	308	193	0.1	3.6	0.9	7.9	58.6	19.9	12.4	30.9	34.5
1.0	215	310	203	0.0	3.6	0.9	8.1	72.2	17.5	2.2	38.7	43.1
1.5	219	311	208	0.0	3.6	0.9	7.5	73.3	16.9	2.2	39.4	43.9
2.0	222	310	211	0.0	3.6	0.9	7.3	73.9	16.6	2.1	39.7	44.3
2.5	225	310	214	0.0	3.6	0.9	7.3	74.0	16.5	2.1	39.7	44.3
3.0	228	309	217	0.0	3.6	0.9	7.3	74.4	16.4	1.8	39.9	44.5
3.5	230	308	219	0.0	3.6	0.9	7.4	74.2	16.4	2.0	39.8	44.3
4.0	234	308	221	0.0	3.6	0.9	7.4	74.1	16.4	2.1	39.7	44.2
4.5	236	307	223	0.0	3.6	0.9	7.4	74.2	16.4	2.1	39.7	44.2
5.0	239	306	224	0.0	3.6	0.9	7.4	74.6	16.2	1.9	39.9	44.5
5.5	242	305	226	0.0	3.6	0.9	7.4	74.6	16.2	1.9	39.9	44.4
6.0	245	304	227	0.0	3.6	0.9	7.4	74.1	16.2	2.3	39.6	44.1
6.5	249	303	228	0.0	3.6	0.9	7.4	74.3	16.2	2.1	39.7	44.2
7.0	252	302	229	0.0	3.6	0.9	7.4	74.5	16.1	2.0	39.7	44.3
7.5	256	301	230	0.0	3.6	0.9	7.4	74.5	16.1	2.0	39.8	44.3
8.0	259	300	231	0.0	3.6	0.9	7.4	74.3	16.1	2.2	39.6	44.1
8.5	263	300	231	0.0	3.6	0.9	7.4	74.4	16.1	2.1	39.6	44.2
9.0	266	299	232	0.0	3.6	0.9	7.4	74.5	16.5	1.7	40.1	44.6
9.5	270	298	232	0.0	3.6	0.9	6.5	74.6	17.2	1.8	41.0	45.7
10.0	273	297	233	0.0	3.6	0.9	5.9	74.9	17.1	2.1	41.5	46.3
10.5	277	296	233	0.0	3.6	0.9	5.9	75.0	16.9	2.2	41.4	46.2
11.0	280	295	233	0.0	3.6	0.9	5.8	75.5	16.1	2.6	41.2	45.9
11.5	283	295	233	0.1	3.6	0.9	5.5	76.7	15.5	2.2	41.8	46.6
12.0	286	294	233	0.2	3.6	0.9	5.6	76.9	15.4	2.1	41.9	46.6
12.5	289	293	233	0.2	3.6	0.9	5.6	77.0	15.3	2.1	41.9	46.7

13.0	292	292	233	0.2	3.6	0.9	5.6	77.1	15.3	2.1	41.9	46.7
13.5	294	291	233	0.2	3.6	0.9	5.6	77.1	15.3	2.0	41.9	46.7
14.0	297	290	233	0.2	3.6	0.9	5.6	77.2	15.3	2.0	42.0	46.8
14.5	299	290	233	0.2	3.6	0.9	5.6	77.2	15.2	2.0	42.0	46.8
15.0	301	289	233	0.2	3.6	0.9	5.6	77.2	15.0	2.2	41.8	46.6
15.5	304	288	232	0.2	3.6	0.9	5.2	78.6	13.8	2.5	42.1	46.9
16.0	305	288	232	0.5	3.6	0.9	4.4	80.5	12.8	2.3	43.1	48.0
16.5	308	287	232	0.5	3.6	0.9	4.7	81.0	12.3	2.0	43.1	47.9
17.0	309	286	232	0.6	3.6	0.9	4.7	81.3	12.1	1.9	43.1	48.0
17.5	311	285	232	0.6	3.6	0.9	4.8	81.5	12.0	1.8	43.1	48.0
18.0	313	284	231	0.6	3.6	0.9	4.8	81.6	11.9	1.8	43.1	48.0
18.5	314	283	231	0.7	3.6	0.9	4.6	82.0	11.8	1.7	43.4	48.3
19.0	315	283	230	0.9	3.6	0.9	4.4	82.5	10.9	2.2	43.2	48.1
19.5	316	282	230	0.9	3.6	0.9	4.1	83.7	10.5	1.8	44.0	48.9
20.0	317	282	230	1.0	3.6	0.9	4.1	84.1	10.1	1.7	44.0	48.9
20.5	319	281	230	1.0	3.6	0.9	4.2	84.2	9.9	1.6	43.9	48.8
21.0	320	280	229	1.0	3.6	0.9	4.3	84.3	9.8	1.6	43.9	48.8
21.5	321	279	229	1.1	3.6	0.9	4.3	84.4	9.7	1.6	43.9	48.8
22.0	321	278	228	1.1	3.6	0.9	4.2	84.5	9.7	1.6	43.9	48.8
22.5	322	278	228	1.1	3.6	0.9	4.3	84.5	9.6	1.6	43.9	48.8
23.0	323	277	227	1.1	3.6	0.9	4.3	84.6	9.6	1.5	43.9	48.8
23.5	324	276	227	1.1	3.6	0.9	4.3	84.6	9.6	1.5	43.9	48.8
24.0	325	275	226	1.1	3.6	0.9	4.3	84.6	9.5	1.6	43.8	48.7
24.5	326	275	225	1.1	3.6	0.9	4.1	85.2	9.0	1.7	44.0	48.9
25.0	326	274	225	1.4	3.6	0.9	3.5	86.2	8.7	1.6	44.7	49.7
25.5	326	274	225	1.5	3.6	0.9	3.6	86.5	8.3	1.6	44.7	49.7
26.0	327	273	224	1.5	3.6	0.9	3.8	86.5	8.2	1.5	44.5	49.4
26.5	328	273	224	1.5	3.6	0.9	3.9	86.6	8.1	1.5	44.4	49.4
27.0	328	272	223	1.6	3.6	0.9	3.9	86.6	8.0	1.5	44.4	49.3
27.5	329	271	223	1.6	3.6	0.9	3.9	86.6	8.0	1.5	44.3	49.3

28.0	330	271	222	1.6	3.6	0.9	3.9	86.7	7.8	1.6	44.2	49.2
28.5	330	270	222	1.6	3.6	0.9	3.5	87.3	8.0	1.1	45.1	50.1
29.0	330	270	221	1.9	3.6	0.9	3.2	87.5	7.1	2.2	44.6	49.5
29.5	330	269	221	2.1	3.6	0.9	3.0	88.4	7.1	1.5	45.4	50.5
30.0	330	269	220	2.3	3.6	0.9	2.7	89.0	6.5	1.8	45.6	50.6
30.5	331	269	220	2.4	3.6	0.9	2.9	89.2	6.2	1.7	45.4	50.4
31.0	331	269	220	2.5	3.6	0.9	3.1	89.2	6.1	1.6	45.2	50.2
31.5	332	268	219	2.5	3.6	0.9	3.1	89.4	6.0	1.5	45.2	50.2
32.0	332	268	219	2.6	3.6	0.9	3.1	89.4	6.0	1.5	45.2	50.2
32.5	315	267	219	2.7	3.6	0.9	3.1	89.3	5.9	1.7	45.1	50.1
33.0	328	266	218	2.7	3.6	0.9	3.1	89.8	5.5	1.6	45.2	50.2
33.5	330	266	217	2.7	3.6	0.9	3.2	89.9	5.5	1.4	45.2	50.2
34.0	332	265	217	2.8	3.6	0.9	3.3	89.9	5.4	1.4	45.1	50.1
34.5	332	265	216	2.8	3.6	0.9	3.3	90.0	5.4	1.4	45.1	50.1
35.0	333	264	216	2.8	3.6	0.9	3.3	89.9	5.4	1.5	45.0	50.0
35.5	333	263	215	2.8	3.6	0.9	3.3	89.8	5.4	1.5	45.0	50.0
36.0	334	263	215	2.9	3.6	0.9	3.4	89.7	5.5	1.4	45.0	49.9
36.5	334	263	214	2.9	3.6	0.9	3.4	89.9	5.4	1.3	45.0	50.0
37.0	334	262	214	2.9	3.6	0.9	3.3	89.8	5.2	1.6	44.8	49.8
37.5	335	262	213	2.9	3.6	0.9	3.3	90.1	5.0	1.7	44.9	49.8
38.0	335	261	212	3.0	3.6	0.9	3.5	89.3	6.6	1.0	45.3	50.3
38.5	338	261	212	2.9	3.6	0.9	4.1	87.8	6.3	1.9	43.7	48.5
39.0	334	260	211	3.4	3.6	0.9	3.9	87.6	6.2	2.3	43.6	48.4

b) GHSV = 737 h^{-1}

time, min	T_1, °C	T_2, °C	T_3, °C	P, bar	v_{H_2in}, Ndm^3/min	v_{CO_2in}, Ndm^3/min	CO_2 %	CH_4 %	H_2 %	N_2 %	LHV, MJ/kg	HHV, MJ/kg
0.0	199	309	177	0	4.0	1.0	6.5	73.3	17.6	2.6	40.4	45.0
0.5	213	314	193	0	4.0	1.0	6.5	73.3	17.6	2.6	40.3	45.0
1.0	219	317	204	0	4.0	1.0	6.5	73.3	17.5	2.6	40.3	44.9

1.5	224	318	210	0	4.0	1.0	6.6	73.3	17.5	2.6	40.2	44.8
2.0	229	317	215	0	4.0	1.0	6.6	73.3	17.5	2.6	40.2	44.8
2.5	232	317	218	0	4.0	1.0	6.6	73.4	17.4	2.6	40.2	44.9
3.0	236	317	222	0	4.0	1.0	6.6	73.4	17.4	2.6	40.2	44.8
3.5	239	316	225	0	4.0	1.0	6.6	73.4	17.3	2.7	40.2	44.8
4.0	242	316	228	0	4.0	1.0	6.6	73.5	17.3	2.6	40.3	44.9
4.5	246	315	230	0	4.0	1.0	6.6	73.6	17.2	2.6	40.2	44.8
5.0	250	315	232	0	4.0	1.0	6.6	73.6	17.2	2.6	40.2	44.8
5.5	253	314	234	0	4.0	1.0	6.6	73.7	17.1	2.7	40.2	44.8
6.0	257	313	235	0	4.0	1.0	6.6	73.7	17.1	2.6	40.2	44.8
6.5	261	312	237	0	4.0	1.0	6.6	73.7	17.0	2.6	40.2	44.8
7.0	265	311	238	0	4.0	1.0	6.6	73.8	17.0	2.7	40.2	44.8
7.5	270	310	239	0	4.0	1.0	6.6	73.9	17.0	2.6	40.2	44.8
8.0	274	309	240	0	4.0	1.0	6.6	73.9	16.9	2.6	40.3	44.9
8.5	278	308	240	0	4.0	1.0	6.6	73.9	16.9	2.6	40.3	44.9
9.0	283	307	241	0	4.0	1.0	6.6	74.0	16.9	2.6	40.3	44.9
9.5	287	306	242	0	4.0	1.0	6.6	74.0	16.9	2.6	40.3	44.9
10.0	291	305	242	0	4.0	1.0	6.6	74.0	16.9	2.6	40.3	44.9
10.5	295	304	242	0	4.0	1.0	6.5	74.0	16.8	2.6	40.3	44.9
11.0	299	303	242	0	4.0	1.0	6.5	74.1	16.8	2.6	40.3	44.9
11.5	303	302	243	0	4.0	1.0	6.6	74.0	16.8	2.6	40.3	44.9
12.0	307	301	243	0	4.0	1.0	6.5	74.1	16.8	2.6	40.3	44.9
12.5	311	300	243	0	4.0	1.0	6.5	74.2	16.8	2.5	40.3	44.9
13.0	314	299	243	0	4.0	1.0	6.5	74.2	16.7	2.6	40.3	44.9
13.5	317	298	243	0	4.0	1.0	6.5	74.2	16.7	2.6	40.3	44.9
14.0	321	297	243	0	4.0	1.0	6.5	74.2	16.7	2.6	40.3	44.9
14.5	323	296	243	0	4.0	1.0	6.5	74.3	16.6	2.6	40.3	45.0
15.0	326	295	242	0	4.0	1.0	6.5	74.3	16.6	2.6	40.4	45.0
15.5	328	294	242	0	4.0	1.0	6.5	74.4	16.6	2.6	40.4	45.0
16.0	330	293	242	0	4.0	1.0	6.5	74.4	16.6	2.6	40.4	45.0

16.5	332	292	242	0	4.0	1.0	6.5	74.4	16.6	2.6	40.4	45.0
17.0	334	292	241	0	4.0	1.0	6.5	74.3	16.6	2.6	40.4	45.0
17.5	335	291	241	0	4.0	1.0	6.5	74.3	16.6	2.7	40.3	44.9
18.0	336	290	241	0	4.0	1.0	6.5	74.3	16.6	2.6	40.3	45.0
18.5	336	289	240	0	4.0	1.0	6.5	74.3	16.6	2.6	40.4	45.0
19.0	337	288	240	0	4.0	1.0	6.5	74.3	16.7	2.6	40.4	45.0
19.5	337	288	240	0	4.0	1.0	6.5	74.2	16.7	2.6	40.4	45.0
20.0	337	287	239	0	4.0	1.0	6.5	74.2	16.8	2.6	40.4	45.0
20.5	337	286	239	0	4.0	1.0	6.5	74.1	16.8	2.6	40.4	45.0
21.0	337	286	238	0	4.0	1.0	6.5	74.1	16.8	2.6	40.3	45.0
21.5	336	285	238	0	4.0	1.0	6.5	74.0	16.9	2.6	40.3	45.0
22.0	336	284	237	0	4.0	1.0	6.5	73.9	17.0	2.6	40.3	45.0
22.5	336	284	237	0	4.0	1.0	6.5	73.8	17.0	2.6	40.3	44.9
23.0	335	283	236	0	4.0	1.0	6.6	73.7	17.1	2.6	40.3	44.9
23.5	335	283	236	0	4.0	1.0	6.6	73.6	17.2	2.6	40.3	44.9
24.0	334	282	236	0	4.0	1.0	6.6	73.6	17.2	2.6	40.2	44.8
24.5	333	281	235	0	4.0	1.0	6.6	73.5	17.3	2.5	40.2	44.8
25.0	333	281	234	0	4.0	1.0	6.6	73.4	17.4	2.6	40.2	44.8
25.5	332	280	234	0	4.0	1.0	6.7	73.3	17.5	2.5	40.2	44.8
26.0	331	280	233	0	4.0	1.0	6.7	73.2	17.6	2.6	40.1	44.7
26.5	331	279	233	0	4.0	1.0	6.7	73.1	17.7	2.6	40.1	44.7
27.0	330	279	232	0	4.0	1.0	6.7	73.0	17.8	2.6	40.1	44.7
27.5	329	278	232	0	4.0	1.0	6.7	72.8	17.9	2.6	40.1	44.7
28.0	329	278	231	0	4.0	1.0	6.8	72.7	18.0	2.6	40.0	44.6
28.5	328	277	231	0.1	4.0	1.0	6.8	72.5	18.1	2.6	40.0	44.6
29.0	327	277	230	0.1	4.0	1.0	6.8	72.4	18.2	2.6	40.0	44.6
29.5	327	276	230	0	4.0	1.0	6.8	72.3	18.3	2.6	40.0	44.5
30.0	326	276	229	0.1	4.0	1.0	6.8	72.2	18.4	2.6	39.9	44.5
30.5	325	275	228	0.1	4.0	1.0	6.9	72.0	18.5	2.6	39.9	44.5
31.0	325	275	228	0	4.0	1.0	6.9	71.9	18.9	2.4	40.1	44.7

31.5	324	274	227	0.1	4.0	1.0	6.4	71.8	19.2	2.6	40.5	45.1
32.0	323	274	227	0.1	4.0	1.0	6.4	71.8	19.2	2.7	40.4	45.0
32.5	323	273	226	0.1	4.0	1.0	6.5	71.5	19.2	2.8	40.2	44.8
33.0	322	273	226	0.1	4.0	1.0	6.2	72.6	17.9	3.3	40.1	44.7
33.5	321	272	225	0	4.0	1.0	5.9	74.0	17.2	2.8	40.9	45.6
34.0	321	272	224	0	4.0	1.0	6.0	74.2	17.2	2.6	41.0	45.7
34.5	320	271	224	0	4.0	1.0	6.0	74.3	17.1	2.7	40.9	45.6
35.0	319	271	223	0.1	4.0	1.0	5.8	74.7	16.4	3.1	40.8	45.4
35.5	319	271	223	0.2	4.0	1.0	5.6	75.9	15.9	2.7	41.4	46.1
36.0	318	270	222	0.2	4.0	1.0	5.6	76.1	15.8	2.5	41.5	46.2
36.5	317	270	222	0.2	4.0	1.0	5.7	76.0	15.8	2.6	41.4	46.1
37.0	316	269	221	0.3	4.0	1.0	5.6	76.0	15.8	2.6	41.4	46.2
37.5	316	269	221	0.4	4.0	1.0	5.7	75.8	15.9	2.6	41.3	46.0
38.0	315	268	220	0.4	4.0	1.0	5.7	75.9	15.9	2.5	41.4	46.2
38.5	314	268	220	0.4	4.0	1.0	5.7	75.8	15.8	2.7	41.3	46.0
39.0	313	267	219	0.4	4.0	1.0	5.5	76.5	15.3	2.7	41.5	46.2
39.5	313	266	218	0.4	4.0	1.0	5.4	77.0	15.0	2.6	41.8	46.5
40.0	312	266	218	0.4	4.0	1.0	5.4	77.1	15.0	2.5	41.8	46.5
40.5	311	265	217	0.4	4.0	1.0	5.4	77.2	15.0	2.4	41.9	46.6
41.0	310	265	217	0.5	4.0	1.0	5.4	77.1	14.8	2.7	41.6	46.3
41.5	310	264	216	0.6	4.0	1.0	5.1	77.9	14.3	2.6	42.0	46.8
42.0	309	264	216	0.6	4.0	1.0	5.1	78.3	14.1	2.6	42.1	46.9
42.5	308	263	215	0.6	4.0	1.0	5.2	78.3	14.0	2.5	42.0	46.8
43.0	307	263	215	0.6	4.0	1.0	5.2	78.3	14.0	2.5	42.0	46.8
43.5	306	262	214	0.7	4.0	1.0	5.1	78.5	13.3	3.1	41.6	46.3
44.0	306	262	214	0.7	4.0	1.0	4.3	80.8	12.3	2.7	43.0	47.9
44.5	305	261	213	0.8	4.0	1.0	4.3	80.0	13.5	2.2	43.4	48.3
45.0	305	260	213	0.8	4.0	1.0	6.8	75.1	15.6	2.6	40.0	44.6
45.5	304	260	212	0.8	4.0	1.0	5.9	75.8	15.3	3.0	40.8	45.4
46.0	302	260	211	1.2	4.0	1.0	4.8	78.3	13.8	3.1	42.0	46.8

46.5	302	260	212	1.2	4.0	1.0	4.2	80.2	12.7	2.9	42.9	47.7
47.0	302	258	210	1.1	4.0	1.0	4.5	80.6	12.3	2.5	42.8	47.6
47.5	301	257	209	1	4.0	1.0	4.6	80.7	12.2	2.4	42.7	47.5
48.0	300	256	208	1	4.0	1.0	4.6	80.9	12.1	2.4	42.7	47.6
48.5	299	256	209	1.1	4.0	1.0	4.7	80.9	12.0	2.4	42.8	47.6
49.0	299	256	209	1.1	4.0	1.0	4.7	80.9	12.0	2.4	42.7	47.6
49.5	298	255	208	1.2	4.0	1.0	4.7	80.9	12.0	2.4	42.7	47.5
50.0	298	255	208	1.2	4.0	1.0	4.6	81.1	11.7	2.6	42.6	47.4
50.5	297	254	207	1.2	4.0	1.0	4.3	82.0	11.3	2.4	43.2	48.0
51.0	297	253	207	1.3	4.0	1.0	4.2	82.4	11.0	2.4	43.2	48.1
51.5	296	253	206	1.3	4.0	1.0	4.4	82.5	10.9	2.3	43.2	48.0
52.0	296	252	206	1.3	4.0	1.0	4.4	82.5	10.9	2.3	43.1	48.0
52.5	295	252	205	1.5	4.0	1.0	4.4	82.5	10.8	2.3	43.1	48.0
53.0	295	251	205	1.5	4.0	1.0	4.4	82.5	10.8	2.2	43.1	48.0
53.5	294	251	205	1.6	4.0	1.0	4.5	82.5	10.9	2.2	43.1	47.9
54.0	294	250	204	1.6	4.0	1.0	4.5	82.4	10.9	2.3	43.0	47.9
54.5	293	250	204	1.6	4.0	1.0	4.5	82.3	10.9	2.2	43.0	47.9
55.0	293	249	203	1.6	4.0	1.0	4.5	82.3	10.9	2.2	43.0	47.8
55.5	292	248	202	1.6	4.0	1.0	4.5	82.2	11.0	2.3	42.9	47.8
56.0	292	248	202	1.6	4.0	1.0	4.5	82.4	10.3	2.8	42.6	47.4
56.5	291	247	201	1.7	4.0	1.0	3.9	84.4	9.1	2.6	43.4	48.3
57.0	291	246	201	1.7	4.0	1.0	3.6	85.6	8.4	2.4	44.0	48.9
57.5	290	246	200	1.7	4.0	1.0	3.7	85.9	8.1	2.2	44.0	48.9
58.0	290	245	200	1.7	4.0	1.0	3.8	86.1	8.0	2.2	43.9	48.8
58.5	289	245	199	2.1	4.0	1.0	3.8	86.2	7.9	2.2	43.9	48.8
59.0	289	245	200	2.3	4.0	1.0	3.8	86.3	7.9	2.0	44.0	48.9
59.5	288	245	200	2.4	4.0	1.0	3.9	86.1	7.8	2.2	43.8	48.7
60.0	288	244	199	2.5	4.0	1.0	3.8	86.4	7.7	2.1	43.9	48.8
60.5	288	244	199	2.5	4.0	1.0	3.8	86.4	7.7	2.1	43.9	48.8
61.0	287	243	199	2.6	4.0	1.0	3.8	86.4	7.7	2.1	43.9	48.8

61.5	287	243	199	2.6	4.0	1.0	3.8	86.3	7.7	2.1	43.9	48.8
62.0	287	242	198	2.7	4.0	1.0	3.9	86.2	7.1	2.9	43.2	48.0
62.5	286	241	197	2.7	4.0	1.0	3.4	86.9	9.4	0.7	45.8	50.9
63.0	286	240	197	2.7	4.0	1.0	4.7	81.7	6.9	6.8	39.4	43.8
63.5	285	240	196	2.7	4.0	1.0	6.9	84.0	9.4	1.3	41.2	45.8
64.0	285	239	196	2.7	4.0	1.0	2.4	85.2	8.3	4.2	44.1	49.0
64.5	283	239	195	3	4.0	1.0	2.0	89.8	4.9	3.2	45.1	50.1
65.0	287	238	196	3.5	4.0	1.0	3.1	90.2	4.8	2.0	44.9	49.8
65.5	282	237	193	4	4.0	1.0	3.2	90.1	4.8	1.9	44.7	49.7
66.0	282	238	194	4.1	4.0	1.0	3.2	90.3	4.6	1.9	44.7	49.7
66.5	282	238	196	4	4.0	1.0	3.2	90.3	4.6	1.9	44.7	49.7
67.0	282	238	196	4	4.0	1.0	3.3	90.4	4.5	1.9	44.7	49.7
67.5	281	237	195	4.1	4.0	1.0	3.3	90.6	4.2	1.9	44.7	49.6
68.0	281	236	195	4.2	4.0	1.0	3.2	90.8	4.2	1.8	44.8	49.7
68.5	281	236	195	4.3	4.0	1.0	3.1	91.1	3.8	2.0	44.8	49.7
69.0	281	235	194	4.4	4.0	1.0	3.0	91.6	3.6	1.9	45.0	49.9
69.5	282	235	195	4.6	4.0	1.0	3.1	91.6	3.4	2.0	44.8	49.8
70.0	266	235	194	4.8	4.0	1.0	3.1	91.9	3.2	1.9	44.9	49.8
70.5	269	234	194	4.9	4.0	1.0	3.0	92.1	3.0	1.9	44.9	49.9
71.0	273	233	193	5.1	4.0	1.0	3.0	92.3	2.8	1.9	44.9	49.8
71.5	274	233	193	5.2	4.0	1.0	3.1	92.4	2.7	1.8	44.9	49.8
72.0	275	233	193	5.5	4.0	1.0	3.1	92.3	2.9	1.7	44.9	49.9
72.5	275	232	192	5.7	4.0	1.0	2.8	91.8	2.9	2.4	44.7	49.7
73.0	277	232	193	5.9	4.0	1.0	2.5	92.6	2.1	2.9	44.8	49.7
73.5	276	232	192	6.1	4.0	1.0	2.4	93.3	2.6	2.1	45.5	50.5
74.0	249	232	192	6.3	4.0	1.0	3.2	85.2	12.5	3.2	44.4	49.4

c) GHSV = 811 h^{-1}

time, min	T_1, °C	T_2, °C	T_3, °C	p, bar	v_{H_2in}, Ndm^3/min	v_{CO_2in}, Ndm^3/min	CO_2 %	CH_4 %	H_2 %	N_2 %	LHV, MJ/kg	HHV, MJ/kg

0.0	198	298	174	0.0	4.4	1.1	6.5	47.6	23.5	20.4	26.3	29.4
0.5	212	310	190	0.1	4.4	1.1	7.9	69.4	19.6	3.0	38.2	42.6
1.0	219	313	202	0.0	4.4	1.1	7.2	71.1	18.9	2.7	39.4	43.9
1.5	224	314	208	0.1	4.4	1.1	7.1	71.4	18.9	2.6	39.6	44.1
2.0	229	314	213	0.1	4.4	1.1	7.1	71.4	18.9	2.6	39.6	44.1
2.5	232	313	216	0.1	4.4	1.1	7.1	71.4	18.9	2.7	39.5	44.1
3.0	236	312	220	0.1	4.4	1.1	7.1	71.4	18.9	2.7	39.5	44.1
3.5	239	311	223	0.1	4.4	1.1	7.1	71.4	18.8	2.7	39.5	44.1
4.0	242	310	226	0.1	4.4	1.1	7.1	71.5	18.7	2.7	39.5	44.1
4.5	246	309	228	0.1	4.4	1.1	7.1	71.5	18.7	2.7	39.5	44.1
5.0	250	308	230	0.1	4.4	1.1	7.1	71.6	18.6	2.7	39.5	44.1
5.5	254	307	232	0.1	4.4	1.1	7.1	71.6	18.6	2.7	39.5	44.1
6.0	259	306	234	0.1	4.4	1.1	7.1	71.7	18.6	2.7	39.5	44.1
6.5	263	305	235	0.1	4.4	1.1	7.1	71.7	18.5	2.7	39.5	44.1
7.0	268	304	236	0.1	4.4	1.1	7.1	71.7	18.5	2.7	39.5	44.1
7.5	273	303	237	0.1	4.4	1.1	7.1	71.7	18.5	2.7	39.5	44.1
8.0	278	302	239	0.1	4.4	1.1	7.1	71.7	18.4	2.7	39.5	44.0
8.5	283	301	239	0.1	4.4	1.1	7.1	71.8	18.4	2.7	39.5	44.1
9.0	288	300	240	0.1	4.4	1.1	7.1	71.7	18.4	2.8	39.5	44.0
9.5	293	299	241	0.1	4.4	1.1	7.1	71.8	18.4	2.7	39.5	44.1
10.0	298	298	241	0.1	4.4	1.1	7.1	71.9	18.4	2.7	39.6	44.1
10.5	302	297	242	0.1	4.4	1.1	7.1	71.8	18.4	2.7	39.5	44.1
11.0	307	296	242	0.1	4.4	1.1	7.1	71.8	18.4	2.7	39.5	44.0
11.5	312	295	242	0.1	4.4	1.1	7.1	71.8	18.4	2.7	39.5	44.1
12.0	316	294	242	0.1	4.4	1.1	7.1	71.8	18.4	2.7	39.5	44.1
12.5	320	293	243	0.1	4.4	1.1	7.1	71.8	18.3	2.8	39.5	44.0
13.0	324	292	243	0.1	4.4	1.1	6.8	72.9	16.4	4.0	38.9	43.3
13.5	327	291	243	0.1	4.4	1.1	6.0	76.2	14.7	3.1	40.5	45.1
14.0	330	291	243	0.4	4.4	1.1	6.0	77.0	14.3	2.7	40.8	45.4
14.5	333	291	243	0.5	4.4	1.1	6.1	77.2	14.0	2.7	40.8	45.4

15.0	336	290	243	0.5	4.4	1.1	6.0	77.4	13.9	2.7	40.8	45.4
15.5	338	289	243	0.5	4.4	1.1	6.0	77.5	13.8	2.7	40.9	45.5
16.0	341	288	243	0.5	4.4	1.1	6.0	77.7	13.7	2.6	40.9	45.6
16.5	343	287	243	0.5	4.4	1.1	6.0	77.8	13.3	2.9	40.7	45.3
17.0	345	286	242	0.6	4.4	1.1	5.6	79.5	12.1	2.8	41.3	45.9
17.5	346	285	242	0.7	4.4	1.1	5.2	80.7	11.5	2.6	41.9	46.6
18.0	348	285	242	0.9	4.4	1.1	5.3	80.9	11.3	2.5	41.8	46.5
18.5	349	284	241	0.9	4.4	1.1	5.3	81.1	11.1	2.5	41.8	46.5
19.0	351	284	241	1.0	4.4	1.1	5.3	81.3	11.0	2.4	41.9	46.6
19.5	352	283	241	1.0	4.4	1.1	5.3	81.4	10.9	2.4	41.9	46.6
20.0	353	282	240	1.0	4.4	1.1	5.3	81.5	10.8	2.3	41.9	46.7
20.5	355	282	240	1.0	4.4	1.1	5.3	81.5	10.8	2.4	41.9	46.6
21.0	356	281	239	1.0	4.4	1.1	5.2	81.9	10.0	2.9	41.6	46.3
21.5	357	280	238	1.1	4.4	1.1	4.1	84.2	9.4	2.3	43.4	48.3
22.0	356	280	237	1.5	4.4	1.1	3.6	85.7	8.1	2.6	43.8	48.7
22.5	358	280	238	1.8	4.4	1.1	4.2	85.8	7.8	2.3	43.4	48.2
23.0	359	280	238	1.9	4.4	1.1	4.4	85.9	7.6	2.2	43.1	48.0
23.5	359	279	237	1.9	4.4	1.1	4.5	86.0	7.4	2.1	43.1	47.9
24.0	360	278	237	2.0	4.4	1.1	4.6	86.1	7.3	2.0	43.1	47.9
24.5	361	278	236	2.0	4.4	1.1	4.4	86.2	7.9	1.5	43.7	48.6
25.0	361	277	235	2.1	4.4	1.1	3.6	86.3	7.7	2.4	43.9	48.8
25.5	361	277	235	2.1	4.4	1.1	3.2	87.8	6.9	2.1	44.6	49.6
26.0	361	276	234	2.4	4.4	1.1	2.9	88.5	6.3	2.3	44.9	49.9
26.5	362	276	234	2.8	4.4	1.1	3.1	88.9	6.0	2.0	44.8	49.8
27.0	361	276	233	2.9	4.4	1.1	3.2	88.9	5.9	2.0	44.7	49.7
27.5	362	275	232	3.0	4.4	1.1	3.3	89.0	5.8	1.9	44.7	49.7
28.0	362	275	232	3.0	4.4	1.1	3.3	89.1	5.7	1.9	44.7	49.6
28.5	362	275	231	3.1	4.4	1.1	3.3	89.4	5.5	1.8	44.8	49.8
29.0	363	274	231	3.1	4.4	1.1	3.2	89.4	5.3	2.1	44.7	49.6
29.5	363	274	230	3.3	4.4	1.1	3.2	89.8	5.2	1.7	44.9	49.9

30.0	363	273	229	3.5	4.4	1.1	3.0	90.1	4.9	2.0	44.9	49.9
30.5	363	273	229	3.6	4.4	1.1	3.0	90.4	4.8	1.8	45.1	50.1
31.0	363	273	228	3.8	4.4	1.1	3.1	90.4	4.7	1.8	45.0	49.9
31.5	365	273	228	4.0	4.4	1.1	3.1	90.6	4.5	1.9	44.9	49.8
32.0	364	272	228	4.0	4.4	1.1	3.1	90.7	4.4	1.8	44.9	49.9
32.5	364	272	227	4.1	4.4	1.1	3.1	90.9	4.3	1.8	45.0	50.0
33.0	364	271	226	4.2	4.4	1.1	3.1	90.9	4.2	1.8	44.9	49.9
33.5	365	271	226	4.2	4.4	1.1	3.2	90.8	4.2	1.9	44.8	49.8
34.0	365	270	225	4.2	4.4	1.1	3.1	90.9	4.0	2.0	44.7	49.7
34.5	365	270	225	4.3	4.4	1.1	3.1	91.3	4.0	1.7	45.1	50.0
35.0	366	270	224	4.5	4.4	1.1	3.0	91.4	3.8	1.8	45.1	50.0
35.5	366	270	224	4.6	4.4	1.1	2.9	91.7	3.6	1.8	45.2	50.2
36.0	366	269	223	4.8	4.4	1.1	3.0	91.8	3.6	1.6	45.2	50.2
36.5	367	269	224	4.9	4.4	1.1	3.1	91.6	3.6	1.7	45.0	50.0
37.0	361	269	223	5.0	4.4	1.1	3.0	91.9	3.4	1.7	45.1	50.1
37.5	365	268	222	5.1	4.4	1.1	3.0	92.1	3.3	1.7	45.1	50.1
38.0	366	268	222	5.2	4.4	1.1	3.0	92.2	3.2	1.7	45.1	50.1
38.5	366	268	221	5.3	4.4	1.1	3.0	92.2	3.1	1.6	45.1	50.1
39.0	367	267	221	5.4	4.4	1.1	3.1	92.6	3.0	1.3	45.3	50.3
39.5	367	267	221	5.5	4.4	1.1	3.1	92.2	3.0	1.6	45.0	50.0
40.0	368	267	220	5.5	4.4	1.1	3.2	92.1	3.0	1.8	44.9	49.8
40.5	368	266	220	5.5	4.4	1.1	3.1	92.4	2.6	1.9	44.8	49.7
41.0	369	266	219	5.6	4.4	1.1	3.2	92.4	3.3	1.1	45.4	50.4
41.5	343	267	219	6.3	4.4	1.1	2.9	92.3	2.8	2.0	44.9	49.9
42.0	354	266	219	6.3	4.4	1.1	2.9	92.8	2.5	1.8	45.2	50.1

d) GHSV = 885 h^{-1}

time, min	T_1, °C	T_2, °C	T_3, °C	p, bar	v_{H_2in}, Ndm^3/min	v_{CO_2in}, Ndm^3/min	CO_2 %	CH_4 %	H_2 %	N_2 %	LHV, MJ/kg	HHV, MJ/kg
0.0	204	299	179	0	4.8	1.2	7.0	70.9	19.3	2.7	21.6	24.2

0.5	217	307	196	0	4.8	1.2	7.0	70.9	19.3	2.7	21.6	24.2
1.0	224	310	206	0	4.8	1.2	7.0	70.9	19.3	2.7	21.6	24.2
1.5	229	310	212	0	4.8	1.2	7.0	70.9	19.3	2.7	21.6	24.2
2.0	233	311	217	0	4.8	1.2	7.0	70.9	19.3	2.7	21.6	24.2
2.5	237	310	221	0	4.8	1.2	7.0	70.9	19.3	2.7	21.6	24.2
3.0	241	310	225	0	4.8	1.2	7.0	70.9	19.3	2.7	21.6	24.2
3.5	245	310	228	0	4.8	1.2	7.0	70.9	19.3	2.7	21.6	24.2
4.0	249	309	230	0	4.8	1.2	7.0	70.9	19.3	2.7	21.6	24.2
4.5	253	309	233	0	4.8	1.2	7.0	70.9	19.3	2.7	21.6	24.2
5.0	258	309	236	0	4.8	1.2	7.0	70.9	19.3	2.7	21.6	24.2
5.5	263	308	238	0	4.8	1.2	7.0	70.9	19.3	2.7	21.6	24.2
6.0	269	308	240	0	4.8	1.2	7.0	70.9	19.3	2.7	21.6	24.2
6.5	275	307	241	0	4.8	1.2	7.0	70.9	19.3	2.5	39.5	44.1
7.0	281	307	243	0	4.8	1.2	7.0	71.4	19.1	2.5	39.8	44.3
7.5	288	306	244	0.1	4.8	1.2	7.0	71.5	19.0	2.5	39.9	44.4
8.0	294	306	246	0.1	4.8	1.2	6.9	71.6	19.0	2.5	39.9	44.4
8.5	300	305	247	0.1	4.8	1.2	7.0	71.6	19.0	2.5	39.9	44.5
9.0	307	304	248	0.1	4.8	1.2	6.9	71.7	18.9	2.5	39.9	44.5
9.5	313	303	248	0.1	4.8	1.2	6.9	71.7	18.9	2.5	39.9	44.5
10.0	319	302	249	0.1	4.8	1.2	6.9	71.7	18.8	2.5	39.9	44.5
10.5	324	301	250	0.1	4.8	1.2	6.8	72.5	16.5	4.2	38.7	43.2
11.0	329	300	250	0.1	4.8	1.2	5.6	77.6	13.8	3.1	41.1	45.7
11.5	333	301	250	0.8	4.8	1.2	5.3	79.3	12.9	2.4	41.9	46.6
12.0	338	301	251	0.8	4.8	1.2	5.4	79.7	12.6	2.3	41.9	46.6
12.5	342	299	252	0.9	4.8	1.2	5.4	80.1	12.3	2.2	42.0	46.7
13.0	345	298	252	1	4.8	1.2	5.3	80.3	12.2	2.2	42.1	46.9
13.5	348	297	252	1	4.8	1.2	5.2	80.6	12.0	2.2	42.2	47.0
14.0	351	296	252	1	4.8	1.2	5.1	80.8	11.8	2.2	42.3	47.1
14.5	353	295	252	1.1	4.8	1.2	5.1	81.0	11.6	2.2	42.3	47.1
15.0	355	294	251	1.1	4.8	1.2	5.1	81.2	11.5	2.1	42.3	47.1

15.5	357	294	251	1.1	4.8	1.2	5.1	81.3	11.4	2.2	42.3	47.1
16.0	359	293	251	1.1	4.8	1.2	5.1	81.5	10.9	2.4	42.1	46.8
16.5	361	292	250	1.1	4.8	1.2	4.5	83.0	10.3	2.2	43.1	47.9
17.0	362	291	250	1.5	4.8	1.2	3.8	84.4	9.6	2.2	43.9	48.9
17.5	364	291	250	1.8	4.8	1.2	3.9	85.1	8.8	2.2	43.8	48.7
18.0	365	290	250	1.9	4.8	1.2	4.2	85.3	8.5	2.0	43.5	48.4
18.5	366	290	249	2	4.8	1.2	4.3	85.5	8.3	1.9	43.4	48.3
19.0	368	289	249	2.1	4.8	1.2	4.4	85.6	8.1	1.8	43.4	48.3
19.5	369	288	248	2.1	4.8	1.2	4.4	85.7	8.0	1.9	43.4	48.2
20.0	370	288	248	2.2	4.8	1.2	4.4	85.8	7.9	1.8	43.4	48.3
20.5	365	287	247	2.2	4.8	1.2	4.3	86.1	7.8	1.8	43.5	48.4
21.0	370	286	247	2.3	4.8	1.2	4.4	86.2	7.7	1.8	43.5	48.3
21.5	372	286	246	2.3	4.8	1.2	4.4	86.3	7.5	1.8	43.5	48.3
22.0	374	285	246	2.3	4.8	1.2	4.3	86.4	7.5	1.7	43.6	48.5
22.5	375	284	245	2.3	4.8	1.2	4.3	86.7	7.2	1.9	43.5	48.4
23.0	376	284	245	2.4	4.8	1.2	4.0	87.3	7.0	1.7	44.0	48.9
23.5	377	284	244	2.6	4.8	1.2	4.2	87.3	6.8	1.7	43.8	48.7
24.0	378	283	243	2.6	4.8	1.2	4.2	87.4	6.5	1.9	43.5	48.4
24.5	379	283	243	2.6	4.8	1.2	3.9	88.2	6.5	1.4	44.3	49.3
25.0	379	283	242	3.1	4.8	1.2	3.8	88.4	6.0	1.9	44.1	49.0
25.5	380	282	242	3.1	4.8	1.2	4.1	88.4	6.0	1.5	44.0	48.8
26.0	380	282	241	3.1	4.8	1.2	4.0	88.5	5.8	1.7	43.9	48.8
26.5	381	282	241	3.1	4.8	1.2	3.9	89.1	5.4	1.6	44.1	49.0
27.0	381	281	240	3.6	4.8	1.2	3.4	89.8	5.1	1.7	44.7	49.6
27.5	381	282	240	3.9	4.8	1.2	3.4	90.3	4.7	1.7	44.7	49.7
28.0	381	281	239	4.1	4.8	1.2	3.6	90.4	4.5	1.5	44.6	49.5
28.5	382	281	239	4.3	4.8	1.2	3.7	90.3	4.6	1.4	44.5	49.4
29.0	358	281	238	4.5	4.8	1.2	3.7	90.3	4.3	1.6	44.3	49.2
29.5	376	281	238	4.6	4.8	1.2	3.7	90.7	4.1	1.5	44.5	49.4
30.0	379	280	237	4.8	4.8	1.2	3.6	90.9	3.9	1.5	44.5	49.4

30.5	381	280	237	4.9	4.8	1.2	3.7	91.1	3.8	1.5	44.5	49.4
31.0	381	279	236	5.1	4.8	1.2	3.7	91.2	3.7	1.5	44.5	49.4
31.5	382	279	236	5.2	4.8	1.2	3.7	91.2	3.6	1.5	44.4	49.3
32.0	382	279	235	5.4	4.8	1.2	3.7	91.3	3.5	1.5	44.4	49.3
32.5	383	279	235	5.5	4.8	1.2	3.8	91.4	3.3	1.5	44.3	49.2
33.0	374	279	234	5.7	4.8	1.2	3.7	91.6	3.2	1.5	44.4	49.3
33.5	372	279	234	6.1	4.8	1.2	3.6	91.9	2.9	1.6	44.4	49.3
34.0	374	278	231	6.4	4.8	1.2	3.9	91.8	2.6	1.7	44.0	48.9
34.5	371	278	233	6.6	4.8	1.2	4.6	91.5	2.0	1.8	43.0	47.7
35.0	377	277	232	6.7	4.8	1.2	6.8	89.8	1.1	2.4	40.2	44.7
35.5	378	276	231	6.7	4.8	1.2	11.7	84.9	6.2	1.7	36.1	40.2
36.0	378	276	230	6.8	4.8	1.2	11.7	84.9	6.2	1.7	36.1	40.2

e) GHSV = 958 h^{-1}

time, min	T_1, °C	T_2, °C	T_3, °C	p, bar	v_{H_2in}, Ndm^3/min	v_{CO_2in}, Ndm^3/min	CO_2 %	CH_4 %	H_2 %	N_2 %	LHV, MJ/kg	HHV, MJ/kg
0.0	204	305	182	0.0	5.2	1.3	7.3	69.2	21.2	2.2	39.6	44.1
0.5	216	313	200	0.1	5.2	1.3	7.2	69.2	21.3	2.3	39.7	44.3
1.0	224	315	208	0.0	5.2	1.3	7.2	69.2	21.3	2.3	39.7	44.3
1.5	230	315	214	0.1	5.2	1.3	7.2	69.2	21.3	2.4	39.6	44.2
2.0	234	315	219	0.1	5.2	1.3	7.2	69.2	21.2	2.4	39.6	44.2
2.5	238	313	223	0.1	5.2	1.3	7.2	69.2	21.2	2.4	39.6	44.2
3.0	243	312	227	0.1	5.2	1.3	7.2	69.3	21.1	2.4	39.6	44.2
3.5	247	311	230	0.1	5.2	1.3	7.2	69.3	21.0	2.4	39.6	44.2
4.0	252	310	233	0.1	5.2	1.3	7.2	69.4	21.0	2.4	39.7	44.2
4.5	257	308	235	0.1	5.2	1.3	7.2	69.5	20.9	2.4	39.7	44.3
5.0	263	307	238	0.1	5.2	1.3	7.2	69.6	20.9	2.4	39.7	44.3
5.5	269	305	240	0.1	5.2	1.3	7.2	69.6	20.8	2.4	39.7	44.3
6.0	276	304	241	0.1	5.2	1.3	7.2	69.7	20.8	2.4	39.7	44.3
6.5	283	302	243	0.1	5.2	1.3	7.1	69.7	20.7	2.4	39.7	44.3

7.0	290	301	244	0.1	5.2	1.3	7.1	69.7	20.7	2.4	39.7	44.3
7.5	298	300	246	0.1	5.2	1.3	7.1	69.8	20.7	2.4	39.7	44.3
8.0	305	299	247	0.1	5.2	1.3	7.1	69.8	20.7	2.5	39.7	44.3
8.5	312	297	248	0.1	5.2	1.3	7.1	69.8	20.7	2.4	39.7	44.3
9.0	319	296	248	0.1	5.2	1.3	7.1	69.8	20.6	2.4	39.7	44.3
9.5	326	295	249	0.1	5.2	1.3	7.1	69.9	20.6	2.4	39.7	44.3
10.0	332	294	250	0.1	5.2	1.3	7.1	69.9	20.6	2.4	39.7	44.3
10.5	338	293	250	0.1	5.2	1.3	7.1	69.9	20.6	2.5	39.7	44.3
11.0	343	292	251	0.1	5.2	1.3	7.0	70.4	19.1	3.6	38.9	43.4
11.5	349	291	251	0.1	5.2	1.3	6.3	73.8	17.0	2.8	40.4	45.0
12.0	353	290	251	0.1	5.2	1.3	6.2	74.9	16.5	2.4	40.9	45.6
12.5	358	289	251	0.1	5.2	1.3	6.1	75.2	16.4	2.3	41.1	45.8
13.0	361	289	252	0.4	5.2	1.3	6.1	75.5	16.2	2.3	41.1	45.8
13.5	365	289	252	0.4	5.2	1.3	6.1	75.6	16.1	2.2	41.2	45.9
14.0	368	288	252	0.4	5.2	1.3	6.0	75.7	16.0	2.3	41.2	45.9
14.5	370	287	252	0.5	5.2	1.3	6.0	76.0	15.4	2.6	40.9	45.6
15.0	373	286	252	0.5	5.2	1.3	5.6	77.4	14.5	2.4	41.6	46.3
15.5	375	286	251	0.5	5.2	1.3	5.5	78.1	14.1	2.2	41.8	46.6
16.0	377	285	251	0.5	5.2	1.3	5.6	78.3	14.0	2.1	41.8	46.6
16.5	379	285	251	0.7	5.2	1.3	5.6	78.4	13.5	2.5	41.6	46.3
17.0	381	284	251	0.7	5.2	1.3	5.2	80.1	12.2	2.5	42.0	46.8
17.5	382	284	250	0.7	5.2	1.3	4.7	81.6	11.5	2.2	42.9	47.7
18.0	384	283	250	0.8	5.2	1.3	4.8	82.0	11.2	2.1	42.8	47.7
18.5	384	283	249	1.2	5.2	1.3	4.8	82.2	11.0	2.0	42.9	47.7
19.0	386	283	249	1.2	5.2	1.3	4.5	83.1	10.5	1.9	43.4	48.2
19.5	387	282	249	1.3	5.2	1.3	3.3	83.8	10.2	2.7	44.2	49.1
20.0	388	282	248	1.3	5.2	1.3	4.9	83.2	9.8	2.1	42.6	47.4
20.5	387	282	247	1.9	5.2	1.3	4.6	83.8	9.8	1.8	43.2	48.1
21.0	390	281	248	1.6	5.2	1.3	4.4	84.1	9.7	1.8	43.4	48.3
21.5	389	281	247	1.6	5.2	1.3	4.4	84.2	9.6	1.8	43.5	48.3

22.0	390	280	246	1.7	5.2	1.3	4.4	84.3	9.5	1.8	43.5	48.4
22.5	391	280	245	1.7	5.2	1.3	4.4	84.4	9.5	1.7	43.5	48.4
23.0	392	280	245	1.7	5.2	1.3	4.4	84.5	9.4	1.7	43.6	48.5
23.5	393	279	244	1.7	5.2	1.3	4.3	84.7	9.3	1.8	43.7	48.5
24.0	394	279	243	1.7	5.2	1.3	4.3	84.7	9.2	1.7	43.6	48.5
24.5	394	279	243	1.8	5.2	1.3	4.3	84.8	8.9	1.9	43.4	48.3
25.0	396	279	242	1.8	5.2	1.3	3.8	85.9	8.9	1.4	44.6	49.6
25.5	397	278	241	1.8	5.2	1.3	3.1	87.0	7.8	2.2	44.8	49.8
26.0	398	278	241	1.8	5.2	1.3	3.7	87.2	7.4	1.7	44.4	49.4
26.5	398	279	240	2.3	5.2	1.3	3.9	87.2	7.3	1.6	44.2	49.1
27.0	398	279	240	2.4	5.2	1.3	4.0	87.3	7.2	1.5	44.2	49.1
27.5	399	279	239	2.5	5.2	1.3	3.9	87.3	7.1	1.6	44.2	49.1
28.0	399	279	239	2.5	5.2	1.3	4.0	87.4	7.1	1.6	44.2	49.1
28.5	400	278	238	2.5	5.2	1.3	4.0	87.5	7.1	1.5	44.2	49.1
29.0	400	278	237	2.6	5.2	1.3	3.9	87.6	6.8	1.7	44.1	49.0
29.5	401	278	237	2.6	5.2	1.3	3.5	88.4	6.5	1.6	44.7	49.6
30.0	402	278	236	2.6	5.2	1.3	3.3	89.1	5.9	1.7	44.9	49.8
30.5	401	278	235	2.8	5.2	1.3	3.5	89.2	5.8	1.5	44.7	49.7
31.0	401	278	235	3.1	5.2	1.3	3.6	89.2	5.7	1.4	44.6	49.6
31.5	402	278	235	3.3	5.2	1.3	3.7	89.2	5.7	1.4	44.6	49.5
32.0	402	278	234	3.3	5.2	1.3	3.7	89.3	5.6	1.4	44.6	49.5
32.5	403	278	233	3.4	5.2	1.3	3.7	89.3	5.6	1.4	44.5	49.5
33.0	403	278	233	3.4	5.2	1.3	3.7	89.3	5.3	1.7	44.3	49.2
33.5	403	277	233	3.4	5.2	1.3	3.3	90.1	5.7	0.9	45.5	50.5
34.0	404	277	232	3.5	5.2	1.3	3.7	89.6	4.4	2.2	43.8	48.7
34.5	404	277	231	3.6	5.2	1.3	4.6	89.3	5.4	0.7	44.0	48.9
35.0	404	278	231	4.1	5.2	1.3	3.6	89.8	5.3	1.3	44.8	49.8
35.5	405	277	230	3.8	5.2	1.3	3.5	90.1	5.2	1.3	45.0	49.9
36.0	405	277	230	3.8	5.2	1.3	3.5	90.0	5.2	1.3	44.9	49.9
36.5	405	277	229	3.8	5.2	1.3	3.5	90.0	5.1	1.4	44.8	49.8

37.0	406	277	228	3.8	5.2	1.3	3.7	90.0	5.1	1.3	44.7	49.6
37.5	406	276	228	3.8	5.2	1.3	3.7	89.9	4.9	1.5	44.5	49.4
38.0	407	276	228	3.8	5.2	1.3	3.4	90.5	5.1	0.9	45.3	50.3
38.5	407	276	227	3.8	5.2	1.3	3.6	90.3	4.5	1.6	44.5	49.4
39.0	408	276	226	3.8	5.2	1.3	3.8	90.2	4.8	1.2	44.5	49.5
39.5	408	276	226	4.2	5.2	1.3	3.6	90.3	4.8	1.2	44.8	49.8
40.0	408	276	226	4.2	5.2	1.3	3.5	90.4	4.8	1.3	44.9	49.8
40.5	409	276	225	4.1	5.2	1.3	3.6	90.3	4.8	1.3	44.7	49.7
41.0	410	276	225	4.1	5.2	1.3	3.6	90.4	4.2	1.8	44.3	49.2
41.5	410	276	224	4.1	5.2	1.3	3.1	91.6	4.5	0.8	45.8	50.9
42.0	411	276	224	4.1	5.2	1.3	2.9	91.2	4.1	1.8	45.2	50.2
42.5	409	275	223	4.8	5.2	1.3	4.7	90.1	3.8	1.4	43.3	48.0
43.0	410	277	222	4.7	5.2	1.3	4.1	90.5	4.8	0.7	44.7	49.6
43.5	405	276	224	4.6	5.2	1.3	2.8	91.4	4.2	1.6	45.5	50.5
44.0	409	275	223	4.7	5.2	1.3	3.1	91.6	3.8	1.4	45.2	50.2
44.5	410	275	222	4.8	5.2	1.3	3.4	91.6	3.8	1.2	45.0	50.0
45.0	411	275	222	4.9	5.2	1.3	3.5	91.6	3.8	1.2	44.9	49.9
45.5	411	275	221	5.0	5.2	1.3	3.5	91.6	3.8	1.2	44.9	49.9
46.0	411	275	221	5.0	5.2	1.3	3.5	91.6	3.7	1.2	44.9	49.8
46.5	411	275	221	5.1	5.2	1.3	3.6	91.6	3.7	1.2	44.9	49.8
47.0	412	275	220	5.1	5.2	1.3	3.5	91.7	3.6	1.2	44.9	49.9
47.5	412	275	220	5.1	5.2	1.3	3.4	91.9	3.5	1.2	45.0	50.0
48.0	412	275	220	5.2	5.2	1.3	3.4	91.9	3.5	1.2	45.0	50.0
48.5	412	274	219	5.4	5.2	1.3	3.5	91.8	3.4	1.2	44.8	49.8
49.0	412	274	219	5.4	5.2	1.3	3.6	91.8	3.5	1.2	44.8	49.7
49.5	413	274	219	5.5	5.2	1.3	3.6	91.8	3.4	1.2	44.8	49.7
50.0	413	274	218	5.5	5.2	1.3	3.6	91.9	3.3	1.3	44.7	49.7
50.5	413	274	218	5.5	5.2	1.3	3.4	92.2	3.2	1.2	45.0	50.0
51.0	414	274	218	5.5	5.2	1.3	3.2	92.4	3.1	1.3	45.2	50.1
51.5	414	274	217	5.8	5.2	1.3	4.0	88.9	0.9	4.7	41.8	46.4

52.0	413	274	217	6.0	5.2	1.3						

f) GHSV = 1032 h^{-1}

time, min	T_1, °C	T_2, °C	T_3, °C	p, bar	v_{H_2in}, Ndm^3/min	v_{CO_2in}, Ndm^3/min	CO_2 %	CH_4 %	H_2 %	N_2 %	LHV, MJ/kg	HHV, MJ/kg
0.0	204	305	182	0.0	5.6	1.4	8.1	67.2	22.4	2.0	38.5	43.0
0.5	215	313	199	0.0	5.6	1.4	7.6	68.0	22.3	2.0	39.4	44.0
1.0	222	315	208	0.0	5.6	1.4	7.5	68.0	22.3	2.1	39.4	44.0
1.5	228	314	214	0.0	5.6	1.4	7.5	68.0	22.3	2.2	39.4	44.0
2.0	234	314	219	0.0	5.6	1.4	7.5	68.1	22.2	2.2	39.4	44.0
2.5	238	312	224	0.0	5.6	1.4	7.5	68.2	22.1	2.2	39.4	44.0
3.0	243	311	228	0.0	5.6	1.4	7.5	68.3	22.0	2.2	39.4	44.0
3.5	249	309	232	0.0	5.6	1.4	7.5	68.4	22.0	2.2	39.5	44.1
4.0	254	308	235	0.0	5.6	1.4	7.4	68.5	21.9	2.2	39.5	44.1
4.5	261	306	238	0.0	5.6	1.4	7.4	68.6	21.8	2.2	39.5	44.1
5.0	268	305	240	0.0	5.6	1.4	7.4	68.7	21.7	2.2	39.5	44.1
5.5	275	303	243	0.0	5.6	1.4	7.4	68.8	21.7	2.2	39.6	44.1
6.0	284	302	245	0.0	5.6	1.4	7.4	68.8	21.6	2.2	39.6	44.1
6.5	292	300	246	0.0	5.6	1.4	7.4	68.9	21.5	2.2	39.6	44.2
7.0	301	299	248	0.0	5.6	1.4	7.4	69.0	21.5	2.2	39.6	44.2
7.5	310	297	249	0.0	5.6	1.4	7.4	69.0	21.5	2.2	39.6	44.2
8.0	318	296	251	0.0	5.6	1.4	7.4	69.0	21.4	2.2	39.6	44.2
8.5	327	295	252	0.0	5.6	1.4	7.4	69.1	21.4	2.2	39.6	44.2
9.0	334	294	252	0.0	5.6	1.4	7.4	69.1	21.4	2.2	39.6	44.2
9.5	342	293	253	0.0	5.6	1.4	7.3	69.1	21.3	2.2	39.6	44.2
10.0	349	292	254	0.0	5.6	1.4	7.4	69.2	21.3	2.2	39.6	44.2
10.5	355	291	255	0.0	5.6	1.4	7.4	69.2	21.3	2.2	39.6	44.2
11.0	361	290	255	0.0	5.6	1.4	7.4	69.2	21.3	2.1	39.6	44.2
11.5	366	289	255	0.0	5.6	1.4	7.3	69.3	21.2	2.1	39.7	44.3
12.0	371	288	256	0.0	5.6	1.4	7.3	69.4	21.2	2.2	39.7	44.3

12.5	375	287	256	0.0	5.6	1.4	7.3	69.5	20.7	2.5	39.4	44.0
13.0	379	286	256	0.1	5.6	1.4	6.8	72.2	17.2	3.8	39.0	43.5
13.5	383	286	256	0.1	5.6	1.4	6.1	75.9	15.8	2.3	41.2	45.8
14.0	386	286	256	0.5	5.6	1.4	6.0	76.6	15.4	2.0	41.4	46.1
14.5	388	286	257	0.6	5.6	1.4	5.8	77.4	14.6	2.2	41.5	46.2
15.0	391	285	257	0.6	5.6	1.4	5.6	78.5	14.0	1.9	42.0	46.8
15.5	392	285	256	0.7	5.6	1.4	5.6	78.9	13.8	1.8	42.1	46.9
16.0	393	284	256	0.8	5.6	1.4	5.6	79.1	13.6	1.7	42.1	46.9
16.5	395	284	256	0.8	5.6	1.4	5.5	79.3	13.5	1.7	42.3	47.0
17.0	396	283	255	0.9	5.6	1.4	5.5	79.5	13.4	1.6	42.4	47.2
17.5	397	283	255	0.9	5.6	1.4	5.4	79.6	13.3	1.7	42.4	47.2
18.0	398	282	254	0.9	5.6	1.4	5.4	79.7	13.3	1.6	42.4	47.2
18.5	400	282	254	0.9	5.6	1.4	5.4	79.8	13.1	1.7	42.4	47.2
19.0	401	282	253	0.9	5.6	1.4	5.5	79.8	13.1	1.6	42.4	47.2
19.5	402	281	253	0.9	5.6	1.4	5.4	80.2	12.6	1.9	42.3	47.0
20.0	404	281	252	0.9	5.6	1.4	5.2	80.8	12.3	1.6	42.7	47.5
20.5	405	281	251	1.0	5.6	1.4	5.2	81.0	12.2	1.5	42.8	47.6
21.0	407	281	251	1.1	5.6	1.4	5.2	81.2	12.2	1.5	42.8	47.7
21.5	408	281	250	1.1	5.6	1.4	5.1	81.3	12.0	1.6	42.8	47.7
22.0	409	281	250	1.1	5.6	1.4	5.2	81.3	12.0	1.5	42.8	47.6
22.5	410	281	249	1.1	5.6	1.4	5.0	81.8	11.5	1.7	42.8	47.7
23.0	411	281	248	1.1	5.6	1.4	4.7	82.7	11.0	1.5	43.3	48.2
23.5	412	281	247	1.3	5.6	1.4	4.8	82.8	10.9	1.4	43.3	48.2
24.0	413	281	247	1.3	5.6	1.4	4.8	82.9	10.8	1.4	43.3	48.2
24.5	414	281	246	1.4	5.6	1.4	4.8	83.1	10.7	1.4	43.3	48.2
25.0	415	281	246	1.4	5.6	1.4	4.8	83.1	10.7	1.4	43.4	48.2
25.5	416	281	245	1.4	5.6	1.4	4.7	83.5	10.3	1.5	43.4	48.3
26.0	416	281	244	1.4	5.6	1.4	4.0	84.6	9.8	1.5	44.2	49.1
26.5	417	281	244	1.6	5.6	1.4	4.2	85.0	9.3	1.4	44.0	49.0
27.0	417	282	243	1.7	5.6	1.4	4.4	85.1	9.3	1.3	43.9	48.8

27.5	418	282	243	1.8	5.6	1.4	4.4	85.1	9.2	1.3	43.9	48.8
28.0	418	282	242	1.8	5.6	1.4	4.4	85.2	9.2	1.2	43.9	48.8
28.5	418	281	241	1.8	5.6	1.4	4.4	85.2	9.1	1.3	43.8	48.8
29.0	419	282	241	1.9	5.6	1.4	4.4	85.3	9.0	1.2	43.9	48.8
29.5	420	282	240	1.9	5.6	1.4	4.4	85.4	9.0	1.2	43.9	48.8
30.0	421	282	239	1.9	5.6	1.4	4.5	85.4	9.0	1.2	43.9	48.8
30.5	421	282	239	1.9	5.6	1.4	4.4	85.3	8.9	1.3	43.8	48.7
31.0	422	282	238	1.9	5.6	1.4	4.3	85.8	8.6	1.3	44.0	48.9
31.5	423	282	237	1.9	5.6	1.4	3.7	86.9	7.9	1.5	44.6	49.6
32.0	423	282	238	2.2	5.6	1.4	3.9	87.2	7.7	1.2	44.5	49.5
32.5	423	283	236	2.3	5.6	1.4	4.0	87.2	7.6	1.2	44.4	49.4
33.0	423	283	236	2.4	5.6	1.4	4.1	87.3	7.5	1.1	44.4	49.4
33.5	424	283	235	2.4	5.6	1.4	4.1	87.3	7.5	1.1	44.4	49.3
34.0	424	283	235	2.5	5.6	1.4	4.1	87.4	7.5	1.1	44.4	49.3
34.5	424	283	234	2.5	5.6	1.4	4.1	87.4	7.4	1.1	44.4	49.3
35.0	424	283	234	2.5	5.6	1.4	4.1	87.4	7.4	1.1	44.4	49.3
35.5	425	283	233	2.5	5.6	1.4	4.0	87.6	7.1	1.3	44.3	49.2
36.0	425	283	232	2.5	5.6	1.4	3.4	88.8	6.7	1.2	45.2	50.2
36.5	425	283	232	2.8	5.6	1.4	3.4	89.4	6.1	1.2	45.2	50.2
37.0	425	283	230	3.1	5.6	1.4	3.7	89.3	6.0	1.0	44.9	49.9
37.5	425	284	231	3.3	5.6	1.4	3.7	89.3	6.0	1.0	44.9	49.8
38.0	425	284	231	3.3	5.6	1.4	3.7	89.3	5.9	1.0	44.9	49.8
38.5	425	283	230	3.4	5.6	1.4	3.7	89.4	5.9	1.0	44.8	49.8
39.0	426	283	230	3.4	5.6	1.4	3.7	89.4	5.8	1.1	44.7	49.7
39.5	426	283	229	3.4	5.6	1.4	3.5	89.5	6.0	0.9	45.2	50.2
40.0	426	284	229	3.4	5.6	1.4	3.7	89.7	5.4	1.1	44.8	49.8
40.5	425	284	229	3.7	5.6	1.4	3.6	89.9	5.5	1.0	45.0	50.0
41.0	426	283	228	3.8	5.6	1.4	3.6	90.0	5.3	1.2	44.8	49.8
41.5	426	283	228	3.8	5.6	1.4	3.5	90.5	5.3	0.7	45.3	50.4
42.0	426	283	227	3.8	5.6	1.4	3.4	90.6	4.9	1.1	45.2	50.2

42.5	426	283	227	4.2	5.6	1.4	3.7	90.6	4.9	0.8	45.0	50.0
43.0	427	283	226	4.2	5.6	1.4	3.7	90.5	4.7	1.1	44.8	49.8
43.5	427	283	226	4.2	5.6	1.4	3.5	90.8	5.1	0.7	45.4	50.5
44.0	427	283	226	4.2	5.6	1.4	3.5	90.8	4.6	1.1	45.0	50.0
44.5	427	283	225	4.5	5.6	1.4	3.2	91.5	4.3	1.1	45.4	50.5
45.0	427	283	225	4.8	5.6	1.4	3.3	91.6	4.1	1.0	45.3	50.3
45.5	427	283	225	4.9	5.6	1.4	3.5	91.6	4.1	0.9	45.2	50.2
46.0	427	283	225	5.0	5.6	1.4	3.5	91.6	4.0	0.9	45.2	50.2
46.5	427	283	224	5.1	5.6	1.4	3.5	91.6	4.0	0.8	45.2	50.2
47.0	427	283	224	5.2	5.6	1.4	3.5	91.6	3.9	0.9	45.1	50.1
47.5	426	283	224	5.2	5.6	1.4	3.5	91.7	3.9	0.8	45.2	50.2
48.0	427	283	223	5.3	5.6	1.4	3.6	91.7	4.0	0.8	45.2	50.2
48.5	428	283	223	5.3	5.6	1.4	3.6	91.6	3.8	1.0	44.9	49.9
49.0	428	283	222	5.4	5.6	1.4	3.8	91.1	4.3	0.9	44.8	49.8
49.5	427	282	222	5.5	5.6	1.4	6.3	87.9	4.2	1.6	41.4	45.9

g) GHSV = 1106 h^{-1}

time, min	T_1, °C	T_2, °C	T_3, °C	p, bar	v_{H_2in}, Ndm^3/min	v_{CO_2in}, Ndm^3/min	CO_2 %	CH_4 %	H_2 %	N_2 %	LHV, MJ/kg	HHV, MJ/kg
0.0	198	309	178	0.0	6.0	1.5	7.3	59.3	23.3	9.3	33.7	37.6
0.5	215	321	202	0.1	6.0	1.5	7.9	67.6	22.1	2.2	38.7	43.2
1.0	224	323	214	0.0	6.0	1.5	8.0	67.4	22.3	2.3	38.7	43.2
1.5	230	324	222	0.1	6.0	1.5	8.0	67.1	22.5	2.3	38.6	43.1
2.0	236	323	228	0.1	6.0	1.5	8.1	66.9	22.7	2.4	38.5	43.0
2.5	241	322	233	0.1	6.0	1.5	8.1	66.7	22.8	2.4	38.5	43.0
3.0	246	320	237	0.1	6.0	1.5	8.1	66.5	23.0	2.4	38.5	42.9
3.5	251	317	240	0.1	6.0	1.5	8.2	66.3	23.1	2.4	38.4	42.9
4.0	257	314	242	0.1	6.0	1.5	8.2	66.1	23.3	2.4	38.4	42.8
4.5	263	311	244	0.1	6.0	1.5	8.3	65.9	23.5	2.4	38.3	42.8
5.0	270	307	245	0.1	6.0	1.5	8.3	65.7	23.7	2.4	38.3	42.7

5.5	277	303	246	0.1	6.0	1.5	8.4	65.4	23.9	2.3	38.2	42.7
6.0	285	300	246	0.1	6.0	1.5	8.4	65.1	24.1	2.4	38.1	42.5
6.5	292	296	246	0.1	6.0	1.5	8.4	64.9	24.2	2.4	38.0	42.5
7.0	300	293	246	0.1	6.0	1.5	8.5	64.8	24.3	2.4	38.0	42.5
7.5	307	290	246	0.1	6.0	1.5	8.5	64.7	24.4	2.4	38.0	42.4
8.0	314	287	245	0.1	6.0	1.5	8.5	64.5	24.5	2.4	37.9	42.4
8.5	321	284	244	0.1	6.0	1.5	8.6	64.5	24.6	2.4	37.9	42.4
9.0	326	281	244	0.1	6.0	1.5	8.6	64.4	24.6	2.4	37.9	42.3
9.5	332	279	243	0.1	6.0	1.5	8.6	64.4	24.6	2.4	37.9	42.3
10.0	337	277	243	0.1	6.0	1.5	8.6	64.4	24.6	2.5	37.8	42.3
10.5	341	275	242	0.1	6.0	1.5	8.6	64.4	24.5	2.5	37.8	42.2
11.0	345	274	242	0.1	6.0	1.5	8.6	64.5	24.4	2.5	37.8	42.2
11.5	349	272	241	0.1	6.0	1.5	8.5	64.7	24.3	2.6	37.8	42.3
12.0	352	271	241	0.1	6.0	1.5	8.5	64.9	23.4	3.2	37.4	41.8
12.5	354	271	241	0.1	6.0	1.5	8.0	67.7	20.9	3.5	37.8	42.2
13.0	357	270	241	0.1	6.0	1.5	7.6	69.7	20.0	2.6	39.0	43.5
13.5	359	270	240	0.3	6.0	1.5	7.5	70.3	19.7	2.5	39.2	43.7
14.0	361	271	241	0.3	6.0	1.5	7.5	70.6	19.5	2.4	39.3	43.8
14.5	363	271	241	0.3	6.0	1.5	7.3	71.4	17.9	3.4	38.7	43.2
15.0	364	272	241	0.4	6.0	1.5	6.8	74.2	16.4	2.7	39.9	44.5
15.5	365	272	242	0.4	6.0	1.5	6.6	75.2	15.8	2.4	40.4	45.0
16.0	365	273	242	0.6	6.0	1.5	6.5	75.6	15.5	2.3	40.5	45.1
16.5	366	274	243	0.7	6.0	1.5	6.5	76.0	15.2	2.3	40.6	45.2
17.0	366	274	243	0.7	6.0	1.5	6.4	76.3	15.0	2.2	40.7	45.3
17.5	367	275	243	0.7	6.0	1.5	6.4	76.7	14.3	2.7	40.4	45.0
18.0	367	275	243	0.8	6.0	1.5	6.0	78.6	12.9	2.5	41.0	45.6
18.5	367	276	244	0.8	6.0	1.5	5.8	79.6	12.4	2.1	41.5	46.2
19.0	367	277	244	1.0	6.0	1.5	5.8	80.0	12.2	2.1	41.6	46.4
19.5	367	278	245	1.1	6.0	1.5	5.7	80.3	11.9	2.1	41.7	46.4
20.0	368	279	245	1.1	6.0	1.5	5.7	80.6	11.8	2.0	41.8	46.5

20.5	368	280	245	1.2	6.0	1.5	5.6	81.0	11.3	2.1	41.8	46.5
21.0	368	280	246	1.2	6.0	1.5	5.4	81.6	11.0	2.0	42.1	46.8
21.5	368	281	246	1.2	6.0	1.5	5.4	81.8	10.8	1.9	42.2	46.9
22.0	368	282	246	1.3	6.0	1.5	5.4	82.1	10.7	1.9	42.2	47.0
22.5	368	283	247	1.4	6.0	1.5	5.4	82.2	10.5	1.9	42.2	47.0
23.0	368	284	247	1.4	6.0	1.5	5.4	82.3	10.4	1.9	42.3	47.0
23.5	368	284	247	1.4	6.0	1.5	5.3	82.5	10.3	1.9	42.3	47.1
24.0	369	285	248	1.4	6.0	1.5	5.3	82.6	10.3	1.7	42.4	47.2
24.5	369	286	248	1.4	6.0	1.5	5.1	82.7	10.5	1.7	42.8	47.6
25.0	369	287	248	1.5	6.0	1.5	4.8	83.0	10.4	1.9	43.0	47.8
25.5	370	287	249	1.5	6.0	1.5	4.4	83.9	9.7	2.0	43.4	48.2
26.0	370	288	249	1.5	6.0	1.5	4.2	84.5	9.4	1.9	43.6	48.5
26.5	370	289	249	1.6	6.0	1.5	4.3	84.7	9.2	1.8	43.6	48.5
27.0	370	290	250	1.8	6.0	1.5	4.3	84.8	9.1	1.7	43.6	48.5
27.5	369	291	250	1.8	6.0	1.5	4.3	84.9	9.0	1.8	43.6	48.5
28.0	370	291	251	1.9	6.0	1.5	4.3	85.0	8.9	1.7	43.6	48.5
28.5	370	292	251	1.9	6.0	1.5	4.4	85.1	8.9	1.7	43.6	48.5
29.0	370	293	251	1.9	6.0	1.5	4.3	85.1	8.9	1.7	43.6	48.5
29.5	370	293	252	2.0	6.0	1.5	4.3	85.1	8.8	1.7	43.6	48.5
30.0	370	294	252	2.0	6.0	1.5	4.3	85.3	8.4	2.0	43.4	48.3
30.5	370	294	252	2.0	6.0	1.5	3.4	86.7	8.4	1.5	45.0	50.0
31.0	371	295	253	2.0	6.0	1.5	3.1	87.6	7.3	2.0	44.8	49.8
31.5	369	296	253	2.7	6.0	1.5	3.6	87.6	7.0	1.7	44.5	49.4
32.0	369	297	254	2.8	6.0	1.5	3.8	87.7	6.9	1.6	44.4	49.3
32.5	369	297	254	3.0	6.0	1.5	3.8	87.8	6.9	1.5	44.4	49.3
33.0	369	297	254	3.1	6.0	1.5	3.8	87.9	6.8	1.5	44.4	49.3
33.5	369	298	255	3.1	6.0	1.5	3.8	88.0	6.8	1.4	44.4	49.4
34.0	368	298	255	3.2	6.0	1.5	3.6	88.0	7.0	1.4	44.8	49.8
34.5	368	298	256	3.3	6.0	1.5	3.5	88.3	6.8	1.5	44.8	49.8
35.0	368	298	256	3.3	6.0	1.5	3.6	88.3	6.7	1.4	44.8	49.8

35.5	368	299	256	3.3	6.0	1.5	3.6	88.4	6.7	1.4	44.8	49.8
36.0	368	299	256	3.4	6.0	1.5	3.6	88.2	6.6	1.6	44.6	49.6
36.5	367	299	257	3.4	6.0	1.5	3.5	88.4	6.7	1.4	44.9	49.8
37.0	367	300	257	3.4	6.0	1.5	3.1	89.0	6.3	1.6	45.2	50.2
37.5	369	300	257	3.6	6.0	1.5	3.3	89.0	6.2	1.6	45.0	50.0
38.0	365	301	257	3.8	6.0	1.5	3.4	89.1	6.1	1.5	44.9	49.9
38.5	366	301	258	4.0	6.0	1.5	3.4	89.0	6.0	1.5	44.9	49.8
39.0	366	301	258	4.0	6.0	1.5	3.4	89.1	6.0	1.4	44.9	49.9
39.5	366	301	258	4.1	6.0	1.5	3.4	89.2	6.0	1.5	44.9	49.9
40.0	366	301	258	4.1	6.0	1.5	3.4	89.0	5.9	1.7	44.7	49.7
40.5	367	301	259	4.2	6.0	1.5	3.4	89.3	5.9	1.4	44.9	49.9
41.0	368	301	259	4.2	6.0	1.5	3.4	89.4	5.8	1.4	45.0	50.0
41.5	367	302	259	4.3	6.0	1.5	3.4	89.4	5.8	1.5	44.9	49.9
42.0	367	302	260	4.4	6.0	1.5	3.4	89.3	5.8	1.5	44.9	49.9
42.5	367	302	260	4.5	6.0	1.5	3.4	89.3	5.8	1.5	44.8	49.8
43.0	368	302	261	4.5	6.0	1.5	3.4	89.4	5.7	1.5	44.8	49.8
43.5	368	302	259	4.6	6.0	1.5	3.5	89.4	5.7	1.4	44.8	49.8
44.0	367	303	261	4.6	6.0	1.5	3.5	89.4	5.7	1.4	44.8	49.8
44.5	368	303	261	4.6	6.0	1.5	3.5	89.4	5.7	1.4	44.8	49.8
45.0	368	303	261	4.6	6.0	1.5	3.5	89.4	5.7	1.4	44.9	49.9
45.5	368	303	262	4.6	6.0	1.5	3.5	89.5	5.7	1.4	44.9	49.8
46.0	369	303	262	4.7	6.0	1.5	3.5	89.5	5.6	1.4	44.9	49.9
46.5	369	305	262	4.7	6.0	1.5	3.5	89.6	5.6	1.3	44.9	49.9
47.0	369	304	262	4.7	6.0	1.5	3.5	89.7	5.6	1.2	45.0	50.0
47.5	369	304	263	4.7	6.0	1.5	3.4	89.7	5.6	1.4	45.0	50.0
48.0	368	304	263	4.7	6.0	1.5	3.4	89.8	5.5	1.3	45.0	50.0
48.5	369	304	263	4.8	6.0	1.5	3.4	89.7	5.5	1.4	44.9	49.9
49.0	369	304	263	4.9	6.0	1.5	3.4	89.7	5.5	1.4	44.9	49.9
49.5	369	305	264	4.9	6.0	1.5	3.4	89.7	5.5	1.4	44.9	49.9
50.0	369	305	264	4.9	6.0	1.5	3.4	89.6	5.6	1.4	44.9	49.9

50.5	367	305	264	5.0	6.0	1.5	3.4	89.7	5.4	1.5	44.8	49.8
51.0	360	304	262	5.1	6.0	1.5	3.4	89.8	5.4	1.4	44.9	49.9
51.5	359	305	265	5.1	6.0	1.5	3.4	89.9	5.3	1.4	44.9	49.9
52.0	365	305	265	5.2	6.0	1.5	3.4	89.9	5.3	1.4	44.9	49.9
52.5	367	305	265	5.2	6.0	1.5	3.4	89.8	5.3	1.5	44.8	49.8
53.0	368	305	265	5.2	6.0	1.5	3.4	89.8	5.3	1.5	23.6	26.2
53.5	368	305	266	5.3	6.0	1.5	3.4	89.8	5.3	1.5	0.3	0.4
54.0	368	305	266	5.3	6.0	1.5	3.4	89.8	5.3	1.5	0.0	0.0

Appendix C

oxygen	STBR	mass flow kg/h				mole fraction							
						process gas				SNG			
		process gas	hydrogen	SNG	water	H_2	CO	CO_2	CH_4	H_2	CO	CO_2	CH_4
11.2 kg/h (OTBR = 0.1)	0.1	132.99	18.01	72.48	78.52	0.40	0.4455	0.0532	0.0760	0.0415	0.0000	0.0048	0.9476
	0.2	140.87	18.01	72.61	86.26	0.45	0.3963	0.0766	0.0504	0.0430	0.0000	0.0053	0.9451
	0.3	147.37	18.00	72.69	92.67	0.48	0.3571	0.0976	0.0351	0.0434	0.0000	0.0057	0.9440
	0.4	152.97	17.99	72.74	98.22	0.51	0.3244	0.1161	0.0254	0.0432	0.0000	0.0058	0.9437
	0.5	157.85	17.98	72.78	103.04	0.52	0.2967	0.1324	0.0188	0.0426	0.0000	0.0060	0.9438
	0.6	162.13	17.97	72.80	107.31	0.54	0.2728	0.1467	0.0143		0.0000	0.0060	0.9441
	0.7	165.92	17.96	72.82	111.07	0.55	0.2522	0.1594	0.0110	0.0413	0.0000	0.0061	0.9445
	0.8	169.28	17.95	72.83	114.40	0.56	0.2342	0.1707	0.0086	0.0406	0.0000	0.0061	0.9450
	0.9	172.27	17.95	72.84	117.37	0.57	0.2183	0.1807	0.0068	0.0399	0.0000	0.0062	0.9455
	1.0	174.96	17.94	72.86	120.04	0.57	0.2043	0.1896	0.0055	0.0393	0.0000	0.0062	0.9459
33.6 kg/h (OTBR = 0.3)	0.1	148.25	20.82	72.77	96.30	0.42	0.3983	0.1250	0.0262	0.0447	0.0000	0.0060	0.9421
	0.2	153.91	20.81	72.80	101.92	0.45	0.3553	0.1483	0.0187	0.0438	0.0000	0.0061	0.9427
	0.3	158.81	20.80	72.82	106.79	0.47	0.3200	0.1680	0.0137	0.0427	0.0000	0.0061	0.9434
	0.4	163.09	20.78	72.83	111.04	0.49	0.2906	0.1848	0.0103	0.0417	0.0000	0.0062	0.9441
	0.5	166.84	20.77	72.84	114.77	0.50	0.2657	0.1993	0.0078	0.0407	0.0000	0.0062	0.9448
	0.6	170.14	20.77	72.85	118.02	0.51	0.2444	0.2118	0.0061	0.0399	0.0000	0.0062	0.9454
	0.7	173.06	20.76	72.86	120.96	0.52	0.2259	0.2227	0.0048	0.0391	0.0000	0.0062	0.9460
	0.8	175.66	20.75	72.87	123.53	0.53	0.2099	0.2323	0.0038	0.0384	0.0000	0.0063	0.9465
	0.9	177.99	20.74	72.88	125.83	0.53	0.1959	0.2407	0.0031	0.0378	0.0000	0.0063	0.9469
	1.0	180.07	20.74	72.89	127.92	0.54	0.1835	0.2482	0.0025	0.0373	0.0000	0.0063	0.9473
56 kg/h (OTBR = 0.5)	0.1	160.33	23.61	72.86	111.09	0.40	0.3425	0.2187	0.0087	0.0421	0.0000	0.0063	0.9435
	0.2	164.62	23.60	72.86	115.35	0.42	0.3061	0.2381	0.0065	0.0408	0.0000	0.0063	0.9446
	0.3	168.33	23.58	72.87	119.05	0.44	0.2762	0.2543	0.0049	0.0397	0.0000	0.0063	0.9454
	0.4	171.57	23.57	72.88	122.28	0.45	0.2512	0.2680	0.0038	0.0388	0.0000	0.0063	0.9461
	0.5	174.40	23.57	72.88	125.08	0.46	0.2301	0.2796	0.0030	0.0380	0.0000	0.0063	0.9468

0.6	176.89	23.56	72.89	127.56	0.47	0.2120	0.2896	0.0023	0.0373	0.0000	0.0063	0.9473
0.7	179.10	23.55	72.90	129.74	0.48	0.1964	0.2983	0.0019	0.0367	0.0000	0.0064	0.9477
0.8	181.07	23.55	72.91	131.72	0.48	0.1828	0.3059	0.0015	0.0362	0.0000	0.0064	0.9481
0.9	182.82	23.54	72.92	133.47	0.49	0.1709	0.3126	0.0012	0.0357	0.0000	0.0064	0.9484
1.0	184.40	23.66	72.67	135.39	0.49	0.1604	0.3186	0.0010	0.0390	0.0000	0.0042	0.9473